AMERICAN UNIVERSITY OF BEIRUT

MODELING PROSTATE CANCER USING PATIENT-DERIVED ORGANOIDS AND CELL LINES: IMPLICATIONS FOR PERSONALIZED MEDICINE

by
KATIA ANIS CHEAITO

A Dissertation
submitted in partial fulfillment of the requirements
for the degree of Doctor of Philosophy
to the Department of Anatomy, Cell Biology & Physiological Sciences
of the Faculty of Medicine
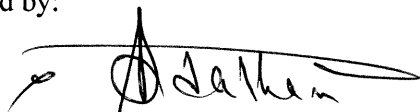at the American University of Beirut

Beirut, Lebanon
May 2019

AMERICAN UNIVERSITY OF BEIRUT

MODELING AND COMPREHENDING PROSTATE CANCER THROUGH PATIENT-DERIVED ORGANOIDS AND CELLS: IMPLICATIONS FOR PERSONALIZED MEDICINE
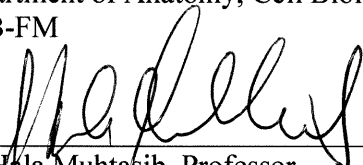
by

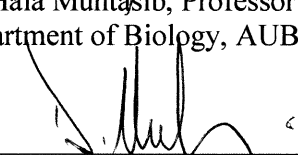## KATIA ANIS CHEAITO

Approved by:

Dr. Marwan El-Sabban, Professor and Vice Chair   Chair
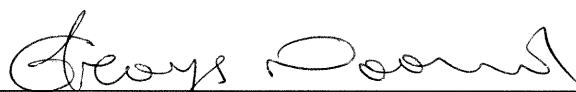Department of Anatomy, Cell Biology & Physiological Sciences
AUB-FM

Dr. Wassim Abou-Kheir, Associate Professor   Advisor
Department of Anatomy, Cell Biology & Physiological Sciences
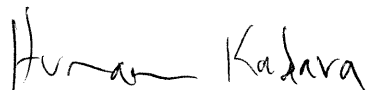AUB-FM

Dr. Hala Muhtasib, Professor   Member
Department of Biology, AUB-FAS
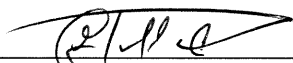
Dr. Deborah Mukherji, Associate Professor   Member
Department of Internal Medicine, AUB-MC

Dr. Georges Daoud, Assistant Professor   Member
Department of Anatomy, Cell Biology & Physiological Sciences
AUB-FM

Dr. Humam Kadara, Associate Professor   External Member
MD Anderson Cancer Center, Houston, USA

Dr. Elias Chalhoub, Associate Professor   External Member
Faculty of Health Sciences, University of Balamand

Date of thesis defense: May 2, 2019

AMERICAN UNIVERSITY OF BEIRUT

THESIS, DISSERTATION, PROJECT RELEASE FORM

Student Name:

Cheaito _____ _Katia_ _____ _Anis_ _____
Last   First   Middle

◯ Master's Thesis   ◯ Master's Project   ⊗ Doctoral Dissertation

☐   I authorize the American University of Beirut to: (a) reproduce hard or electronic
copies of my thesis, dissertation, or project; (b) include such copies in the archives and digital
repositories of the University; and (c) make freely available such copies to third parties for
research or educational purposes.

☒   I authorize the American University of Beirut, to: (a) reproduce hard or electronic
copies of it; (b) include such copies in the archives and digital repositories of the University;
and (c) make freely available such copies to third parties for research or educational purposes
after:

> One --✓ year from the date of submission of my thesis, dissertation, or project.
> Two ---- years from the date of submission of my thesis, dissertation, or project.
> Three ---- years from the date of submission of my thesis, dissertation, or project.

Katia _____   _May 13, 2019_ _____
Signature   Date

ACKNOWLEDGMENTS

The route towards fulfilling my PhD dissertation was bumpy and challenging but full of exciting and enriching experiences. This laborious journey was made possible in the presence of cheering companions to whom I owe my deepest gratitude.

I am extremely appreciative to my thesis advisor Dr Wassim Abou-Kheir. His continuous guidance and support were key to bring this dissertation into light. I thank him for his positive outlook and perseverance which enabled me to look at personal and scientific challenges from a different perspective. He is an advisor from whom I keep on learning, a counselor who is always available to listen, but most importantly a friend who believes in my potential. Thank you for being supportive and understanding during the toughest times.

I would like to express my gratitude for the committee members for their valued input and meticulous remarks and questions. Thank you for the time spent in reviewing this dissertation. Thank you Dr Marwan El-Sabban for chairing the thesis committee. It is a privilege to learn from you and your critical way of thinking. I am appreciative for your challenging remarks and questions.

To my big family in the WAK laboratory, I am thankful for each one of you. The team spirit and cooperative work environment were essential to fulfill this thesis project. Thank you Dr Hisham Bahmad for being an enthusiastic and hardworking colleague and friend, your contributions were essential at times of need. Thank you to Dr Ola Hadadeh, Alissar Monzer, Hiba Msheik, Emane Saleh, Zaki Abou Mrad and Hiba Jalloul for

contributing to this project. Your dedication, work ethics and caring attitude were essential to finalize different experiments I could not address by myself. Thank you to all lab members for the beautiful friendship that I will always cherish.

To my family, I dedicate this work. Thank you Ziad for being a loving husband and friend. Thank you for your endless support and understanding during this journey. You give me strength during the hardest days and you make me smile during the saddest moments, and for that I am forever grateful. Thank you to my parents for their unconditional love and for always believing in me since I was a little child. Thank you to my brother Hassan, you were always my safety net, my comforting person and my cheerleader. Despite the heavy load of your absence, your endless love, your confidence and your leadership skills still guide my steps and push me to become a better person.

Lastly, the presence of a support system and teamwork are key to reach our goals in life; and I was blessed with supporting family, friends and colleagues.

AN ABSTRACT OF THE DISSERTATION OF

Katia Anis Cheaito   for   PhD in Biomedical Sciences
                                       Discipline: Physiology

Title: Modeling Prostate Cancer Using Patient-Derived Organoids and Cell Lines: Implications for Personalized Medicine

Background: In Lebanon, Prostate cancer (PCa) is the one of the most commonly diagnosed malignancy in men. It is a heterogeneous disease associated with large-scale genomic rearrangements and extensive copy number alterations involving multiple chromosomes. The currently available cancer models fail to recapitulate the progression of PCa, its metastasis, and its progression to castration-resistant states. The epithelial-mesenchymal transition (EMT), marks a key step in the invasion and malignant progression of PCa, and plays a substantial role in therapeutic resistance to antiandrogens and radiotherapy. Therefore, the identification of the onset of metastatic dissemination through assessment of molecular markers of EMT is highly needed to further aid in the development of a novel system for predicting the prognosis of PCa. In addition, the three-dimensional (3D) organoid culture systems are rapidly emerging as potential models to investigate both basic developmental processes and disease mechanisms, where patient-derived organoids have demonstrated the ability to mimic genetically and phenotypically the tumor of origin.

Objective: The overall aim of this thesis is to establish novel models to elucidate the mechanisms of PCa progression. Our first aim was to demonstrate that EMT status can model the progression status of the disease and predict the prognosis/recurrence. Our second aim was to employ fresh tissue specimens from a treatment-naïve cohort to establish 3D patient-derived organoids as an in vitro disease model for PCa progression and drug response. The third aim was to optimize the previously established extensive organoids culture system in the attempt to increase the formation efficiency and reduce the costly requirements. Knowing the difficulty in establishing primary PCa cell lines, our last aim was to generate novel PCa patient-derived cell lines.

Methods: For the first aim, a total of 122 radical prostatectomy (RP) specimens from patients with locally-advanced PCa were analyzed. Sections were examined using

immunofluorescence staining for CK8/VIM co-expression (EMT score). Then, we investigated the correlation between EMT score on one hand and the various clinicopathological parameters among PCa patients on the other hand. For the second aim, fresh radical prostatectomy specimens were collected from a total of 35 treatment-naïve patients (one unaffected and one tumor). Briefly, fresh tissue samples were digested enzymatically, and the resulting cell suspensions were plated in a 3D environment that employs Matrigel as an extracellular matrix. A cocktail of essential factors was used to enhance the establishment of organoids. Organoids and the corresponding tissue specimens were characterized using immunofluorescent analysis and immunohistochemistry. Furthermore, patient-derived organoids were employed for the assessment of drug response. For the third aim, we developed an assay system in which we examined the effect of withdrawal of individual components from the pool of previously employed culture medium components on the formation of PCa organoids. For the fourth aim, PCa patient-derived cell lines were generated and their culture conditions were optimized. These cells were further characterized using immunofluorescent analysis. Statistical analyses were performed using Graphpad prism 6 and SPSS software to test for the significance of results.

Results: Our results indicated that the co-expression of CK8/Vim (EMT score), was associated with increasing Gleason group. A highly significant linear association was detected wherein higher Gleason group was associated with higher mean EMT score. Our data also confirmed that the EMT score can predict PSA (Prostate specific antigen) failure irrespective of Gleason group, pathological stage, or surgical margins. Out of the 70 fresh specimens (35 patients) received, more than 90% were successfully established as organoids. 2D cells were generated along with the organoids using the same culture media and were continuously maintained for up to 30 passages. The presence of prostate luminal (Cytokeratin 8, Androgen Receptor, Prostate Specific Antigen) and basal (Cytokeratin 5, Cytokeratin 14, and P63) epithelial lineages was confirmed by immunofluorescent analysis. In addition, the results showed differential drug response between patient samples. Moreover, our results demonstrated the ability to grow and maintain patient-derived organoids using only 5 factors components instead of the 12 components included in the initial protocol. In addition, we optimized the culture and maintenance of patient-derived 2D cells by plating on collagen type I and we have reduced the medium requirement to include EGF only as an essential component.

Conclusion: This study underscores the importance of EMT markers for predicting the prognosis of PCa. The results revealed that the mean EMT score increases significantly as disease becomes more poorly differentiated reflected by higher Gleason group. Moreover, this study provides a repertoire of novel patient-derived organoids and cells from a unique cohort of treatment-naïve patients, as our results demonstrate that we succeeded in delineating the essential components needed to grow prostate organoids and primary cells with a high success rate and long-term maintenance in culture.

CONTENTS

ILLUSTRATIONS

TABLES

ABBREVIATIONS

ADT: Androgen Deprivation Therapy

AMACR: Alpha Methylacyl CoA Racemase

AR: Androgen Receptor

AUB: American University of Beirut

AUBMC: American University of Beirut Medical Center

Bica: Bicalutamide

BMP: Bone Morphogenetic Protein

BPH: Benign Prostatic Hyperplasia

BSA: Bovine Serum Albumin

CCLE: Cancer Cell Line Encyclopedia

CK: Cytokeratin

CRPC: Castration-Resistant Prostate Cancer

DAB: Diaminobenzidine

DHT: Dihydrotestosterone

DMSO: Dimethyl Sulfoxide

Doc: Docetaxel

ECM: Extracellular Matrix

EGF: Epithelial Growth Factor

EMT: Epithelial-Mesenchymal Transition

Enza: Enzalutamide

FBS: Fetal Bovine Serum

FFPE: Formalin-Fixed Paraffin-Embedded

FGF: Fibroblast Growth Factor

G: Generation

H&E: Hematoxylin and Eosin

IF: Immunofluorescence

IHC: Immunohistochemistry

IRB: Institutional Review Board

ISUP: International Society of Urological Pathology

Lgr5: Leucine-Rich Repeat-Containing G-Protein-Coupled Receptor

LVI: Lymphovascular Invasion

MTT: 3-(4, 5-dimethylthiazol-2-yl)-2, 5-diphenyltetrazolium bromide

NAC: N-acetylcysteine

NGS: Normal Goat Serum

NOG: Noggin

OD: Optical Density

OFC: Organoids Forming Count

PBS: Phosphate Buffered Saline

PCa: Prostate Cancer

PDX: Patient-Derived Xenograft

PFA: Paraformaldehyde

PGE2: Prostaglandin E2

PIN: Prostatic Intraepithelial Neoplasia

PNI: Perineural Invasion

PSA: Prostate-Specific Antigen

PSM: Positive Surgical Margin

ROCK: Rho-Associated Kinase

ROS: Reactive Oxygen Species

RP: Radical Prostatectomy

RSPO: R-spondin

SB: SB202190

SVI: Seminal Vesicle Invasion

TF: Transcription Factors

TGF-β: Transforming Growth Factor-Beta

CHAPTER I

INTRODUCTION

A. Prostate Cancer

1. *Prostate Cancer Epidemiology*

Cancer prevalence is on the upsurge, driven by aging societies and unhealthy standard of living. In 2018, the incidence rates recorded for cancer were one in five men and one in six women, and the mortality rates were one in eight men and one in ten women with numbers reaching 18.1 million cancer diagnosis and 9.6 million deaths in 185 countries [1]. Moreover, it is predicted that by 2030, 13 million people will die from this disease yearly [1].

Prostate Cancer (PCa) is the second most frequently diagnosed cancer and the second most frequent cause of cancer-related death in men worldwide [1, 2]. Nonetheless, the incidence of PCa varies extremely from one region to the other; according to Globocan (2018), it is the leading cancer among males in Western Europe and North America, while it ranks as the tenth most frequent cancer among males in Asia. These differences are associated with population-related factors including genetic susceptibility, age structure, metabolic syndrome and diet, or healthcare system-related including the quality of healthcare services and the variability in the adapted screening procedures mainly for prostate-specific antigen (PSA) [2-4]. In Lebanon, PCa is the most commonly diagnosed

malignancy in men, affecting 20.3% of male cancers in 2008 with estimates predicting that this percentage will continue to rise reaching 22.1 % in 2020 [5, 6].

2. *Anatomy and Histology*

The prostate is an endodermal tissue that develops during the third trimester of embryogenesis through ductal budding from the urogenital sinus epithelium and mesenchyme under the influence of testicular androgen synthesis [7]. At the beginning of puberty and in response to intensified levels of androgen stimulation, the gland starts increasing in size to attain the adult weight of nearly 20 g by 25–30 years of age. It resembles a truncated cone in shape and extends from the bladder neck to the urogenital diaphragm [8, 9].

The main function of the prostate gland is to secrete around 30% of the semen fluid [7]. It is the chief male reproductive gland implicated in male fertility since the prostatic fluid includes several components that are essential for semen liquefaction and sperm motility [10]. These factors include: Kallikreins such as prostate-specific antigen (PSA), a serine protease; citrate, an intermediate in the Krebs cycle; Zn^{2+}, a trace element that is highly accumulated in the normal prostate [10].

The human prostate lacks discernible lobes but is separated into different anatomical zones; peripheral, transition, and central as illustrated in Figure 1 [11-14]. The outermost peripheral zone (pz) comprises most prostatic glandular tissue and is the site where carcinoma, chronic prostatitis, and post-inflammatory atrophy most commonly take place [7]. The transition zone (tz) comprises a small proportion of the glandular tissue but is

implicated in the incidence of age-related benign prostatic hyperplasia (BPH) and, less frequently, adenocarcinoma [7, 12]. The central zone (cz) resembles a cone at the base of the prostate gland that surrounds the ejaculatory duct and comprises around 20% of the prostatic tissue [15]. In addition, the anterior external surface is shielded with a non-glandular anatomic region constituted of thick fibromuscular zone (fz) and covered with a fibrous capsule [11, 12]. The seminal vesicles are positioned above the base of the prostate and converge with the vas deferens on each side to constitute the ejaculatory ducts. The seminal vesicles are resilient to most of the disease courses that affect the prostate but get invaded with cancer at late stages of the disease [13, 14].

The architecture of the prostate can be described as a branched duct gland constituted of epithelial acini within a fibromuscular stromal network [16]. At the histological level (Figure 2), each gland or duct is lined with pseudostratified epithelium with three differentiated epithelial cell types; a luminal secretory cell layer expressing distinctive markers including cytokeratins (CK) 8 and 18 and prominent levels of Androgen receptor (AR) and PSA; an underlying basal cell layer expressing p63 and the high-molecular-weight keratins CK5 and 14 but low or indiscernible levels of AR and PSA; and basally localized neuroendocrine cells characterized by chromogranin A and synaptophysin expression but AR negative [17, 18]. In addition, an intermediate cell population referred to as intermediate or transit amplifying cells co-expresses luminal and basal markers [7, 18].

The mesenchymal compartment of the prostate comprises a number of differentiated cell types including a significant population of mature fibroblasts that produce extracellular matrix, entailing fibrillar proteins, glycoproteins and proteoglycans that enable growth factor signaling [19]. In addition, a layer of contractile smooth muscle cells lines the epithelium to enable expulsion of prostatic fluid [20]. Other constituents of the stroma
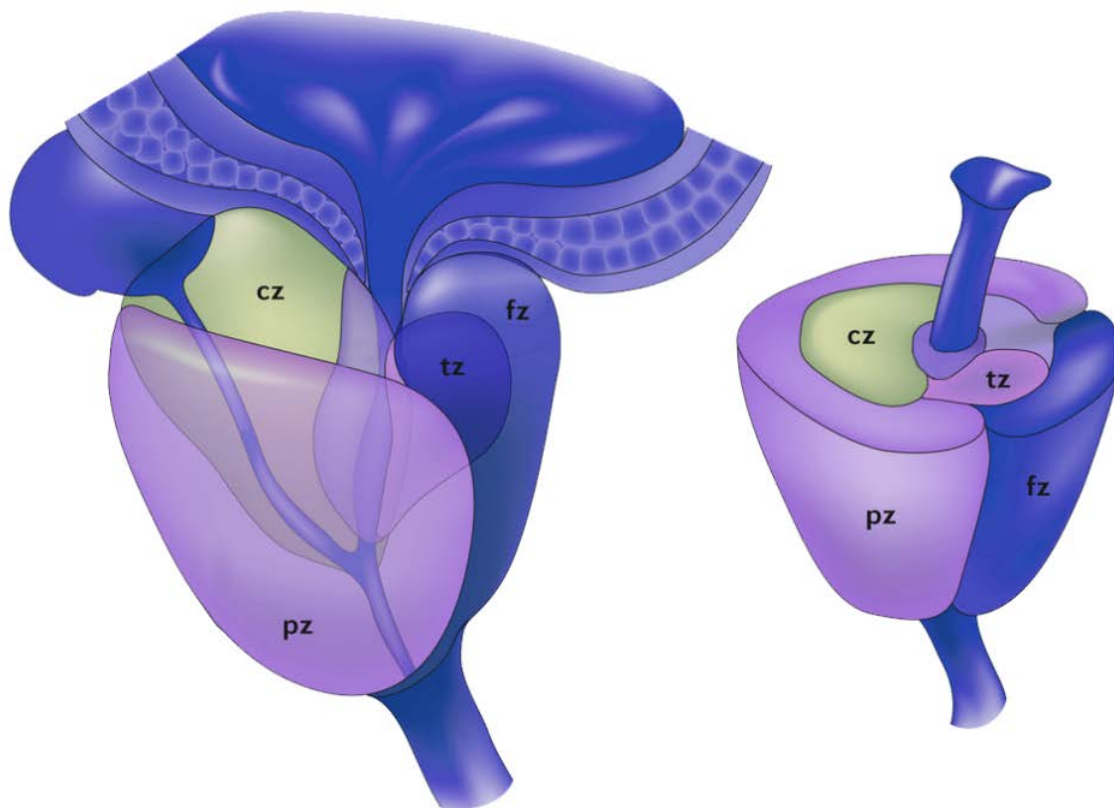
include nerves, blood vessels, lymphatics, and immune cells [15].

Figure 1. Prostate Anatomy. A schematic representation illustrating the different anatomical zones in the prostate gland. Abbreviations: pz: peripheral zone, fz: fibromuscular zone, tz: transitional zone, cz: central zone. Adapted and modified from De Marzo *et al.* (2007) [14].
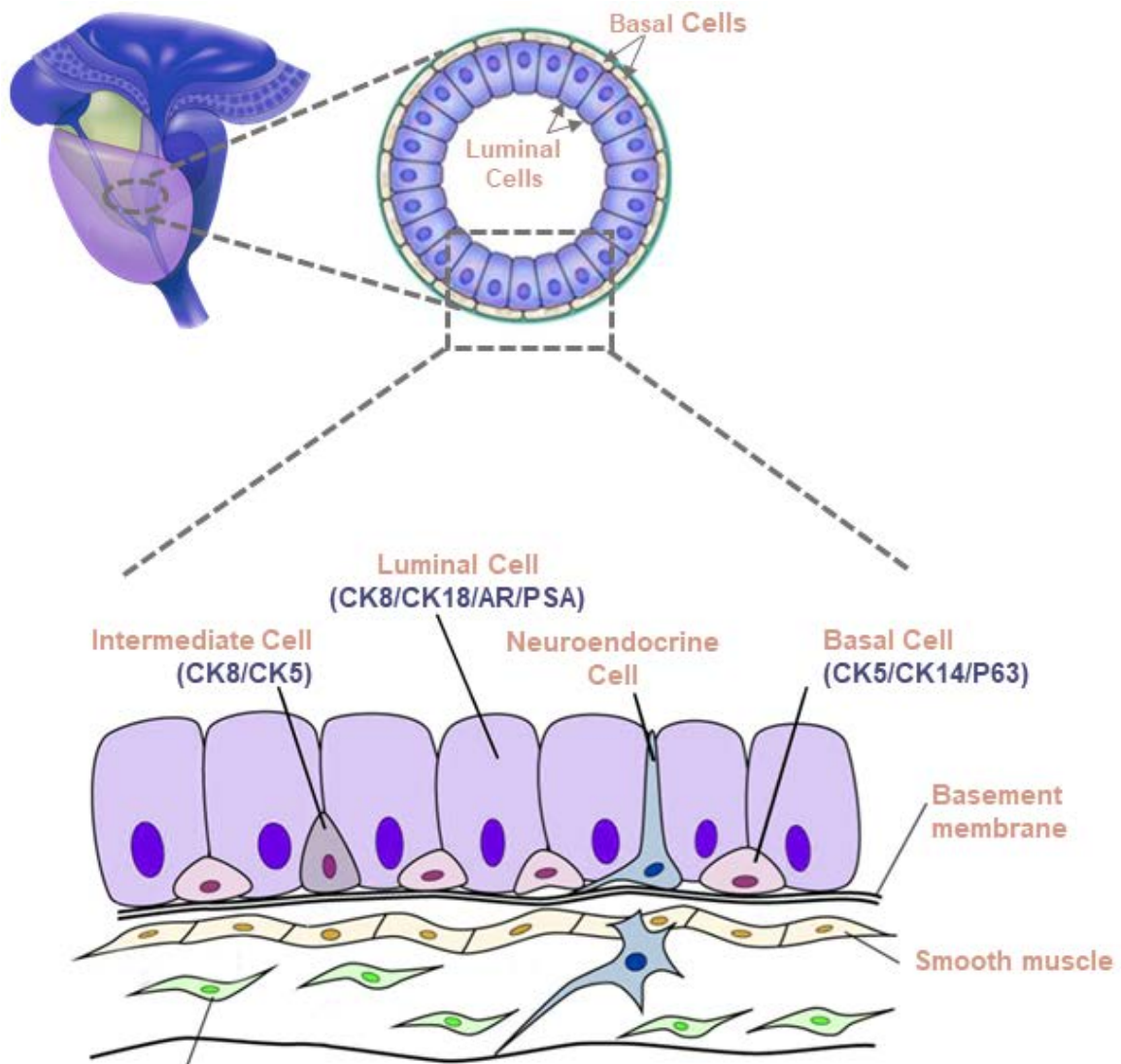
Figure 2. Prostate Histology. A schematic representation illustrating the histology of each gland or duct within the prostate where it is lined with pseudostratified epithelium with three differentiated epithelial cell types; a luminal secretory cell layer, an underlying basal cell layer; and basally localized neuroendocrine cells. Abbreviations: CK: cytokeratin, AR: Androgen receptor, and PSA: prostate specific antigen.

3. *Pathology of the Prostate*

The prostate gland can be disturbed by several benign and malignant disorders including prostatitis, BPH and PCa [10].

a. <u>Prostatitis</u>

It is a widespread urinary tract disease in men; the third after PCa and BPH [21]. It affects men of all age groups, with a prevalence of around 11–13% among adult men [22] . It can be either acute or chronic, bacterial with urinary tract infections, or non-bacterial with chronic pelvic pain, or even asymptomatic [21]. Bacterial prostatitis can induce various andrological complications and eventually provoke impaired male fertility [23]. Furthermore, prostatic inflammation might predispose for the development of BPH and PCa [24].

b. <u>Benign Prostatic Hyperplasia</u>

Benign prostatic hyperplasia (BPH) is one of the common conditions affecting approximately 70% of men over the age of 70 years [25, 26]. In BPH, the proliferation of prostatic cells increases significantly resulting in an enlarged prostate, urethral blockade, and lower urinary tract symptoms [27]. Histologically, it is defined as nodules with hyperplasia of mainly stromal cells, that take place in the transitional zone, where stromal and epithelial cells interrelate [25, 28]. BPH coexists with PCa, nonetheless it is not a premalignant lesion [29]. Despite shared risk factors, such as inflammation, BPH and PCa

demonstrate significant differences related to histology and localization in the prostate gland [30]. Moreover, wide-scale epidemiological studies have demonstrated a relationship between BPH and risk of developing PCa and PCa-related mortality, yet the causal association remains questionable [30].

4. *Histopathological Subtypes of Prostate Cancer*

Prostate cancer, unlike other epithelial tumors such as breast cancer, lacks distinct well-defined histopathological subtypes with foreseeable prognosis and therapeutic response [7]. The most common type is acinar adenocarcinoma, while other categories such as mucinous carcinoma, ductal adenocarcinoma, and signet ring cell carcinoma are infrequent [31]. In addition, the neuroendocrine subtype labels less than 2% of PCa cases and is most commonly described as treatment recurrent since it is detected mainly after prostatectomies or hormonal therapies [31, 32]. It is attributed to earlier relapse and progression to castration-resistant prostate cancer (CRPC) explained by the lack of AR expression in these cells [33]. Non-epithelial malignant neoplasms can take place infrequently in the prostate including sarcomas (mesenchymal) and lymphomas (hematolymphoid) [34].

a. Intraductal Carcinoma

It is described as intra-acinar and/or intraductal epithelial proliferation that packs acini and prostatic ducts, without loss of basal cells [34]. It typically takes place at late

stages of PCa progression and is commonly linked to high-grade and advanced stage invasive adenocarcinoma [35].

b. Invasive Adenocarcinoma

Prostatic adenocarcinoma is characterized by atypical architecture with infiltrative small glands or irregular large cribriform glands [34]. Other characteristic attributes include the loss of basal cells and nuclear atypia with prominent nuclei and nucleoli [34].

The International Society of Urological Pathology (ISUP) recently modified the gleason grading system to segregate the patterns of growth observed in prostatic adenocarcinoma as illustrated in Figure 3 [36]. The five grade groups as defined by the ISUP are as follows:

- Grade group 1 consists of individual, separated, and well-formed glands that might be crowded or infiltrative to stroma (Gleason score ≤6).

- Grade group 2 comprises mainly well formed-glands with a small constituent of poorly-defined, fused, and cribriform glands (Gleason score 3+4=7).

- Grade group 3 includes mainly poorly formed, fused, or cribriform glands with a minor constituent of well-formed glands (Gleason score 4+3=7).

- Grade group 4 contains only poorly-defined, fused, and cribriform glands, or mainly well-formed glands and a minor constituent lacking glands, or mainly lacking glands and a minor constituent of well-formed glands (Gleason score 4+4=8; 3+5=8; or 5+3=8)

- Grade group 5 lacks gland formation and consists of sheets of tumor individual cells, cords, linear arrays, and solid nests (or with necrosis) with or without poorly formed, fused, and cribriform glands (Gleason scores 9 –10).

These new categories segregate patients by pathological outcome and prognosis [37]. Several studies have demonstrated that Group 1 is associated with a low risk of progression after radical prostatectomy (RP) [38]. As for group 2 and 3, despite both having a Gleason score of 7, group 3 exhibits a more adverse pathologic stage and biochemical recurrence rates when compared with group 2 [39]. The prognosis exacerbates substantially with Gleason score 8 tumors, then the risk doubles with

Grade group 1
Closely-packed but separate, uniform and well-formed glands (Gleason score ≤6).

Grade group 2
Well formed-glands with a small constituent of poorly-defined and less uniform glands (Gleason score 3+4=7).

Grade group 3
Separate glandular units with poorly formed, fused, or cribriform glands with a minor constituent of well-formed glands (Gleason score 4+3=7).

Grade group 4
Mostly poorly formed, fused microacinar and large cribriform glands (Gleason score= 8).

Grade group 5
lacks gland formation and consists of sheets of tumor individual cells or with necrosis surrounded by papillary, cribriform glands (Gleason score= 9).

Gleason scores 9 to 10 [37].

Figure 3. The modified grading system for PCa as defined by the ISUP. Adapted and modified from Papadakis *et al.* (2016) [40].

5. *Molecular Subtypes of Prostate Cancer*

The heterogeneity of PCa on a clinical level complicates the classification of this disease into discernible subtypes. Nonetheless, during the last decade, significant advancement in grasping the molecular basis and the genomic alterations underlying PCa took place, which enabled the classification of PCa into potential distinctive molecular subtypes [41]. Based on the Cancer Genome Atlas (TCGA), most PCa cases can be categorized into two general classes; ETS positive and ETS negative [42]. The rearrangements in ETS family transcription factors (TF) include ERG, ETV1, ETV4, and FLI1 among others with common alterations in PI3K and P53 signaling pathways, while ETS-fusion negative PCa exhibits recurrent mutations in SPOP, FOXA1, and IDH1 with overexpression of SPINK1 being specific to this group [43-46].

a. ETS family members

The most frequent ETS family rearrangement, accounting for 90% of these rearrangements, is the TMPRSS2:ERG fusion; the 5′ untranslated region of *TMPRSS2* gene fuses with the ETS family of TFs, most commonly ERG and ETV [44, 47, 48]. The TMPRSS2:ERG fusion has been detected in almost 50% of PCa cases [49]. The ETS rearrangements are associated with early stages of PCa and have been frequently identified in high grade prostatic intraepithelial neoplasia [50]. Nonetheless, it seems that ERG rearrangements might be associated with increased risk of progression [51].

b. <u>Non-ETS family members</u>
  i.   <u>SPOP/CHD1</u>

SPOP encodes the substrate-binding subunit of E3 ubiquitin ligase (SPOP). It is the

most recurrent point mutation in PCa which accounts for 5-15 % of cases [52]. *SPOP*-

mutant tumors are most likely associated with early stages of PCa [53]. It is associated

with recurring somatic deletions at the *CHD1* locus: an ATP-dependent chromatin-

remodeling enzyme [53]. Interestingly, *SPOP*-mutant/*CHD1*-deleted primary PCa cases

seem to exhibit a homogenous gene expression with increased DNA methylation, and

overexpressed *SPINK1* [42].

  ii.   <u>SPINK1</u>

SPINK1 is a secreted serine peptidase inhibitor Kazal type 1 [54]. It is

overexpressed in a subset of ETS-negative cancers (including SPOP-mutant cancers),

exclusive from *ERG* rearrangements [42]. Tumors overexpressing *SPINK1* were found to

be associated with higher Gleason scores and earlier biochemical recurrence [54].

Interestingly, being an extracellular protein, SPINK1 seems to be an amenable target for

therapies and non-invasive diagnosis [41].

  iii.   <u>FOXA1</u>

Forkhead Box A1 (*FOXA1*), also known as hepatocyte nuclear factor 3α (*HNF3α*),

is a pioneering transcription factor targeting androgen signaling [42, 55]. It is essential for

normal prostate development while its overexpression can result in PCa progression [41,

56]. Beside *SPOP*-mutant cancers, *FOXA1* mutants show the highest levels of AR

11

transcriptional activity [42]. *FOXA1* mutants are found in around 4% of PCa cases including both localized PCa and CRPC [56].

6. *Initiation and Progression of Prostate Cancer*

The cancerous transformation of the prostate includes a multistep course, that starts with prostatic intraepithelial neoplasia (PIN), followed by the development of localized PCa, that acquires the ability to invade neighboring lymph nodes before metastasizing to distant sites[7].

PCa is a heterogeneous disease associated with large-scale genomic rearrangements and extensive copy number alterations involving multiple chromosomes. One of the initiating events in prostate tumorigenesis is downregulation of the homeobox gene *NKX3.1*, which is described as the "gatekeeper" for PCa initiation [52]. Indeed, this tumor suppressor gene is frequently downregulated in primary prostate tumors [7]. Several investigations have established an upsurge in *MYC* gene copy number detected before the onset at the PIN phase, at early stages and in a subset of advanced PCa [57, 58]. Chromosomal rearrangements involving the *ETS* family of transcription factors, such as *TMPRSS2-ERG* fusions, are mostly detected after initiation and not as an initial event, thus they are commonly associated with cancer progression [7, 44]. Loss of *PTEN* (phosphatase and tensin homologue) through deletion and mutation is detected in around 40% of PCa cases and correlates with a higher Gleason score, adverse prognosis, and increased metastatic potential [43]. *Pten* loss induces activation of the *AKT*–mammalian target of

rapamycin (*mTOR*) pathway primarily in castration-resistant PCa [59, 60]. The histone

methyltransferase enzyme *EZH2* is a key oncogene that is overexpressed in metastatic PCa

[61]. Other aberrations that are implicated in the emergence of androgen independence

include the Wnt signaling pathway [62].

7. *Metastatic Prostate Cancer*

Metastasis is the leading cause of PCa-associated deaths [63]. Metastatic PCa

exhibits a five-year survival rate of less than 30% in comparison with the 100 % five-year

survival for organ-confined tumors [64]. The primary site of PCa invasion are the adjacent

lymph nodes, which is detected in around 10% of PCa patients with organ-restricted disease

[65, 66]. Patients with lymph node metastases demonstrate a poor prognosis with increased

biochemical recurrence [66]. PCa distant metastasis involves most frequently bones

followed by lungs, liver, pleura, and adrenals [63, 67]. Most patients with advanced disease

will suffer from incurable bone metastases, where around 90% of patients who die of PCa

have metastatic disease to bone [68]. Moreover, PCa metastasis to bone is often manifested

as osteoblastic lesions resulting in debilitating symptoms such as severe pain,

hypercalcemia, recurrent fractures, and eventually death [67, 69].

a. Androgen Deprivation and the Emergence of Castration Resistance

A fundamental characteristic of PCa is being hormone-dependent. In 1941, this

feature was initially demonstrated by showing that castration can induce PCa regression

[70]. Moreover, advanced disease is associated with aberrations in androgen signaling

pathway and the standard of care for PCa is androgen deprivation therapy (ADT) [68]. Alas, ADT does not represent a curative option, and most tumors eventually recur and develop resistance to this therapy [71]. This deterioration in the context of deprived testosterone serum levels is referred to as castration resistance which remains lethal despite recently developed drugs [68]. The molecular mechanisms triggering castration resistance are mostly associated with the transcriptional activity of the androgen receptor (AR) [62]. During normal development of the prostate gland and early-stage PCa, cell survival relies principally on AR signaling [72]. The active hormone dihydrotestosterone (DHT) binds to AR and activates its translocation to the nucleus where it triggers the transcription of genes involved in cell survival and proliferation [72]. Despite the importance of androgens for the survival of prostate cells, these cells acquire the ability to bypass androgen ablation therapy through various mechanisms that include amplification or mutations affecting the AR. This amplification is detected in around a third of men with CRPC while it is nonexistent in hormone-dependent PCa [73]. Androgen independence can also be acquired through other survival pathways independent of AR such as neuroendocrine differentiation and deactivation of apoptotic genes [74].

b. Epithelial-Mesenchymal Transition

The epithelial-mesenchymal transition (EMT) is a crucial cellular mechanism that directs morphogenesis during normal embryonic development [75]. This process also predominates during disease progression, particularly in fibrosis and cancer metastasis [75, 76]. During EMT, epithelial cells lose their adhesion molecules and gain a motile

14

mesenchymal phenotype [77]. Particularly, EMT is characterized by loss of E-cadherin and decreased expression of cytokeratins and tight junctions, such as zona occludens and occludin, complemented with an increase in mesenchymal markers such as vimentin and N-cadherin [78]. This shift in cytoskeletal dynamics results in loss of polarized sheets of epithelium and breakdown of cell-to-cell or cell-to-extracellular matrix (ECM) adhesions prompting the development of spindle shaped mesenchymal cells capable of invading the ECM [79, 80].

This essential developmental process plays an ominous role during tumor progression where the expression of EMT markers represents a crucial step in the malignant progression of several cancers, such as prostate, breast, ovarian, and colon cancers [79, 81-84]. The role of EMT in PCa metastasis has been studied [80] revealing significant interplay between EMT-related genes and alterations in signaling pathways involved in prostate organogenesis such as transforming growth factor-beta (TGF-β) [85], IL-6 [86-88], AR variants [89, 90], fibroblast growth factor (FGF) [91], and Wnt/β-catenin [92-94].

Indeed, EMT takes place during the progression of PCa from a primary stage to an advanced and metastatic castration-resistant PCa (mCRPC) where it endorses the invasiveness of PCa cells due to increased mobility and migratory ability [80]. In addition to the role of EMT in PCa progression, it has been identified as playing a substantial role in PCa therapeutic resistance to anti-androgens and radiotherapy [95]. Therefore, it has been postulated that targeting EMT may improve the overall survival of patients with PCa [80].

In a previous study, we have reported increased co-expression of epithelial CK8 and mesenchymal vimentin (VIM) markers in androgen-independent PLum-AI murine PCa cell lines, which represent advanced stages of PCa, when compared with androgen-dependent PLum-AD cells which represent primary PCa [96]. CK8/Vim co-expression was also reported in other murine PCa cell lines, including PLum-P and PLum-C *Pten-/- TP53-/-* murine prostate epithelial progenitor cells [97].
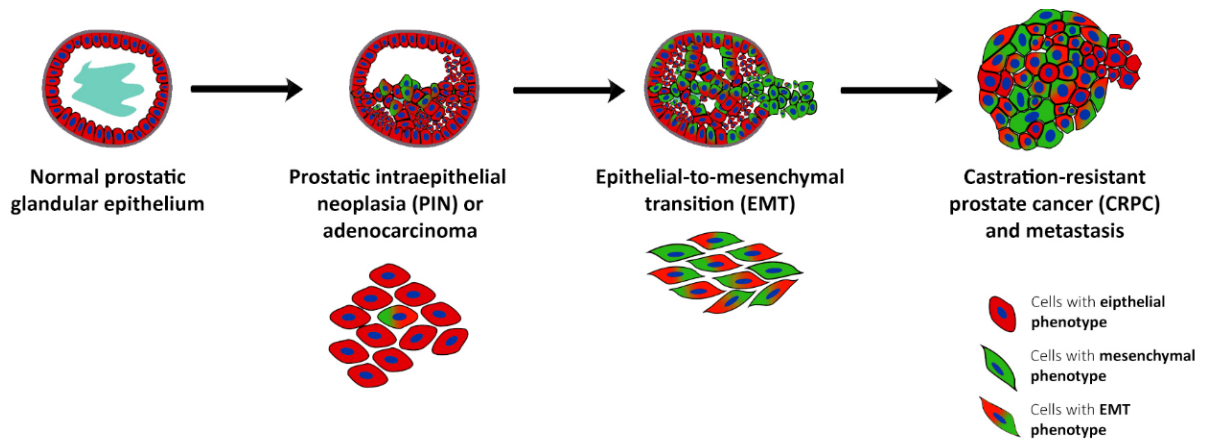
Figure 4. Schematic diagram illustrating the epithelial-mesenchymal transition that takes place during the progression from normal prostate to castration-resistant prostate cancer.

8. *Treatment of Prostate Cancer*

a. Treatment of Localized PCa

Localized PCa, which is depicted with no discernable lymph nodes or distant metastases, exhibits different therapeutic approaches depending on the disease stage and

clinical manifestations [98]. These include expectant management with either active surveillance where monitoring the progression is followed up through PSA testing and physical examinations, or watchful waiting where the symptoms are treated [99]. For more advanced disease, when PSA level is higher than 10 ng/mL or when nodules are detected on digital rectal examination, radical prostatectomy (RP) and radiation remain the therapy of choice [98].

b. Treatment for Metastatic Prostate Cancer

Androgen deprivation therapy (ADT) remains the standard treatment for metastatic PCa [64]. ADT includes AR antagonists that block this receptor by competitive inhibition [100]. The developed compounds include first-generation agents such as bicalutamide which provides limited efficiency and enhanced second-generation agents such as enzalutamide which provide higher binding efficiency to AR and blockade of its nuclear translocation and DNA binding [101]. Abiraterone exhibits another approach in ADT which inhibits testosterone biosynthesis in prostatic tissue, adrenal glands and testes [102]. Nonetheless, this therapy has been associated with resistance and recurrence of PCa, as well as toxicity and adverse effects such as sexual dysfunction and reduced bone density [98, 103]. Despite a high initial response rate, hormone sensitive PCa becomes unresponsive in most patients where it is hypothesized that ADT exerts a clonal selection and allows androgen- independent cells to thrive [104, 105]. Moreover, it was shown that chemotherapy can extend survival and delay the castration-resistance when compared with ADT alone [106]. Consequently, taxanes such as docetaxel and cabazitaxel are approved

therapies for CRPC and bone metastases [106]. Other therapies with evidence of reduced

mortality among men with metastatic CRPC include immunotherapeutic vaccine

sipuleucel-T, and bone-selective radium-223 [107, 108].

B. Two-dimensional Models of Prostate Cancer

1. *Prostate Cancer Cell Lines*

a. Advantages and Limitations

Ever since the HeLa cell line was successfully developed, cancer cell lines have

been essential to understand tumorigenesis as well as to predict therapeutic response and

resistance mechanisms. Currently, there are ~1,500 cancer cell lines available worldwide

[109]. These cell lines embody the backbone of tumor biology and allow drug discovery

through feasible experimental manipulation, general and detailed mechanistic studies, and

numerous high-throughput applications [110]. Indeed, the Cancer Cell Line Encyclopedia

(CCLE) represents a combination of gene expression, chromosomal copy number and

parallel sequencing data from 947 human cancer cell lines [110]. This CCLE allowed the

combination of genomic profiles with pharmacological profiles for several anticancer drugs

and enabled the identification of lineage and gene-expression-based predictors of drug

sensitivity and resistance [111-115].

In vitro cancer cell lines provide several advantages including, first, unlimited

growth; second, minimal medium requirements; third, docility to high throughput screening

[113, 116]. Nonetheless, it remains problematic to translate cancer genomic data into

knowledge of tumor biology and therapeutic promises. In this challenge, the currently

available 2D cell lines have numerous limitations. Foremost, most cancer types generate

cell lines with low efficiency, and only a limited number of cancer type subsets have

available established cell lines. This selection process results in cancer cell lines that

underrepresent tumor types and do not recapitulate the diversity of human cancer [116].

Second, continuous passaging and adaptation to *in vitro* culture conditions generally leads

to loss of heterogeneity and changes in gene expression profiles, by epigenetic or genetic

mechanisms [117, 118]. Third, most currently available cell lines were established at a time

when germline DNA and clinical annotation was unattainable, which confounds the

connection with patient disease progression and treatment profiles [109]. Fourth, a large

repertoire of cell lines is needed to study each specific lineage and capture the diversity of

genetic alterations and their effect on drug sensitivity [116]. Other drawbacks of cell lines

comprise the scarcity of control cell lines derived from normal tissue as reference and the

absence of stromal constituents [119].

    b.   <u>Available Cell Lines of Prostate Cancer</u>

Prostate cancer (PCa) exemplifies the most extreme example of cancer types with a

very limited number of available cell lines [109]. Despite its prevalence, PCa has proven

problematic to establish as cell lines in culture and is highly underrepresented with only 7

cell lines in public repositories [120-125]. Moreover, the available human PCa cell lines

grow independently of AR signaling, which makes them poor models for the assessment of

PCa pathogenesis and therapy response [126, 127]. From 1970 to the present, a large

number of human prostate cell lines have been designated and employed in research, but turned out to be either derivatives of previously established cell lines, or were contaminated with HeLa or T24 bladder carcinoma cell lines [128, 129]. The three "classical" prostate carcinoma cell lines include DU 145, LNCaP, and PC3, and were all established from metastatic lesions [130]. PC3 cell line was derived from poorly-differentiated, highly aggressive, metastatic to bone, human prostatic adenocarcinoma [121]. DU 145 represents moderately aggressive, metastatic to bone, human prostate adenocarcinoma [131]. Both DU-145 and PC-3 cell lines are unresponsive to androgens and lack PSA expression [130]. LNCaP cell line was established from human prostatic, relatively indolent, metastatic to lymph node lesion of adenocarcinoma [120]. In contrast to PC3 and DU 145, LNCaP cells express AR and PSA and show an androgen-dependent behavior [130]. In addition, other non-classical cell lines include 22rv1 that was derived from a human prostatic carcinoma xenograft and expresses both AR and PSA [124].

The heterogeneity of PCa remains a challenge when developing representative models. Indeed, prostate tumorigenesis and progression have been recently designated in a catalog of numerous genetic lesions, many of which remain not denoted in currently available models [132]. To add to these challenges, in CRPC, the selection pressure exerted by therapies results in increased heterogeneity, that would require a large repository of cell lines to represent the numerous mechanisms of resistance [56].

C. Three-Dimensional Modeling of Prostate Cancer

1. *A Brief History of Three-Dimensional Cultures*

The original use of "three-dimensional structures" in culture dates to 1989, where Barcellos-Hoff *et al.* (1989) described the reorganization of cells into the exogenous matrix-embedded 3D structures [133]. Consequently, and prior to 2005, the term "organoid" was used to refer to all 3D cultures. Specifically, it was used to describe the organ-like structures formed in various types of 3D gels after enzymatic and mechanical digestion of small tissue fragments, typically epithelial tissues [134]. The last 10 years observed the return of the "organoid", after the development of intestinal organoid culture in 2009, which was considered a breakthrough in the stem cell field. The novelty in this method was employing endogenous stem cell niche components to create a stable, long term, near-physiological culture system. This culture system was the outcome of various crucial discoveries starting as early as 1998 when the role of Wnt signaling in maintaining stem cells of murine small intestine was outlined [135]. Afterwards, the Wnt target gene leucine-rich repeat-containing G-protein-coupled receptor 5 (*Lgr5*) was delineated as an indicator of stemness in the small intestine and colon, followed by the observation that R-spondin, an Lgr5 ligand, elicits crypt hyperplasia [136, 137]. All these discoveries highlighted the boundless ability of intestinal stem cells to proliferate and regenerate in vivo, which was translated in vitro by the establishment of a culture system that allows

expansion of intestinal stem cells and conserves the architecture of the intestine [138]. This system enabled the unlimited 3D proliferation of organoids including all cell types of the intestinal epithelium with differentiated crypt and villus compartments [138].

2. *Defining Organoids*

Lately, the definition of "organoids system" expanded to include various cell culture techniques. As defined by Shamir and Ewald (2014), the term organoids can refer to "primary explants of epithelial ducts into 3D extracellular matrix (ECM) gels, clonal derivatives of primary epithelial stem cells that are grown without mesenchyme, or epithelial–mesenchymal co-cultures that are derived from embryonic stem cells or induced pluripotent stem cells" [139]. Lancaster and Knoblich (2014) defines an organoid as a structure "containing several cell types that develop from stem cells or organ progenitors and self-organize through cell sorting and spatially restricted lineage commitment, similar to the process in vivo" [140]. A similar definition was iterated by Clevers (2016) where he defines an organoid as "a 3D structure grown from stem cells and consisting of organ-specific cell types that self-organizes through cell sorting and spatially restricted lineage commitment" [141]. A more elaborate definition was stated by Fatehullah et al. (2016) where they define an organoid "as an in vitro 3D cellular cluster derived exclusively from primary tissue, embryonic stem cells, or induced pluripotent stem cells, capable of self-renewal and self-organization, and exhibiting similar organ functionality as the tissue of origin" [142]. All these delineations agree on defining an organoid as an in vitro 3D cluster

of stem cells capable of recapitulating the architecture and functionality of the in vivo tissue of origin. This culture system exploits the unlimited growth potential of stem cells; whether embryonic stem cells or induced pluripotent stem cells, or organ restricted adult stem cells [141]. This promising technology has the potential to bridge the traditional 2D in vitro models and in vivo models, with boundless potential for clinical relevance particularly in cancer research [119].

3. *Organoids as Disease Models*

Organoids are rapidly emerging as an effective tool to investigate both basic developmental processes and disease mechanisms [119]. Interestingly, this near-physiological 3D model can be used to define a vast range of biological processes including tissue renewal, stem cell/niche functions, drug and genetic screening [142]. In addition, it can enhance our ability to understand the molecular mechanisms leading to a specific disease, identify potential biomarkers, and optimally develop personalized platforms for drug testing [119].

Currently, organoids are being established from a variety of organs , including the colon, stomach, prostate, kidney, liver, pancreas, thyroid, inner ear, retina, pituitary gland and brain [127, 136, 143-154]. Colorectal cancer is taking the lead and intestinal organoids are being extensively exploited in understanding stem cell behavior, gene editing and disease modeling [138, 155, 156]. An organoid biobank was established from 20 patients with genetically diverse colorectal cancer with their matched normal tissue-derived

organoids [157]. These patient-derived organoids showed reproducible and differential responses to preclinical and clinical compounds: for instance tumor organoids carrying a specific mutation in the Wnt regulator *RNF43* showed extreme sensitivity to Wnt inhibitors demonstrating that organoids can help us identify specific gene-drug associations [157].

The ability to grow unaffected and diseased organoids from patients enables clinical screens for drug combinations that selectively target the diseased tissue, and identify more effective therapies with minimal side effects [142]. Cystic fibrosis patient-derived organoids confirmed that this in vitro model can be used to successfully predict the likelihood for patients carrying rare mutations to benefit from a specific therapy. The authors demonstrated a positive correlation between in vitro therapeutic responses in rectal organoids and clinical results [158].

A large biobank of breast cancer organoids was derived from more than 100 patients recapitulating most breast cancer subtypes [159] . This biobank demonstrated that organoids can preserve the histopathological and genetic attributes of the tissue of origin, where most of the patient-derived organoids maintained the expression of specific breast cancer biomarkers including estrogen and progesterone receptors [159]. In addition, this study provided an evidence about the correlation between HER2 status and sensitivity of organoids to drugs targeting the HER signaling pathway [159].

In a study employing murine and human pancreatic cancer organoids, it was shown that organoids represent an achievable platform to unravel novel genes and pathways associated with disease development [160]. Herein, they demonstrate that neoplastic

organoids, when transplanted orthotopically, can recapitulate the full range of tumor

progression by establishing early-grade neoplasms capable of progressing into metastatic

carcinomas [160].

Cerebral organoids derived from human iPSCs delineated specific mechanisms that

drive congenital microcephaly disorders [153]. Brain organoids were further utilized to

show that neural progenitor cells impact migration abnormalities and surface folding with

PTEN deletion [161]. Cerebral organoids were taken a step further to demonstrate a

possible causal connection between the Zika virus and microcephaly where infection with

this virus led to impairment of cortical growth and folding in organoids [161]. Human-

derived iPSC organoid models provide the distinctive potential to assess mechanisms of

cortical malformation syndromes, including outer radial glial dysfunction and migration

abnormalities [162]. Using cerebral organoids, Bershteyn et al. extended our understanding

of a severe cortical malformation syndrome, Miller-Dieker syndrome, through identifying a

mitotic defect in a neural progenitor cell type essential for human neocortical development

but deficient from rodent models [163].

4. *Organoids as Models for Prostate Cancer*

The attempt to culture human prostate tissues Ex-vivo dates back to the 1970s

following the derivation of mouse prostate cell lines [164]. Although various culture

methods have been introduced, the culture of human PCa tissues remains challenging [165].

Luckily, in 2014, Karthaus *et al. and* Gao *et al.* adapted the organoids culture method to

PCa and described an Rspondin1-based 3D culture method through which normal human

and murine prostate epithelial cells can be cultured indefinitely without genetic manipulation, in a 3D system that models prostate glandular structure [116, 166]. This system has been optimized for human metastatic prostate specimens to generate new lines that express previously-identified common genetic alterations seen in advanced PCa [116, 167]. The culture media employed in this system was considered a leap forward since it allows highly efficacious and unlimited growth of both normal and tumor prostate cells without the need for genetic alterations [166, 167].

Until now, prostate organoids were successfully derived from PCa patients specimens [146, 168, 169], from PCa cell lines [170-172], and from transformed primary normal prostate cells [171, 173]. In 2014, Gao *et al.* reported the successful generation of fully-characterized organoid lines from 6 metastatic tissue biopsies and one circulating tumor cells specimen [116]. The methodology adapted by this group provided a success percentage of 20% and maintenance in culture for only 1-2 months [116]. Furthermore, PCa organoids demonstrated their potential use in personalized drug treatments [119]. Patient-derived organoids harboring AR amplification were more sensitive to the anti-androgen enzalutamide than AR-negative PCa organoids [116]. In the same issue, an accompanying manuscript was published describing the development of a methodology that maintains murine and human benign prostate organoids for a long period of time with verified preserved morphologies and genetics over 7 generations [166]. In 2016, a culture protocol was described by the same group as the sole method that maintains the growth of both the luminal and basal prostatic epithelial lineages [146].

Later, Puca *et al* reported the derivation of tumor organoids from metastatic lesions of 4 patients focusing on the neuroendocrine phenotype of PCa [168]. Beshiri *et al.* established organoids using 20 models from the LuCaP mCRPC Patient-derived Xenografts (PDX) cohort, comprising adenocarcinoma and neuroendocrine subtypes [170]. They show conserved genomic heterogeneity between the PDXs and organoids that provides a platform to investigate responses to therapies; specifically, the cytotoxicity to PARP inhibitor olaparib in $BRCA2^{-/-}$ organoids reflected the patients' response in the clinic [170]. However, the long-term maintenance in culture of PDX-derived organoids could not be demonstrated [170].

More recently, the addition of stromal cells in the protocol described by Richards *et al*. increased formation efficiency and viability of human 3D prostate organoids in a co-culture system [169]. This model demonstrated the ability to further optimize the organoids culture system to incorporate additional components that recapitulate the tissue of origin more faithfully.

a. Understanding the Prostate Organoids protocol

i. General requirements of organoids culture

Notably, organoid technology is adaptable where cultures can commence from small tissue samples, typically biopsy or surgical specimens, without the need for stem cell purification [174]. The Matrigel constituent is used to substitute the extracellular matrix, and the medium is supplemented with specific growth factor cocktails that mimic the

endogenous stem cell niches. This combination allows stem cells to differentiate and self-organize into structures that resemble native tissue architecture [142].

The Matrigel component represents an ex-vivo basement membrane alternative that is essential to enable the 3D architecture of organoids [119]. This gelatin-line protein mix is secreted by Engelbreth-Holm-Swarm (EHS) murine sarcoma cells [175]. The major components include adhesive proteins such as laminin, collagen, entactin and heparan sulfate proteoglycans, which resembles the extracellular matrix in various tissues [176].

In general, organoids derived from different tissues are cultured under serum free-conditions in a medium that includes various growth factors and small molecule inhibitors [177]. There are minor differences between various tissue types but in general they include most of the following components: epidermal growth factor, fibroblast growth factor (FGF) 7 and 10, hepatocyte growth factor, bone morphogenetic protein (BMP) inhibitor (Noggin), a WNT agonist and ligand of LGR5 (R-spondin-1), a mitogen (prostaglandin E2), nicotinamide , N-acetylcysteine, a Rho kinase inhibitor (Y27632), a TGF-β inhibitor (A-83-01), and a p38 MAPK inhibitor (SB202190) [177].

ii.   Requirements of Prostate organoids culture

The prostate organoids culture system includes the following components:

- B27 is a serum-free supplement that was originally developed with defined components to support the growth of nerve tissue [178, 179].

- Epithelial growth factor (EGF) is a fundamental growth factor for epithelial tissues [180]. It binds to its receptor EGFR and activates the RAS/ERK MAP kinase and PI3K/Akt signaling pathways which results in increased cell proliferation in the epithelium [181, 182]. In addition, EGF plays a substantial role in stimulating cell motility and migration of epithelial cells from various tumors including PCa [183, 184].

- FGF signaling plays a crucial role in maintaining the stemness of prostate cells [185], thus its importance in the enhanced maintenance of organoids in culture. For instance, FGF 10 is a highly expressed growth factor in the mesenchyme of a developing prostate gland, while its deletion was shown to impede branching morphogenesis [186]. FGFs are essential for the development and maintenance of the normal prostate, nonetheless, they endorse tumor growth through their mitotic and angiogenic properties [187]. FGF 2 or basic fibroblast growth factor performs a substantial role in prostate carcinogenesis and is associated with adverse clinic-pathological characteristics in PCa [188]. FGF 2, as well as other FGFs, can induce metalloproteinases, thus facilitate invasion and metastatasis of various tumor types including PCa [187].

- The R-spondins belong to the superfamily of thrombospondin type 1 repeat-containing proteins [189]. They are agonists of the canonical Wnt/β-catenin signaling pathway, where R-spondin binds to its receptor leucine-rich repeat-containing G-protein-coupled receptor (Lgr5) and activates the Wnt pathway [190]. Since Lgr5 is a known marker of adult stem cells, R-spondins are considered potent

activators of adult stem cell proliferation [189]. The Wnt∕β-catenin pathway is essential to maintain intestinal crypt homeostasis and R-spondin 1 was delineated as an essential component to grow intestinal epithelial organoids [138].

- Noggin, the BMP antagonist, is essential for stem cell expansion and plays a critical role during prostate development by counteracting BMP-4 inhibitory effect on cell proliferation [142, 191].

- TGF-β signaling blocks proliferation of prostate cells and embodies a defense mechanism that suppresses tumorigenesis in various cancer types [192-194]. A83-01, the Alk3/4/5 inhibitor, plays a substantial role to relieve the growth barrier and enhance the organoids growth by obstructing the TGF-β signaling pathway.

- The substantial function of p38 MAPK signaling pathway in PCa was highlighted in various studies [195, 196]. The activation of this pathway has been related to EMT in primary tumors and consequently invasion, migration and metastasis [197, 198]. On the contrary, the inhibition of p38 MAPK can block anoikis which enables circulating cancerous cells to survive [199]. Consequently, the p38 MAPK inhibitor SB202190 was included as a requirement for the long-term culture of organoids [143]. Nonetheless, it was recently shown that this component might not be essential for all CRC-derived organoids and its removal showed increased efficiency [200].

- Prostaglandin-E2 (PGE2) belongs to the family of proinflammatory eicosanoids which perform substantial roles in inflammatory reactions [201]. In addition, PGE2 has been connected to a large number of disorders including cancer where it

can contribute to tumorigenesis through activating cell proliferation [202], angiogenesis [203] and metastasis [204].

- Nicotinamide is the amide form of niacin, which belong to the vitamin B3 family [205]. It has been commonly employed to target disorders such as diabetes, Alzheimer's disease, and cancer [206-208]. Nicotinamide was also shown to expand adult stem cells derived from various tissues including pancreas and colon [147, 209]. Furthermore, it can enhance cell survival by inhibiting the Rho-associated protein kinase (ROCK) [205].

- N-acetylcysteine (NAC) is a synthetic precursor of the amino acid cysteine that is crucial in the synthesis of glutathione, consequently it plays a substantial role as an antioxidant and inhibitor of reactive oxygen species (ROS)-dependent apoptosis [210-212]. Moreover, NAC is frequently used in different clinical situations including chronic obstructive pulmonary disorder and neurological conditions such as Alzheimer and epilepsy [210, 213].

- ROCK inhibitor (RI) plays a substantial role in enhancing the survival of stem/progenitor cells with an epithelial phenotype by blocking the dissociation-induced Rho/ROCK-mediated apoptosis [214]. Subsequently, it is primarily critical during and after tissue digestion, organoids dissociation for propagation, and primary cells splitting in culture.

b. Limitations of the Organoids Culture System

Despite the huge potential of the organoid technology, it is essential to understand its limitations. First, when compared with the 2D system, organoid culture is more laborious, time consuming and costly [119]. Second, this methodology employs undefined factors such as Matrigel as ECM substitute. Third, organoid culture systems fail at faithfully recapitulating the in vivo microenvironment since they do not include stromal, immune or endothelial cells [215].

Moreover, five years after the development of PCa organoids protocol, it remains a challenge to culture prostate organoids with a high success rate, where only a very limited number of publications report the successful establishment of patient derived organoids from PCa patients specimens [146, 168, 169], from PCa cell lines [170-172], or from transformed primary normal prostate cells [171, 173]. The reported success percentage does not exceed 20% of samples while the long-term maintenance is variable and limited [116].

D. Aims

The overall aim of this dissertation is to establish novel models to elucidate the mechanisms of prostate cancer progression. We hypothesized that the epithelial-mesenchymal transition status can model the progression status of the disease and predict the prognosis/recurrence; and fresh tissue specimens from treatment-naïve cohort can be employed to establish 3D patient-derived organoids as an in vitro model of drug response

and genomic landscape. Altogether, this will lead to better understanding of PCa etiology and might lead to better management of the disease.

- **Specific aim 1:** To develop a novel scoring system to quantify EMT expression in patients with locally-advanced PCa using the radical prostatectomy institutional database (1998-2016) of the American University of Beirut Medical Center (AUBMC), then explore the correlation between this score and the different clinicopathological outcomes.

- **Specific aim 2:** To establish and characterize the culture system of PCa organoids derived from fresh tissues obtained from consented treatment-naïve patients undergoing radical prostatectomies at AUB-MC.

  - *Sub-aim 1*: To examine the efficiency of the organoids culture system by assessing the organoids growth (% success rate), quantifying the number of organoids forming count (OFC), calculating the average size (diameters), and evaluating the maintenance time in culture (number of generations/ days).

  - *Sub-aim 2*: To characterize the organoids formed by assessing the expression of prostate epithelial lineage and stem cell markers using immunofluorescence, immunohistochemistry and RT-PCR.

  - *Sub-aim 3*: To investigate the validity of the organoids culture system as a model for personalized treatment of PCa by assessing the effect of classical therapies on organoids derived from unaffected vs. tumor tissue from the same patient, as well as the differences between various patients.

33

- **Specific aim 3:** To enhance the previously established extensive organoids culture system in the attempt to increase the formation efficiency and minimize the costly requirements.

- **Specific aim 4:** To generate novel patient-derived cell lines from the 3D organoids representing unaffected and tumor prostate tissues.
    - *Sub-aim 1*: To examine the efficiency of the novel cell lines derivation by assessing their maintenance time in culture (number of passages).
    - *Sub-aim 2*: To characterize the cell lines formed by assessing the expression of prostate epithelial lineage and stem cell markers using immunofluorescence and RT-PCR.
    - *Sub-aim 3*: To optimize the requirements needed to maintain primary prostate epithelial cells in culture.

CHAPTER II

MATERIALS AND METHODS

A. Experimental Methods

1. *Patients Selection*

The study with all its experimental protocols was conducted under the Institutional Review Board (IRB) approvals of the American University of Beirut (AUB) and American University of Beirut Medical Center (AUBMC). The work described herein has been carried out in accordance with relevant guidelines and regulations, and in agreement with The Code of Ethics of the World Medical Association (Declaration of Helsinki) for experiments involving human subjects.

Retrospectively, using the radical prostatectomy institutional database (1998-2016) of the AUBMC, 122 patients were identified with locally-advanced PCa. Those patients had adverse pathological features with more than 30 months of follow-up.

Prospectively, fresh tissue samples from distinct stages of human prostate adenocarcinomas were obtained from consented patients undergoing RP at AUBMC. If a consented patient was undergoing any prostate surgery, a primary sample was collected only if it does not compromise the sample for diagnosis or staging. For RP specimens, a core biopsy was taken from the area most likely to be involved with cancer and another

core biopsy from the unaffected area according to a pathologist recommendation guided by imaging reports of the prostate.

2. Antibodies and Reagents

Antibodies used in this study were as follows: mouse monoclonal anti-CK8 (1/200 dilution; Biolegend), rabbit polyclonal anti-CK5 (1/200 dilution; Covance, CA), rabbit polyclonal anti-CK14 (1/200 dilution; Santa Cruz Biotechnology, CA), mouse monoclonal anti-CD44 (1/50 dilution; Santa Cruz Biotechnology, CA), rat monoclonal anti-CD49f (1/50 dilution; BD pharmingen), rabbit monoclonal anti-AR (1/50 dilution) (Abcam), mouse monoclonal anti-Sox2 (1/50 dilution) (Santa Cruz Biotechnology, CA), rabbit polyclonal anti-Vim (1/50 dilution) (Santa Cruz Biotechnology, CA), rabbit monoclonal anti-AR (1/50 dilution) (Abcam), anti-PSA (1/200 dilution) (Abcam), mouse monoclonal P63 (Bond^{TM}), and rabbit monoclonal anti-AMACR (BioGenex), Alexa 568 goat anti   mouse (Life Technologies), Alexa 488 goat anti-rabbit (Invitrogen, CA), and Alexa 488 goat anti-rat (Life Technologies). All secondary Alexa Fluor antibodies were used at 1/200 dilution. Fluoro-gel II with DAPI (Electron Microscopy Sciences, PA) was used for mounting.

Reagents used were as follows: Triton X-100 (Biorad, cat. no. 1610407), Bovine Serum Albumin (BSA; Amresco, cat. no. 0332), Normal Goat Serum (NGS; Invitrogen, cat. no.16210064), Fetal Bovine Serum (FBS; Sigma, cat. no. F9665), Tween-20 (Amresco, cat. no. 0777), ImmPACT diaminobenzidine (DAB) Horseradish Peroxidase (HRP) substrate (cat. no. SK-4105), TRIZOL Reagent (Ambion, cat. no. 15596018),

paraformaldehyde (PFA), Dimethyl sulfoxide (DMSO; Scharlau), MTT (Sigma-Aldrich, cat. no. M5655), Collagenase Type II (Life Technologies, cat. no. 17101-015), TrypLE Express (Life Technologies, cat. no. 12605-010), Advanced DMEM/F12 (adDMEM/F12; Life Technologies, cat. no. 12634-034), GlutaMAX 100× (Life Technologies, cat. no. 35050-038), Penicillin-streptomycin (Biowest, cat. no. L0022-100), Plasmocin Prophylactic (Invivogen, ANT-MPP), Hepes (Life Technologies, cat. no. 15630-056), Phosphate buffered saline (Sigma, cat. no. D8537), Matrigel^{TM} Growth Factor Reduced (Corning, cat. no. 354230), Histogel (Thermo-Scientific), B27 supplement 50x (Life Technologies, cat. no. 17504-044), Nicotinamide (Sigma-Aldrich, cat. no. N0636), N-acetylcysteine (Sigma-Aldrich, cat. no. A9165), A83-01 (Tocris Bioscience, cat. no. 2939), Y-27632 (ROCK Inhibitor; RI) (Santacruz, cat. no. sc-281642A), Human FGF10 (PeproTech, cat. no. 100-26), Recombinant human Noggin (Peprotech, cat. no. 120-10C), Recombinant human R-spondin (Peprotech, cat. no. 120-38), Prostaglandin E2 (Tocris Bioscience, cat. no. 2296), SB202190 (Sigma-Aldrich, cat. no. S7076), (DiHydro)Testosterone (DHT; 5α-Androstan-17β-ol-3-one) (Sigma-Aldrich, cat. no. A8380), Recombinant Human FGF-basic (Gibco, PHG0261), Human EGF (R&D systems, cat. no. 236-EG).

3. *Clinicopathological Variables*

Preoperative serum PSA level, Gleason group, pathological stage, positive surgical margin (PSM), perineural invasion (PNI), seminal vesicle invasion (SVI), lymphovascular invasion (LVI), and tumor volume in the PCa specimens were recorded.

4. *Tissue Sampling and Gleason Scoring and Grouping*

The tumor tissues were harvested and fixed in 4% formalin overnight, rinsed well in PBS and transferred to 70% ethanol before standard processing to obtain paraffin-embedded sections. The tumor grade and clinical stage were reviewed, and the Gleason scores were assigned by two independent pathologists according to the International Society of Urological Pathology (ISUP) criteria. This new five–grade group system has been suggested by the ISUP and accepted by the WHO (World Health Organization) in 2016, in order to address the deficiencies in the previous gleason scoring systems [216]. In this system, grade group 1 includes Gleason score ≤6, grade group 2 comprises Gleason score 7(3+4), grade group 3 includes Gleason score 7(4+3), grade group 4 includes Gleason score 8, while grade group 5 consists of Gleason scores 9 and 10 [36]. The sections were immunostained and analyzed for CK8/Vim co-expression, and the EMT score was then compared between three different Gleason groups that we assigned: category A (grade groups 1 and 2); category B (grade group 3); and category C (grade groups 4 and 5).

5. *IF evaluation of tissue sections and EMT scoring*

Using a 40× objective and a Carl Zeiss Axio Observer.Z1 epifluorescent microscope, the number of glands presenting CK8/VIM double staining (double positive immunoreactivity) was manually quantified by counting the number of glands with at least one cell that is co-expressing CK8/VIM, and all numbers were plotted as percentages out of

the total number of glands counted per tissue section. This percentage is referred to as EMT score. CK8/VIM staining was graded as double positive only when cytoplasmic staining was detectable.

6. Human Prostate Growth Medium Components

The "Human prostate growth medium" included advanced DMEM/F12 containing penicillin/streptomycin, 10mM HEPES and 2mM GlutaMAX, in addition the factors specified in the table below were added fresh on a weekly basis. RI was added fresh to the culture medium on the same day medium is changed for the first week after plating.

Table 1. Overview of specific components and their respective concentrations added to prepare human prostate organoids culture medium. Adopted and modified from Drost *et al.* [146].

Component	Stock concentration	Solvent	Final concentration
B27	50X	-	1X
Nicotinamide	1M	PBS	10mM
NAC	500 mM	PBS	1.25 mM
EGF	500 µg/mL*	PBS	10 ng/mL*
A83	5 mM	DMSO	500 nM
NOG	100 µg/mL*	PBS + 0.1% BSA*	50 ng/mL*
RSPO	500 µg/mL*	PBS + 0.1% BSA*	250 ng/mL*
DHT	10 µM	Ethanol	1 nM
FGF2	100 µg/mL*	PBS + 0.1% BSA*	6 ng/mL*
FGF10	0.1 mg/mL	PBS + 0.1% BSA	10 ng/mL
PGE2	10 mM	DMSO	1 µM
SB	10 mM	DMSO	10 µM
RI	10 mM	PBS + 0.1% BSA	10 µM

Abbreviations: PBS: phosphate buffered saline; BSA: bovine serum albumin; DMSO: dimethyl sulfoxide; NAC: N-acetylcysteine; EGF: epidermal growth factor; A83: A83-01, TGFβ kinase/activin receptor-like kinase (ALK 5) inhibitor; NOG: noggin; RSPO: R-spondin; DHT: dihydrotestosterone; FGF2: basic fibroblast growth factor (bFGF or FGF-β); FGF10: fibroblast

growth factor 10; PGE2: prostaglandin E2; SB: SB202190, p38 MAP kinase inhibitor, RI: ROCK inhibitor

* modifications applied to the protocol described by Drost *et al.* [146].

7. *Establishing Patient-derived Organoids*

According to the protocol described by Drost *et al.* [146], with some modifications, freshly collected prostate tissue fragments designated "unaffected/normal" and "tumor" were minced using sterile scalpel blades before being digested in 2 mL of 5 mg/mL collagenase type II (Gibco) in Advanced DMEM-F12 medium (adDMEM/F12, Gibco) with RI, overnight at 37°C. The following day, digested tissue pellet was washed with adDMEM/F12 and then centrifuged at 200g for 5 min. The pellet was resuspended in 1mL TrypLE with RI and digested for approximately 15 min at 37°C. TrypLE was inactivated with an equal volume of adDMEM/F12 medium then centrifuged at 200g for 5 min. The pellet was then resuspended in adDMEM/F12 medium and passed through a 40 µm cell strainer (Sigma-Aldrich) to get rid of tissue debris and obtain single cell suspensions. The derived cell count was estimated using trypan blue. A specific cell count, depending on the size and quality of samples we receive, was frozen as P0 cells as a stock of patient's derived cells for later use. All cells were kept as a stock in liquid nitrogen. The needed cell count was resuspended in Matrigel$^{\text{TM}}$, with the ratio of 20,000 cells per 40 µl of 90% Matrigel$^{\text{TM}}$. Out of a master mix, 40 µl droplets are plated in the center of wells of a 24-well plate with the fraction of one droplet per well. The plate is then placed upside down in the 37°C incubator for 30 min to allow the Matrigel$^{\text{TM}}$ to solidify. Pre-warmed (37°C) human prostate growth medium plus RI (10 µM) was added gently into each well. Media

40

was replenished every 2-3 days using human prostate growth medium plus RI (the RI was added during the first week only). The size and shape of organoids was assessed using Zen Software. Organoids were counted manually under a bright field microscope. The
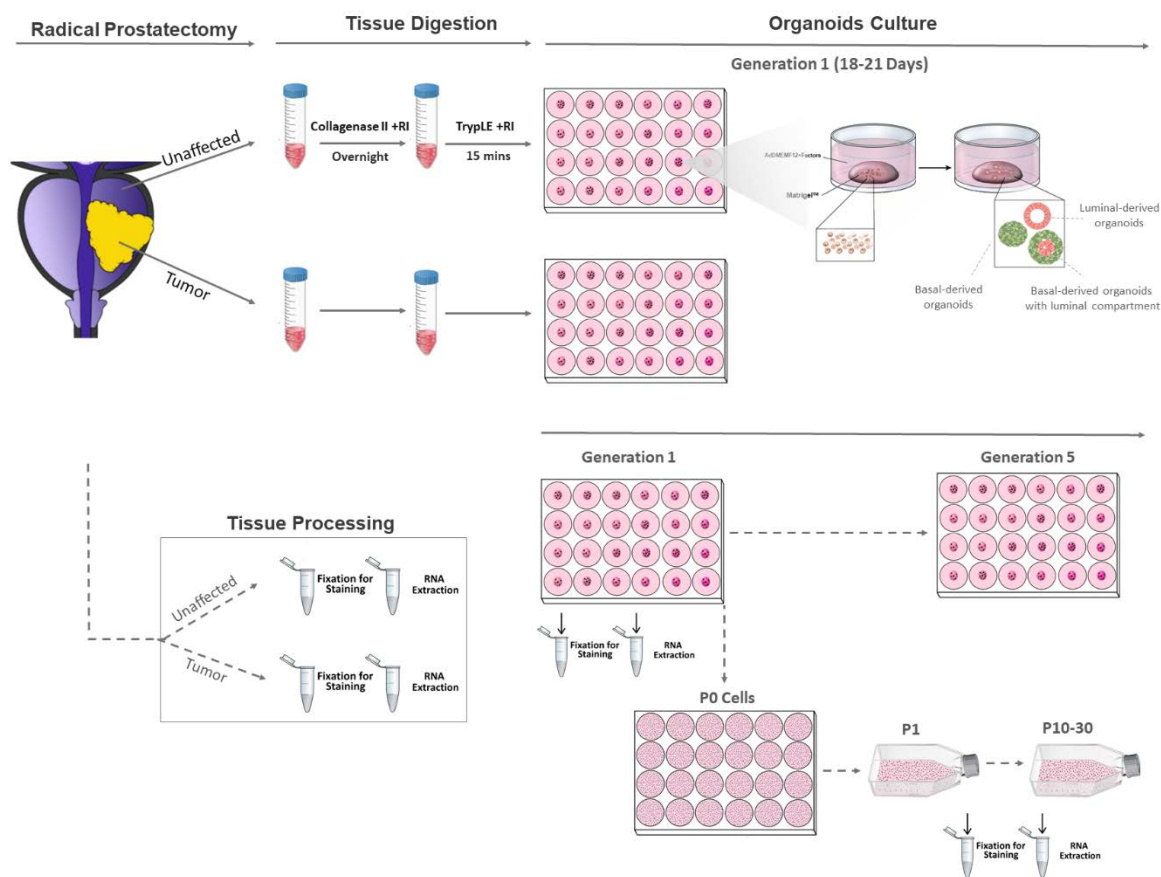
harvesting and propagation of organoids from Generation 1 (G1) to G2 was performed after 18 to 21 days or more depending on the sample. The percent organoids-forming efficiency was calculated by dividing the number of organoids counted by the number of input cells and then multiplied by 100.

Figure 5. Schematic diagram for the experimental plan adapted for patient-derived organoids and cells establishment. Freshly prostate tissue fragments designated minced

41

using sterile scalpel blades before being digested in 5 mg/mL collagenase type II in Advanced DMEM-F12 medium) with RI (ROCK inhibitor). After 18-24 hours, tissue pellet was further digested in TrypLE with RI which results in completely dissociated cells. Then cell suspensions are plated in droplets of 90% Matrigel™ and supplemented with human prostate growth medium as described in table 1. After 18-21 days, organoids were propagated into Generation 2 and maintained in culture up to G5 whenever possible. In parallel, 2D cells remaining in 2D were collected and maintained in culture for downstream characterization. Fragments of tissue specimens were also fixed in PFA or snap frozen for RNA extraction.

8. *Passaging of the Newly Established Organoids*

After approximately 18-21 days, organoids were collected in ice-cold culture medium and transferred to 2 ml eppendorfs or 15mL Falcon tube depending on the number of wells collected. Then, ice-cold adDMEM/F12 was added to dissolve residual Matrigel™, centrifuged at 200g for 5 min at 4°C. Then, organoids were dissociated enzymatically using TrypLE for 5 min at 37°C then pipetted up and down gently for 15–20 times. TrypLE was inactivated by adding an equal volume of adDMEM/F12. Organoids were then centrifuged at 200g for 5 min at 4°C. Then, ice-cold adDMEM/F12 was added to dissolve residual Matrigel™, centrifuged at 200g for 5 min at 4°C, and the pellet (including cell clumps) of one well was suspended in 80µL of 90% Matrigel™ (split ratio 1:2). As before, 40µL drops were plated into the middle of one well of a 24-well dish (total 2 wells). The dish was placed upside down in the 37°C incubator for 30 min to allow the Matrigel™ to solidify. Finally, 500µL of pre-warmed human prostate growth medium plus RI was added into each well.

The previous steps were repeated for a minimum of 5 generations, thereby keeping the primary cell culture growing for more than 4 months when needed. When possible and

depending on the cell count obtained from tissue digestion as starting material, and the efficiency of organoids establishment, which differs from one patient to the other, additional wells are collected and digested in a similar procedure to obtain a pellet for RNA extraction. In addition, for immunophenotyping, organoids were fixed in situ, embedded in Histogel and paraffin, and sectioned for subsequent characterization using immunological staining (please see section 14 below). Organoids were also collected similarly, without digestion using TrypLE, fixed and stained in suspension (please see section 13 below). Also, when possible and while passaging organoids, a portion of the dissociated organoids were frozen using FBS + 10% DMSO to have a stock of organoids culture.

9. *Establishment of Novel 2D Cell Lines*

We observed 2D cells growing underneath the organoids 3D Matrigel^{TM} culture, and so we decided to examine them as a potential source of novel patient-derived cell lines. After passaging the organoids, cells were detached using TrypLE and then transferred to T25 plates previously coated with 1% collagen-I. Cells were supplemented with human prostate organoids culture medium plus RI and incubated at 37°C in a CO_2 incubator. These patient-derived 2D cells were split at a ratio of 1:2 every 3-4 days where 50 % of cells were frozen down in FBS +10% DMSO and stored in liquid nitrogen, and 50% were maintained in culture using same conditions and medium.

10. Treatments of Patient-derived Organoids and Cells

Cell suspensions derived from fresh digested tissues were plated in Matrigel^{TM} as mentioned above. Then, human prostate organoids culture medium was added to each well, in the presence or absence of different drugs in duplicates per treatment. The culture medium was changed every 2-3 days, and organoids were counted after 18-21 days. All drugs were dissolved in DMSO to generate a final concentration of 0.1% in all drug-treated groups. Drugs tested included the following: Bicalutamide (Sigma-Aldrich) (AR signaling pathway, 1st generation drugs; 1 and 10uM), Enzalutamide (MDV3100; Selleckchem) (AR signaling pathway, 2nd generation drugs; 1 and 10uM), and Docetaxel (Sigma-Aldrich) (common chemotherapeutic agent used in the treatment of PCa; 1 and 50 nM). In addition, we evaluated combinatorial therapies such as combining Enzalutamide with Docetaxel. Moreover, we subjected the organoids to radiation therapy. To assess the effect of irradiation on organoids, we performed irradiation with 2 Gy dose (a clinically achievable dose) on day 1 of plating cell suspensions in Matrigel^{TM}. Corresponding controls were sham irradiated. After approximately 18-21 days, at the end of G1 and before propagation to G2, we analyzed two main outcomes reflecting the effect of drugs on proliferation and survival of cells. In that regard, sizes and counts of organoids were assessed. A minimum number of 50 organoids were analyzed to calculate diameter measurements using the ZEN 2013 software. Total number of organoids was counted manually under bright field light microscopy and the OFC was calculated by organoids forming count (OFC) was estimated by plating 20,000 cells per well in duplicates and then counting the total number of organoids formed per well after 18-21 days.

11. Optimization of Culture Conditions of Organoids

Cell suspensions derived from fresh digested tissues or frozen p0 cells were plated in Matrigel^{TM} as mentioned above. Then, to assess the importance of each factor of the 13 factors added to the culture medium, variations of the human prostate organoids culture medium were prepared by removing one factor at a time as follows: control condition prepared as described in table 1, condition -NAC included all other factors except N-acetylcysteine, condition -Nog included all other factors except Noggin, condition -RSPO included all other factors except R-spondin, condition - A83 included all other factors except A83-01, condition -PGE2 included all other factors except Prostaglandin E2, condition -DHT included all other factors except Dihydrotestosterone, condition -FGF10 included all other factors except FGF10, condition -FGF2 included all other factors except FGF2, condition -EGF included all other factors except EGF, condition -SB included all other factors except SB202190. This experiment was performed on samples derived from 3 patients; the tumor tissue sample and the corresponding unaffected tissue sample, in duplicates per condition.

In the follow up experiment, essential factors including B27, N-acetylcysteine, Nicotinamide, Noggin and A83-01 were designated 5F. The variations of the human prostate organoids culture medium were prepared as follows: 5F with R-spondin, 5F with SB202190, 5F with Prostaglandin E2, 5F with FGF2, 5F with FGF10, 5F with EGF. Organoids were plated in duplicates per condition. After approximately 18-21 days, at the end of G1 and before propagation to G2, we analyzed two main outcomes reflecting the

effect of variations of the medium on proliferation and survival of cells. In that regard, sizes and counts of organoids were assessed. A minimum number of 50 organoids was analyzed to calculate diameter measurements using the ZEN 2013 software. Total number of organoids was counted manually under bright field light microscopy and percent organoids forming efficiency was calculated by dividing the number of organoids counted by the number of input cells and then multiplied by 100.

12. Immunofluorescent and Immunohistochemical Staining Procedure for Tissues

Unstained formalin-fixed paraffin-embedded (FFPE) 4 µm tissue sections were deparaffinized, and antigen retrieval was performed in a citrate buffer in a steamer at 100°C for 40 min.

For immunofluorescence (IF), protein blocking was performed using the blocking buffer (3% BSA, 0.1% Triton x-100, and 10% NGS in PBS) for one hour at room temperature. Then slides were incubated overnight at 4°C using the different primary antibodies including mouse monoclonal anti-CK8 (1/200 dilution) (Biolegend), rabbit polyclonal anti-CK5 (1/200 dilution; Covance, CA), rabbit polyclonal anti-CK14 (1/200 dilution; Santa Cruz Biotechnology, CA), rabbit polyclonal anti-Vim (1/50 dilution), mouse monoclonal anti-Sox2 (1/50 dilution) (Santa Cruz Biotechnology, CA). Sections were then incubated with the corresponding secondary antibodies; Alexa 568 goat anti -mouse (Life Technologies), Alexa 488 goat anti-rabbit (Invitrogen), for 1 hour at room temperature. After gentle washing with PBS containing 0.1% Tween-20, tissue sections were incubated

with the corresponding secondary antibodies, then washed gently and mounted with anti-fade Fluoro-gel II with DAPI.

For immunohistochemistry (IHC), after deparaffinization and antigen retrieval, the Novolink™ polymer detection system (Leica Biosystems) was employed, then sections were incubated overnight at 4°C using the different primary antibodies including rabbit monoclonal anti-AR (1/50 dilution) (Abcam), anti-PSA (1/200 dilution) (Abcam), mouse monoclonal anti-P63 (Bond™), and rabbit monoclonal anti-AMACR (BioGenex). Then sections are incubated with Post Primary and Novolink™ Polymer for 30 mins each, before developing the peroxidase activity using ImmPACT DAB peroxidase substrate for 1-10 mins depending on the antibody. Finally, sections are counterstained with hematoxylin, dehydrated and mounted using Permount medium.

13. Immunofluorescence and Morphological Analysis of Organoids in Suspension

Indirect immunofluorescence analysis was used to characterize the 3D organoids. To preserve the 3D architecture, immunofluorescence analysis was performed in suspension. Organoids were collected when they reach the appropriate size and confluency for passaging (18-21 days after plating). Matrigel™ was dissolved using ice-cold medium as mentioned above. After that, the pellet was fixed in 4% PFA for 30 min. Then organoids were permeabilized with 0.5% Triton X-100 for 30 min at room temperature, followed by a blocking buffer (0.1% BSA, 0.2% Triton X-100, 0.05% Tween-20 and 10% NGS in PBS) for 1 hr at room temperature. Organoids were then incubated overnight with primary antibodies at 4°C. Antibodies used included: mouse monoclonal anti-CK8 (1/200 dilution)

(Biolegend), rabbit polyclonal anti-CK14 (1/200 dilution; Santa Cruz Biotechnology, CA), mouse monoclonal anti-CD44 (1/50 dilution; Santa Cruz Biotechnology, CA), rat monoclonal anti-CD49f (1/50 dilution; BD pharmingen). After gentle washing with PBS containing 0.1% Tween-20, organoids were incubated with the corresponding secondary antibodies; Alexa 568 goat anti-mouse (Life Technologies) (Invitrogen), Alexa 488 goat anti-rat (Life Technologies), then washed gently and mounted with anti-fade reagent Fluoro-gel II with DAPI.

14. Immunofluorescence and Immunohistochemical Staining of Organoids Sections

Immunofluorescence and immunohistochemical staining were also performed FFPE sectioned organoids to further assess the architecture and morphology of organoids in comparison with corresponding tissue sections. To embed organoids, droplets of Matrigel™ containing organoids were fixed in pre-warmed 4% PFA for 30 min to keep the Matrigel™ intact, then the droplet of Matrigel™ is collected carefully using a spatula. Histogel is liquefied at 60°C and used to surround the droplet of Matrigel™ in a sandwich of Histogel. Then it is allowed to solidify on ice for 10 mins before transferring it into a tissue cassette to be incubated in 10% formalin overnight. Finally, it is processed for paraffin embedding and sectioning into 4 μm sections. Organoids sections were stained using the procedure adapted for tissue sections as described in section 12.

15. Immunofluorescence and Morphological Analysis of Cells Grown as Monolayer

Indirect immunofluorescence analysis was used to characterize prostate epithelial lineage markers including monoclonal anti-CK8 (1/200 dilution) (Biolegend), rabbit polyclonal anti-CK5 (1/200 dilution; Covance, CA), rabbit polyclonal anti-CK14 (1/200 dilution; Santa Cruz Biotechnology, CA), rabbit polyclonal anti-VIM (1/50 dilution). Cells were grown on collagen-I coated coverslips. Adherent cells were then fixed using 4% PFA in PBS for 20 min, then permeabilized with 0.5% Triton X-100 in PBS for 20 min. Non-specific sites were blocked by incubation in blocking buffer (0.1% BSA, 0.2% Triton X-100, 0.05% Tween-20 and 10% NGS in PBS) for one hour. Cells were then incubated overnight with specific primary antibodies at 4°C. After washing with PBS containing 0.1% Tween-20, cells were incubated with the corresponding secondary antibodies, then washed gently and mounted with anti-fade reagent Fluoro-gel II with DAPI.

16. RNA extraction and quantitative real time PCR (qRT PCR)

TRIZOL/RNeasy Micro Kit (Qiagen) were used to extract total RNA from organoids, cells and tissues. 2µg of total RNA was then reverse transcribed into cDNA using the QuantiTect® Reverse Transcription kit (Qiagen) according to the manufacturer's instructions. Specific transcripts were quantified by real time RT-PCR (Bio-rad CFX^{TM} manager) using 2X SYBR Green PCR master mix. The amplification of cDNA was performed over the following cycles: 95 °C for 5 min, followed by 40 cycles at 95 °C for 10 s, 60 °C for 30 s and 72 °C for 1 min. Fold changes in gene expression were calculated by ΔCt method of relative quantitation using GAPDH as an endogenous reference gene. All

reactions were run in triplicates using the primers designed using Primer3-BLAST as listed in Table2.

Table 2. List of primers used in qRT PCR

Gene Symbol	Direction	Primer Sequences 5' → 3'
VIM	Forward	AGGTGGACCAGCTAACCAAC
	Reverse	TCTCCTCCTGCAATTTCTCC
CDH1	Forward	TTCTGCTGCTCTTGCTGTTT
	Reverse	TGGCTCAAGTCAAAGTCCTG
AR	Forward	CCTGGCTTCCGCAACTTACAC
	Reverse	GGACTTGTGCATGCGGTACTCA
CK8	Forward	GCTGACCGACGATCAACT
	Reverse	CCATGGACAGCACCACAGAT
SOX2	Forward	AACCCCAAGATGCACAACTC
	Reverse	GCTTAGCCTCGTCGATGAAC
TP63	Forward	ACCTCCTCAGGGAGCTGTTA
	Reverse	ATACTGGGCATGGCTGTTCC

17. Cell Viability (Trypan Blue Exclusion Method)

Unaffected and tumor patient-derived prostate cells from three patients were seeded, in triplicates, in 12-well plates at a density of 5×10^4 cells per well. Cells were then cultured under the three different culturing conditions: (i) condition 1 "All factors" included adDMEM/F12 medium + all 12 prostate organoids culture components, (ii) condition 2 "All factors – EGF" includes prostate organoids growth medium without EGF, and (iii) condition 3 "EGF alone" includes adDMEM/F12 with EGF only (10 ng/ml). Viable cells were collected and counted using trypan blue dye exclusion method after 72 hours [217]. Cell viability was expressed as percentage growth relative to condition 1. The data are derived from the mean of triplicates wells.

18. MTT

MTT ([3-(4, 5-dimethylthiazol-2-yl)-2, 5-diphenyltetrazolium bromide]) cell growth assay was used to measure the *in vitro* proliferative effects of EGF on the growth of patient derived 2D cells. Cells derived from tissue samples from 3 different patients, including the unaffected and the tumor sample, were seeded at a density of 4×10^3 cells/well in 100 µL in triplicates under three different conditions; (i) condition 1 "All factors" included adDMEM/F12 medium + all 12 prostate organoids culture components, (ii) condition 2 "All factors – EGF" includes prostate organoids growth medium without EGF, and (iii) condition 3 "EGF alone" includes adDMEM/F12 with EGF only (10 ng/ml). MTT assay was performed as described by manufacturers [218-220]. In brief, unaffected and tumor patient-derived prostate cells from three patients were seeded, in triplicates, at a density of 5×10^3 cells/well in 100 µL of cell growth media in a 96-well culture plate and incubated overnight at 37°C in a humidified incubator containing 5% CO_2, before being exposed to the different culturing conditions for 72 hours. Media was changed at 24 and 48 hours. At 72 hours, media was removed and replaced with fresh media along with 10 µL/well of 5 mg/mL (in 1x PBS) MTT yellow dye and incubated at 37°C, 5% CO_2 for 4 hours, after which 100 µL/well of the solubilizing agent (isopropanol) was added. After overnight incubation, the reduced MTT optical density (OD) was measured by the microplate ELISA reader (Multiscan EX) at a wavelength of 595 nm. The percentage of cell viability was presented as percentage growth using the OD ratio of cells exposed to conditions (ii) and (iii) relative to condition (i). The average percentage cell viability in each condition was derived from the mean of triplicate wells of three independent experiments.

51

19. Microscope Specifications

Microscopic analyses were performed using Carl Zeiss Axio Observer.Z1 epifluorescent microscope and Zeiss LSM 710 laser scanning confocal microscope when needed and images were acquired and analyzed using the Carl Zeiss ZEN 2013 image software. Images of IHC staining were acquired using Olympus CX41 light microscope and processed using Vanguard software.

20. Statistical Analysis

The EMT score was categorized into less than 25% and more than or equal to 25%. This cutoff of 25% was assigned based on the EMT score distribution where 95.1% (116) of the total population clustered in the "less than or equal to 50% EMT score". Student *t*-test of independent variables was used to compare the EMT score between the three assigned gleason groups A, B and C. Chi-square test and two-tailed unpaired Student's *t*-test of independent variables were used to assess the association of the EMT score categorized into two groups with the sample clinicopathological characteristics such as age, PCa pathological stage, preoperative PSA, PSA failure, percentage of tumor volume involved, prostate size, perineural invasion, seminal vesicle invasion, lympho-vascular invasion, and surgical margins. A Mantel-Haenszel test of trend was run to determine whether a linear association existed between the EMT score categories and the different gleason groups. In a secondary analysis, a linear regression model was built to examine the

effect of the gleason group on the EMT score while adjusting for the pathological stage and the surgical margins. EMT score in addition to the gleason group, pathological stage and surgical margins (the three clinicopathological variables which showed statistically significant difference between the two EMT score categories) were entered as covariates in the cox regression model. P-values less than or equal to 0.05 were considered significant. Statistical analysis was performed using the Statistical Package for the Social Sciences statistical package 21.0 software (SPSS, Inc.).

For in vitro assays, statistical analysis was performed using GraphPad Prism 7.0 Software. The significance of the data was analyzed using one-way or Two-way ANOVA statistical test, followed by multiple comparisons test using Bonferroni post hoc analysis. Statistical significance was reported when the P-value was less than 0.05 (* P<0.05; ** P<0.01; £ P<0.001).

CHAPTER III

RESULTS

A. A Novel Scoring System to Quantify EMT Expression in Patients with Locally-Advanced PCa

Our first aim was to develop a novel scoring system to quantify EMT expression (EMT score) in patients with locally-advanced PCa using the radical prostatectomy institutional database (1998-2016) of the American University of Beirut-Medical Center (AUB-MC), then explore the correlation between this score and the different clinicopathological outcomes. This work was recently published in Frontiers in Oncology [221].

1. *Clinicopathological Characteristics of PCa Patients and their Correlation with the EMT Score*

    a. Gleason Scoring and Assigned Gleason Groups

The Gleason scores were assigned by two independent pathologists according to the International Society of Urological Pathology (ISUP) criteria. After reviewing the different Gleason scores, three groups were created as follows: group A, includes patients with
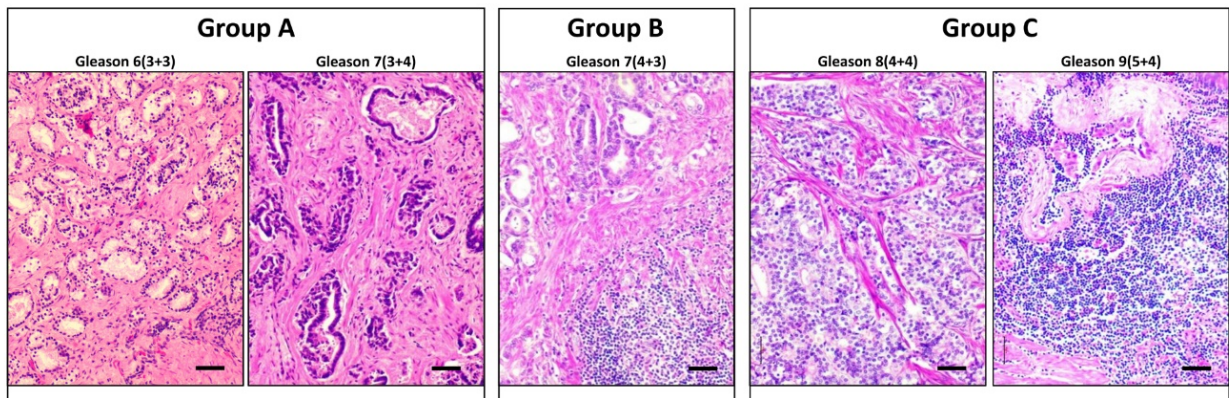
Gleason scores 6 and 7(3+4); group B, includes patients with Gleason score 7(4+3); group C, includes patients with Gleason scores 8 and 9. Cross-sections of PCa tissues representing each of the three Gleason groups were stained with Hematoxylin and Eosin (H&E) for general assessment (Fig. 6).

Figure 6. Representative H&E staining of PCa tissue sections that represent each of the three Gleason groups. The left panel represents group A that includes Gleason scores 6 and 7(3+4). The middle panel represents Group B that includes Gleason score 7(4+3). The right panel represents group C that includes Gleason scores 8 and 9. Scale bars = 50μm.

55

b. The Clinicopathological Characteristics of Patients

A total of 122 radical prostatectomy (RP) specimens were analyzed. The specimens of RP were collected from patients with a mean diagnostic age of 62.1 ± 6.5 years at AUBMC. All patients underwent open or laparoscopic prostatectomies. Samples were collected from January 1998 to January 2016. It was observed that 89.3% were diagnosed at age less than 70 years. Patients of GS group A, B and C were distributed as 51.6% 24.6% and 23.8% respectively.

Table 3. Clinicopathological characteristics of the 122 patients with PCa included in our study.

Clinicopathological Variable	Total N	Categories	n (%)
Age (in years)	122	Mean (±SD)	62.1(± 6.5)
		< 70	109 (89.3%)
		≥ 70	13 (10.7%)
Gleason groups	122	A: Gleason scores 6 and 7(3+4)	63 (51.6%)
		B: Gleason score 7(4+3)	30 (24.6%)
		C: Gleason scores 8 and 9	29 (23.8%)
Lympho-vascular invasion	61	Absent	55 (90.2%)
		Present	6 (9.8%)
Perineural invasion	94	Absent	28 (29.8%)
		Present	66 (70.2%)
Seminal vesicle invasion	118	Absent	96 (81.4%)
		Present	22 (18.6%)
Lymph node Invasion	28	Absent	25 (89.3%)
		Present	3 (10.7%)
Pathological stage	120	pT2	35 (29.2%)
		≥ pT3	85 (70.8%)

Preoperative PSA (in ng/mL)	116	Mean (±SD)	10.7(± 9.8)
		< 10	76 (65.5%)
		≥ 10	40 (34.5%)
Prostate size (in g)	120	Mean (±SD)	58.3(± 59.5)
		< 50	65 (54.2%)
		≥ 50	55 (45.8%)
Tumor volume (in cc)	113	Mean (±SD)	14.9(± 21.9)
		< 5	26 (23%)
		≥ 5	87 (77%)
PSA failure	87	No	45 (51.7%)
		Yes	42 (48.3%)

c. <u>Association between Clinicopathological Variables and EMT Score</u>

In studying the sample distribution statistics between the two categories of the EMT score (less than 25% and more than or equal to 25%) a significant statistical difference was detected between the two categories in terms of Gleason group (p = 0.014), pathological stage (p = 0.014) and surgical margins (p = 0.006). No significant differences in the patient's age, pre-operative PSA, PSA failure (defined by an increase in blood PSA level at or above 0.2 ng/mL following surgery), and tumor volume were observed (**Table 2**).

Table 4. Correlation of EMT score with the patients' clinicopathological variables.

Clinicopathological Variable		**EMT score**			**P-value**
		< 25	**≥ 25**	**Total**	
		N (%)	N (%)	N (%)	
Age (in years)	Mean (±SD)	61.6 (± 6.2)	63.6 (± 7.2)	62 (± 6.5)	0.167
	< 70	85 (93.4%)	22 (81.5%)	107 (90.7%)	0.061

	≥ 70	6 (6.6%)	5 (18.5%)	11 (9.3%)	
	Total	91 (100%)	27 (100%)	118 (100%)	
Gleason groups	A: Gleason scores 6 and 7(3+4)	51 (56%)	9 (33.3%)	60 (50.8%)	**0.014**
	B: Gleason score 7(4+3)	24 (26.4%)	6 (22.2%)	30 (25.4%)	
	C: Gleason scores 8 and 9	16 (17.6%)	12 (44.4%)	28 (23.7%)	
	Total	91 (100%)	27 (100%)	118 (100%)	
Lympho-vascular invasion	Absent	32 (88.9%)	22 (91.7%)	54 (90%)	0.725
	Present	4 (11.1%)	2 (8.3%)	6 (10%)	
	Total	36 (100%)	24 (100%)	60 (100%)	
Perineural invasion	Absent	15 (23.1%)	10 (38.5%)	25 (27.5%)	0.137
	Present	50 (76.9%)	16 (61.5%)	66 (72.5%)	
	Total	65 (100%)	26 (100%)	91 (100%)	
Seminal vesicle invasion	Absent	74 (83.1%)	19 (73.1%)	93 (80.9%)	0.251
	Present	15 (16.9%)	7 (26.9%)	22 (19.1%)	
	Total	89 (100%)	26 (100%)	115 (100%)	
Lymph node invasion	Absent	11 (91.7%)	13 (86.7%)	24 (88.9%)	0.681
	Present	1 (8.3%)	2 (13.3%)	3 (11.1%)	
	Total	12 (100%)	15 (100%)	27 (100%)	
Pathological stage	pT2	21 (23.6%)	13 (48.1%)	34 (29.3%)	**0.014**
	≥ pT3	68 (76.4%)	14 (51.9%)	82 (70.7%)	
	Total	89 (100%)	27 (100%)	116 (100%)	
PSA failure	No	32 (49.2%)	11 (55%)	43 (50.6%)	0.625
	Yes	33 (50.8%)	9 (45%)	42 (49.4%)	
	Total	65 (100%)	20 (100%)	85 (100%)	
Surgical margins	Negative	17 (18.7%)	12 (44.4%)	29 (24.6%)	**0.006**
	Positive	74 (81.3%)	15 (55.6%)	89 (75.4%)	
	Total	91 (100%)	27 (100%)	118 (100%)	
Preoperative PSA (in ng/mL)	Mean (±SD)	10 (± 7.1)	13.7 (± 16.4)	10.9 (± 9.9)	0.289
	< 10	55 (63.2%)	17 (68%)	72 (64.3%)	0.66
	≥ 10	32 (36.8%)	8 (32%)	40 (35.7%)	
	Total	87 (100%)	25 (100%)	112 (100%)	
Prostate size (in g)	Mean (±SD)	58.5 (± 67.7)	60.1 (± 24.8)	58.9 (± 60.4)	0.903
	< 50	48 (53.9%)	13 (48.1%)	61 (52.6%)	0.598
	≥ 50	41 (46.1%)	14 (51.9%)	55 (47.4%)	
	Total	89 (100%)	27 (100%)	116 (100%)	
Tumor volume (in cc)	Mean (±SD)	16.1 (± 24.7)	12.3 (± 9.4)	15.2 (± 22.2)	0.461
	< 5	18 (21.4%)	7 (28%)	25 (22.9%)	0.493

≥ 5	66 (78.6%)	18 (72%)	84 (77.1%)
Total	84 (100%)	25 (100%)	109 (100%)

2. *Immunofluorescence Characterization of Paraffin-embedded Tissue Sections*

The specimens were examined using immunofluorescence staining for CK8/Vim co-expression (EMT score) (Figure 7). EMT scoring was performed manually using a 40× objective and a Carl Zeiss Axio Observer.Z1 microscope. It was done by screening the whole tissue section in a systematic manner and counting the total number of glands, then counting the number of glands with at least one cell co-expressing CK8 and Vim. Then, the percentage was calculated by dividing the number of glands with at least one double positive cell by total number of glands, multiplied by 100. This percentage is referred to as EMT score. CK8/Vim staining was graded as double positive only when cytoplasmic staining ws detectable. The EMT score was categorized into two groups (less than 25% and more than or equal to 25%).
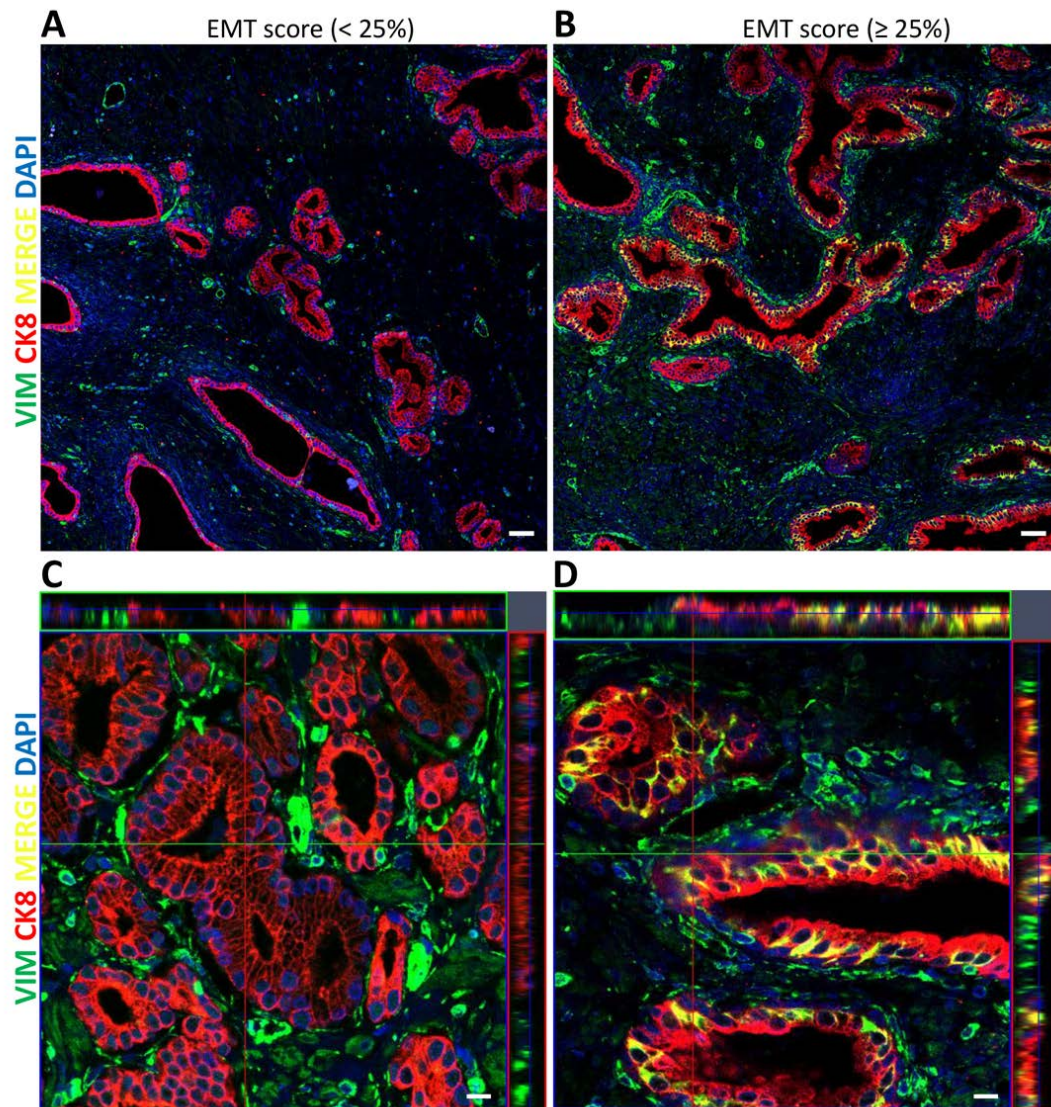
Figure 7. Representative immunofluorescent images of the co-expression of CK8/Vim molecular markers in PCa tissue specimens. Tissue sections were stained with CK8 (red), Vimentin (green) and DAPI (blue)**. (A)** Tile scan image (5x5) of PCa tissue showing EMT score < 25% (scale bar = 50μm). **(B)** Tile scan image (5x5) of PCa tissue stained showing EMT score ≥ 25% (scale bar = 50μm). **(C)** Z-stack with maximal and orthogonal projection of PCa tissue showing low EMT score < 25% (scale bar = 10μm). (D) Z-stack with maximal and orthogonal projection of PCa tissue showing high EMT score ≥ 25% (scale bar = 10μm).

3. *High Mean EMT Score is Significantly Associated with Higher Gleason Group*

To investigate the difference in the mean EMT score between the assigned Gleason groups, an independent *t*-test was performed. There were 60 patients in group A, 30 patients in group B and 28 patients in group C. There was no statistical difference in the mean EMT score between groups A and B. Nonetheless, the mean EMT score was higher in group B (M=15.3%, SD=21.3%) than group A (M=10.7 %, SD=11.6%), with a mean difference (M = -4.62, 95% CI [-13.04;3.8], p = 0.274). When comparing the mean EMT score of the 60 patients in the Gleason group A (M=10.7 %, SD=11.6%) to the 28 patients in group C (M=26.8%, SD=29.1%), a significant difference with quite high mean difference was recorded (M=-16.09, 95% CI [-27.71; -4.47], p = 0.008). The mean EMT score comparison between groups B and C revealed no significant difference, although a higher mean was recorded in the higher Gleason group (M= -11.47, 95% CI [-24.99; -2.06], p = 0.091) (Table 5).

Table 5. Comparison of the mean EMT scores between Gleason groups.

	Gleason group	N	Mean (± SD)	Mean Difference (95% CI)	P-value
Mean EMT score	A: Gleason scores 6 and 7(3+4)	60	10.7 (± 11.6)	-4.62 [-13.04; 3.8]	0.274
	B: Gleason score 7(4+3)	30	15.3 (± 21.3)		

	Gleason group	N	Mean (± SD)	Mean Difference (95% CI)	P-value
Mean EMT score	B: Gleason score 7(4+3)	30	15.3 (± 21.3)	-11.47 [-24.99; 2.06]	0.091
	C: Gleason scores 8 and 9	28	26.8 (± 29.1)		

	Gleason group	N	Mean (± SD)	Mean Difference (95% CI)	P-value
Mean EMT score	A: Gleason scores 6 and 7(3+4)	60	10.7 (± 11.6)	-16.09 [-27.71; -4.47]	**0.008**
	C: Gleason scores 8 and 9	28	26.8 (± 29.1)		

a. Mean Plot of EMT score versus the Different Gleason Groups

Next, we sought to determine if there was any association between EMT scores and the different Gleason Groups. In fact, a linear association was demonstrated between mean EMT score and the assigned Gleason groups where the mean percentage EMT score showed a drastic increase with increasing Gleason groups (from A to C) (Fig. 8).

Figure 8. Mean plot of mean EMT score in percentage versus different Gleason groups showing a linear association. Gleason groups A; Gleason scores 6 and 7(3+4), group B; Gleason score 7(4+3), and group C; Gleason scores 8 and 9.

Mantel-Haenszel Test of Trend between EMT Score and Gleason Groups

In addition to the previous data, a Mantel-Haenszel test of trend was run to determine whether a linear association existed between the two EMT scores and the assigned Gleason groups. The Mantel-Haenszel test of trend showed a statistically significant linear association between them ($\chi^2(1) = 7.547$, $p < .007$, $r = 0.254$), where higher Gleason group was associated with a higher EMT score (Table 6).

Table 6. Gleason group distribution among the EMT score categories.

Gleason Group	EMT Score		
	< 25	**≥ 25**	**Total**
A: Gleason scores 6 and 7(3+4)	51 (56%)	9 (33.3%)	60 (50.8%)
B: Gleason score 7(4+3)	24 (26.4%)	6 (22.2%)	30 (25.4%)
C: Gleason scores 8 and 9	16 (17.6%)	12 (44.4%)	28 (23.7%)
Total	91 (100%)	27 (100%)	118 (100%)

c. A Scatterplot between EMT Score and the Gleason Groups

65

Furthermore, A scatter plot is shown to demonstrate the linear association detected by Mantel-Haenszel test between the two EMT scores and the assigned Gleason groups (Figure 9.

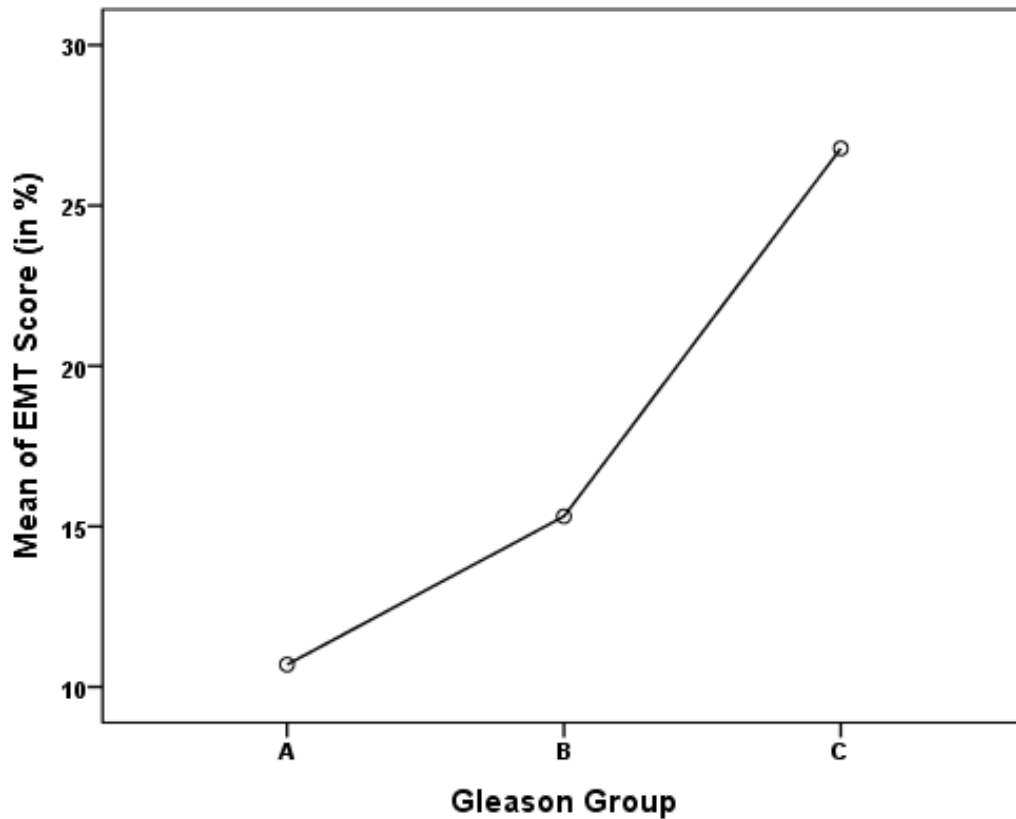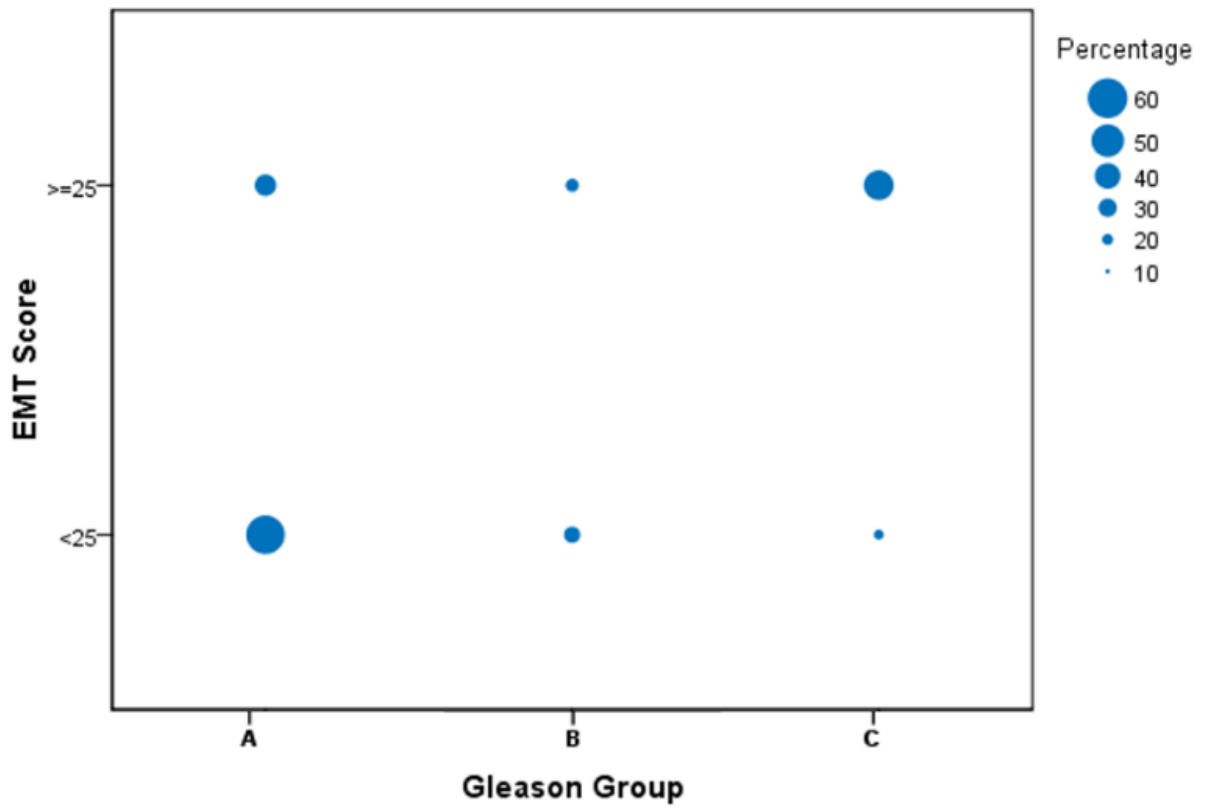**Figure 9. Scatterplot of the EMT score versus different Gleason groups showing a linear association.** Groups A; Gleason scores 6 and 7(3+4), group B; Gleason score 7(4+3), and group C; Gleason scores 8 and 9.

4. *Gleason Groups Can Predict EMT Score Irrespective of the Pathological Stage and Surgical Margins*

A multiple regression model was built to study if the Gleason group can be used to predict the EMT score. In addition, to assess if this predictive relationship is exclusive between the EMT score and the Gleason group, we adjusted for the variables that showed a statistically significant difference between the two EMT score categories; the pathological stage and surgical margins (Table 4). The multiple regression model showed a significant predictive ability of the EMT score, $F_{(3,112)} = 7.037$, $p < 0.001$ and the Gleason group was the only variable that added statistical significance to the prediction, $p = 0.001$. Regression coefficients and their P-values can be found in Table 7.

Table 7. Regression coefficients of the multiple regression model.

Clinicopathological variable	B (95% CI)	P-value
Gleason group	7.38 [8.2;45.63]	**0.001**
Pathological stage	-6.79 [3.06;11.71]	0.118
Surgical margins	-7.08 [-15.32;1.74]	0.122

5. *The Correlation of EMT Score with PSA Failure*

To study the correlation between EMT score and PSA failure, a Cox regression model was built. Time to PSA failure was considered time to event, and EMT score, Gleason group, pathological stage and surgical margins were added as covariates to the model using forward method. Interestingly, EMT score was found to be an independent predictor of PSA failure, where biochemical recurrence was higher in patients with EMT score $\geq$ 25% (OR: 2.23, 95% CI [1.018; 4.895], p = 0.045). The overall model has a χ^2 of 4.221, with a P-value of 0.04. Biochemical recurrence-free survival curve estimating PSA
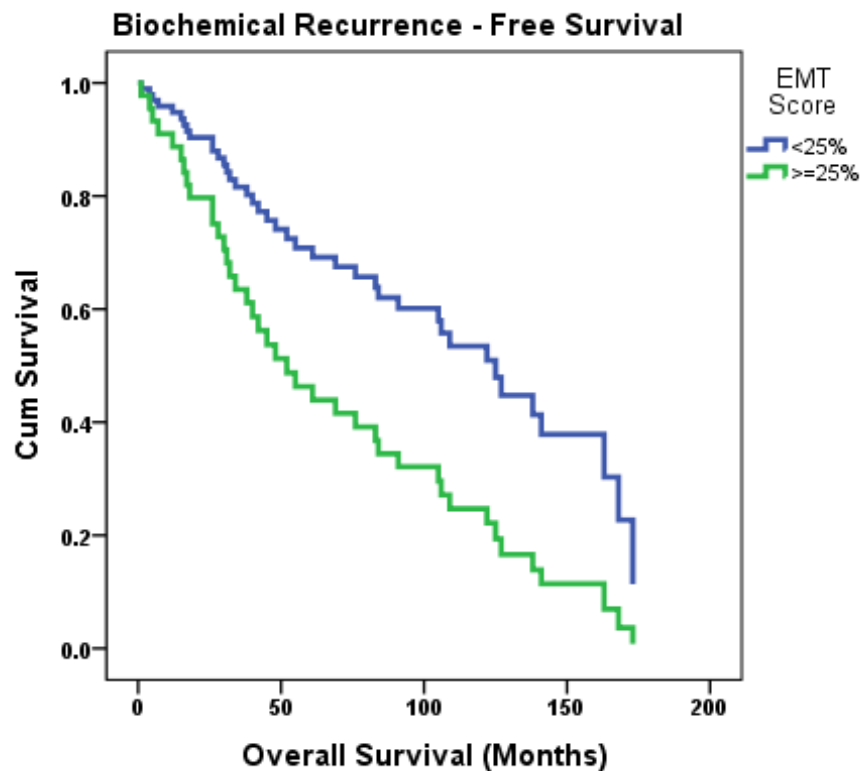
failure based on the patients' EMT score is shown in **Figure 10**.

Figure 10. Biochemical recurrence-free survival curve estimating PSA failure based on the patients' EMT score. Biochemical recurrence was found to be higher in patients with EMT score $\geq$ 25% (p = 0.045).

B. Characteristics of the Prostate Cancer Specimens Established as Organoids

Knowing that the organoids technology is very promising and exhibits boundless potential for clinical relevance, and despite the expected challenges in modeling PCa, our second aim was to establish and characterize patient-derived PCa organoids from patients undergoing radical prostatectomies.

1. *The Efficiency of Organoids Culture system*

Between May 2017 and Feb 2019, fresh radical prostatectomy specimens were received from a total of 35 treatment-naïve patients with 47% belonging to Gleason group (GG) A, 41% to GG B, and 12% to GG C. From each patient, 2 samples were received, one from the "unaffected" side and one from the "tumor" side according to a pathologist and processed according to the diagram in Figure 11. Out of the 70 specimens, more than 90% were successfully established as organoids. It is worth noting that for most of the unestablished samples, primary alive cells (p0) were not successfully derived after the initial tissue digestion, which indicates that the quality of tissue received is a major factor

91.43% Established
8.57% Not Established
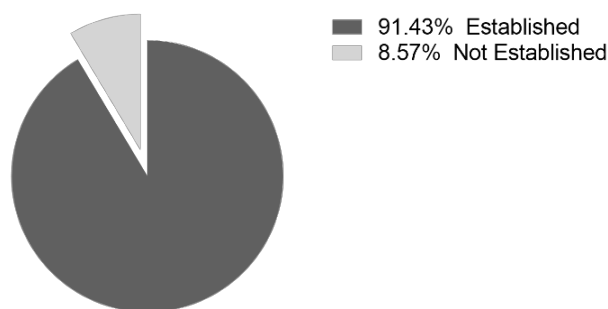
N=35 patients; 70 specimens

that affects organoids derivation.

Figure 11. Pie chart showing the percentage success rate of deriving PCa patient-derived organoids.

    a.   <u>Assessment of Organoids Counts for Unaffected and Tumor Samples</u>

For organoids establishment, and after tissue digestion overnight, a total of 20,000 cells were plated per 40 µl droplets of 90% Matrigel[TM]. Organoids were plated in duplicates or triplicates per condition depending on the total cell count successfully derived from the tissue specimens. One major limitation was the small size of tissue fragment received (less than 3 mm). To determine the suitable organoid count per droplet of Matrigel[TM], organoids counts ranging from 10,000 to 100,000 cells per droplet were plated. The count of 20,000 gave the highest organoids count while preventing the overcrowding that confines the organoids size. The average number of organoids forming count (OFC) was estimated by plating 20,000 cells per well in duplicates and then counting the total number of organoids formed per well after an average of 18-21 days. The OFC ranges between 227 (1.135%) and 841 (4.205%) organoids from unaffected specimens, and between 142 (0.71%) and 607 (3.03%) organoids from tumor specimens

Organoids Forming Count
n=20

70
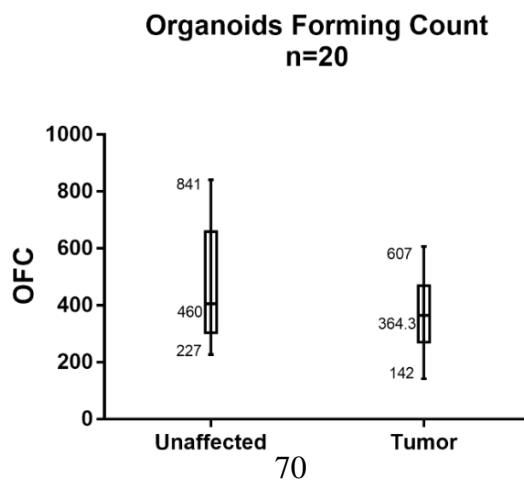
(Figure 12).

Figure 12. Optimal Organoids count. Box and Whiskers plot representation showing the average, minimum and maximum organoids forming count (OFC) of PCa patient-derived organoids starting with 20,000 cells (Unaffected; n=10, Tumor; n=10).

  b. Assessment of Organoids (average size) for Unaffected and Tumor Samples

A minimum number of 50 organoids per well were analyzed to calculate the

average diameter measurements using the ZEN 2013 software. To further assess the

variations between one patient sample and the other, and between unaffected and tumor

samples, the calculated averages of organoids diameter derived from 10 unaffected and 10

tumor samples were further analyzed to estimate the overall average. The overall average

size ranged between 63.2 and 110 μm from unaffected specimens, and between 61.8 and

106 μm from tumor specimens (Figures 13, 14).
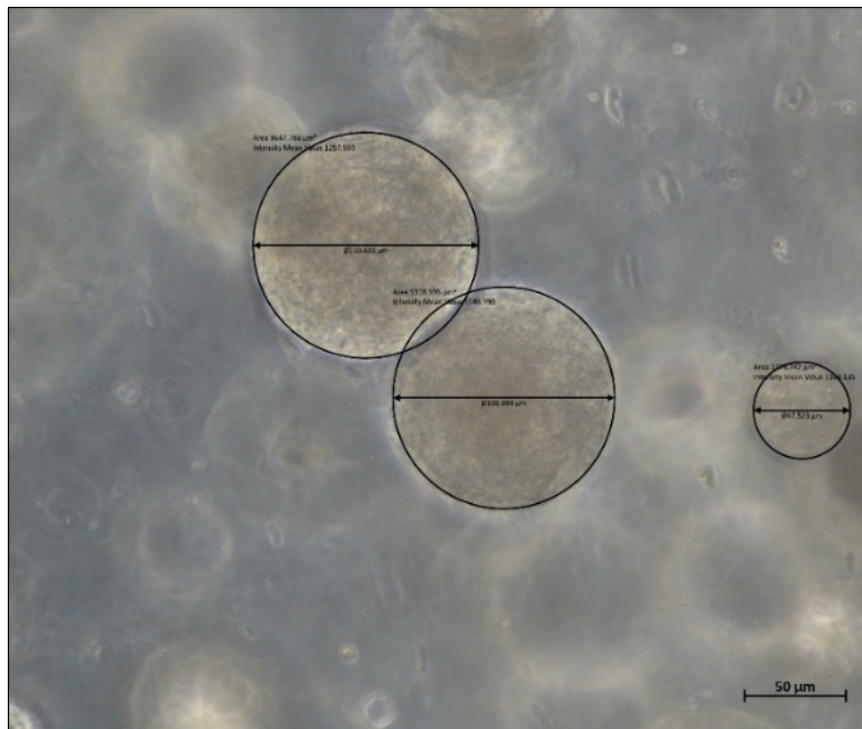
Figure 13. Measurement of organoids size. Representative bright-field image showing the method adapted to estimate the size of a specific organoid using ZEN 2013 software. To estimate the average diameter for a specific condition, the average of a total of 50 organoids per well is calculated. Scale bar = 50μm.

Organoids Average Size
n=20
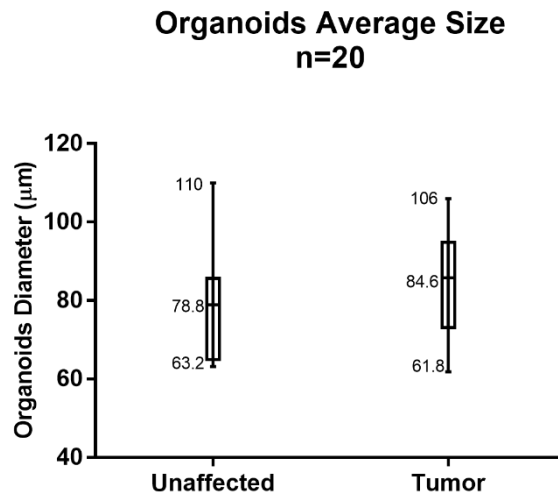
Figure 14. Distribution of organoids sizes. Box and Whiskers plot representation showing the average, minimum and maximum organoids diameter of PCa patient-derived organoids starting with 20,000 cells (Unaffected; n=10, Tumor; n=10).

2. Characterization of the Established PCa Patient-derived Organoids

a. Representative H&E and IHC Images of PCa Patient-derived Organoids and their Corresponding Tissue Specimens

Patient-derived organoids were characterized by assessing the expression of prostate epithelial lineage markers using immunohistochemistry. Patient-derived organoids were grown and supplemented with human prostate organoids culture medium plus RI for an

72

average of 18 days, then fixed with PFA and embedded in histogel and paraffin, then sectioned and immunostained, as described in the methods section. The sections were probed for different markers including luminal markers (Androgen receptor (AR) and prostate specific antigen (PSA), basal marker (P63), and tumor marker (Alpha -methylacyl   ).CoA racemase (AMACR) specimens were also fixed with PFA and embedded in paraffin, then sectioned and immunostained with the same markers. The results obtained revealed a strong nuclear expression of AR in tumor organoids in parallel with the corresponding tumor tissue (Figure 15). A strong P63 expression was detected in all organoids assessed and matching with the tissue of origin. The expression of the secretory protein PSA was not confirmed. Indeed, the highest proportion of organoids cells expressed basal marker p63, which might explain the low undetectable levels of luminal distinctive marker PSA despite the high levels of PSA in the original tissue. Nonetheless, PSA was noticed in tumor organoids derived from patients (Figure 15). Notably, these expression patterns recapitulated the architecture of prostate tissues where a luminal secretory cell layer expresses prominent levels of AR and PSA, and an underlying basal cell layer expresses p63 but low or indiscernible levels of AR and PSA [17, 18]. Moreover, AMACR is a peroxisomal and mitochondrial enzyme that is not discernible in normal prostate tissues but over-expressed in PCa [222]. This enzyme was only detected in tumor tissue of patients; however, it was absent in the corresponding organoids (Figure 15-18).

Figure 15. Immunophenotype of patient-derived prostate organoids compared with the corresponding tissue specimen. Immuno-histochemistry images of organoids and the corresponding tissue specimens of patient 7 sample with Gleason group A (GS 7 (3+4)) stained with H&E, with the prostate lineage epithelial markers P63, AR, and PSA and the tumor marker AMACR. Scale bars = 50μm. Representative microscopy images were acquired using the Olympus CX41 light microscope 10X objective.

74

Figure 16. Immunophenotype of patient-derived prostate organoids compared with the corresponding tissue specimen. Immuno-histochemistry images of organoids and the corresponding tissue specimens of patient 8 sample with Gleason group A (GS 6) stained with H&E, with the prostate lineage epithelial markers P63, AR, and PSA and the tumor marker AMACR. Scale bars = 50μm. Representative microscopy images were acquired using the Olympus CX41 light microscope objective.

Figure 17. Immunophenotype of patient-derived prostate organoids compared with the corresponding tissue specimen. Immuno-histochemistry images of organoids and the corresponding tissue specimens of patient 18 sample with Gleason group B (GS 7(4+3) stained with H&E, with the prostate lineage epithelial markers P63, AR, and PSA and the tumor marker AMACR. Scale bars = 50μm. Representative microscopy images were acquired using the Olympus CX41 light microscope 10X objective.

Figure 18. Immunophenotype of patient-derived prostate organoids compared with the corresponding tissue specimen. Immuno-histochemistry images of organoids and the corresponding tissue specimens of patient 25 with Gleason group B (GS 7(4+3). stained with H&E, with the prostate lineage epithelial markers P63, AR, and PSA and the tumor marker AMACR. Scale bars = 50μm. Representative microscopy images were acquired using the Olympus CX41 light microscope 10X objective.

77

b. <u>Representative Immunofluorescence Analysis of Patient-derived Organoids</u>

Patient-derived organoids were characterized by assessing the expression of prostate epithelial lineage markers using immunofluorescence analysis. For that, patient-derived organoids were grown and supplemented with human prostate organoids culture medium plus RI for an average of 18 days, then fixed with PFA and embedded in histogel and paraffin, then sectioned and immunostained as described in the methods section. The sections were probed for different markers including the luminal marker CK8, basal markers CK5 and CK14, mesenchymal marker VIM, and stem cell marker SOX2. The expression of luminal CK8 and basal CK5 and CK14 markers confirmed the presence of both prostate epithelial lineages in the established organoid cultures, with organoids expressing only luminal, only basal, or luminal and basal double-positive cells within the same organoid as shown in Figures 19-22. Moreover, luminal CK8-positive cells were detected around a lumen-like and surrounded by basal CK5-positive cells in organoids derived from patient 22 (Figure 20), which recapitulated the histological architecture observed in prostate tissues where each gland is lined with pseudostratified epithelium with three differentiated epithelial cell types; a luminal secretory cell layer expressing distinctive markers including CK8, and surrounded by an underlying basal cell layer expressing the high-molecular-weight keratins CK5 and CK14 [17, 18]. In addition, an intermediate cell population is found referred to as intermediate or transit amplifying cells that co-expresses luminal and basal markers [7, 18]. This population was also detected in organoids including cells that co-express luminal CK8 and basal CK5. Positive nuclear staining of stem cell marker SOX2 was identified in both unaffected and tumor derived organoids which

78

confirms the presence of stem-like/ progenitor cells within the bulk of our patient-derived

organoids (Figure 22).
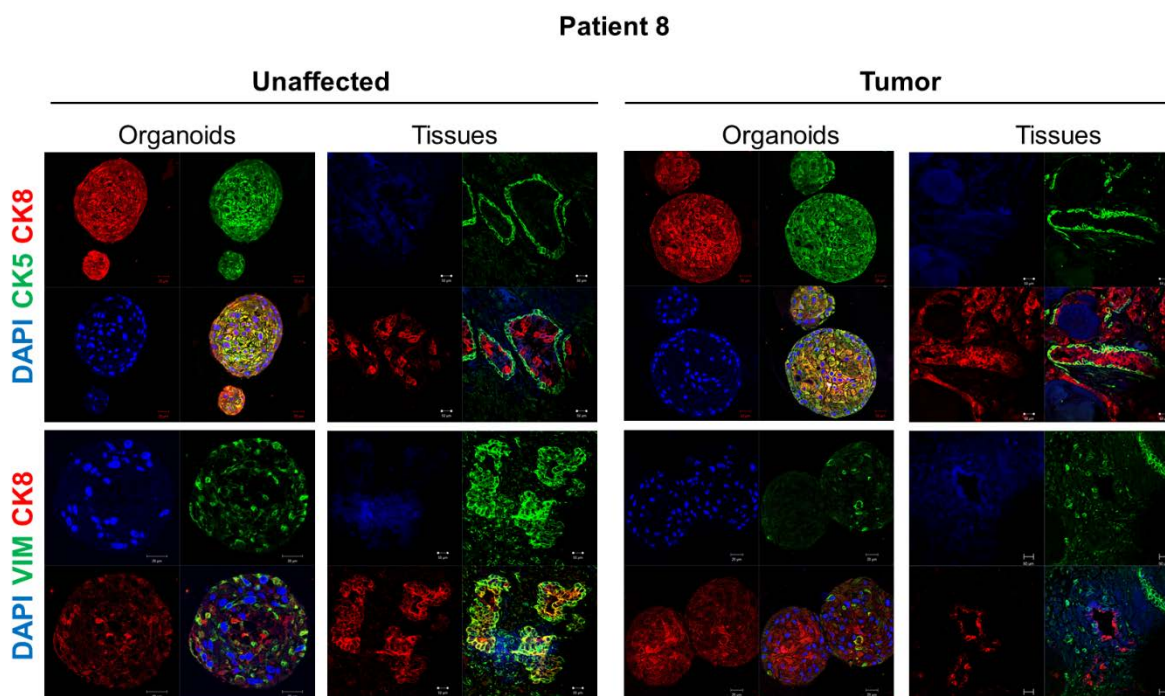
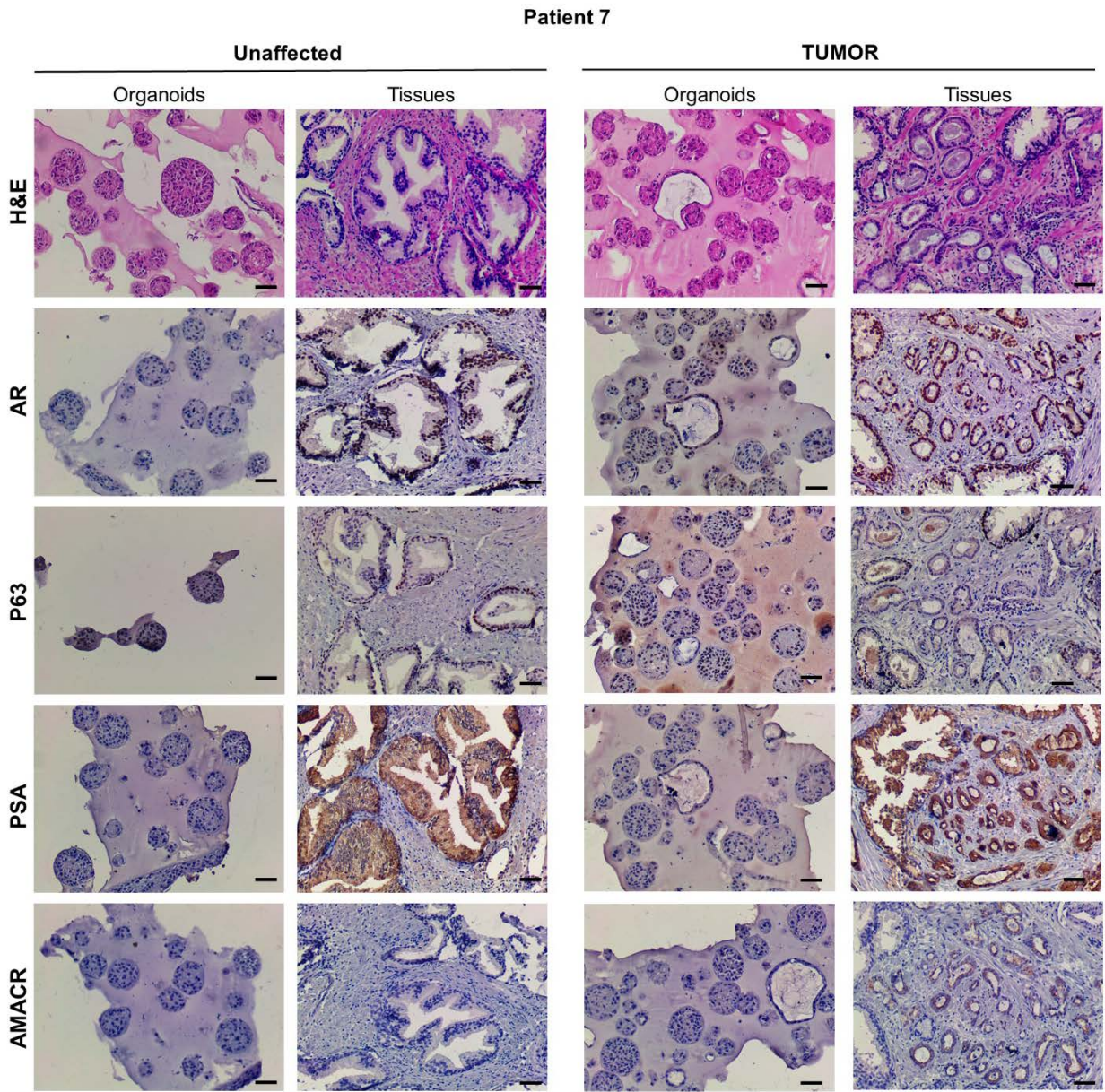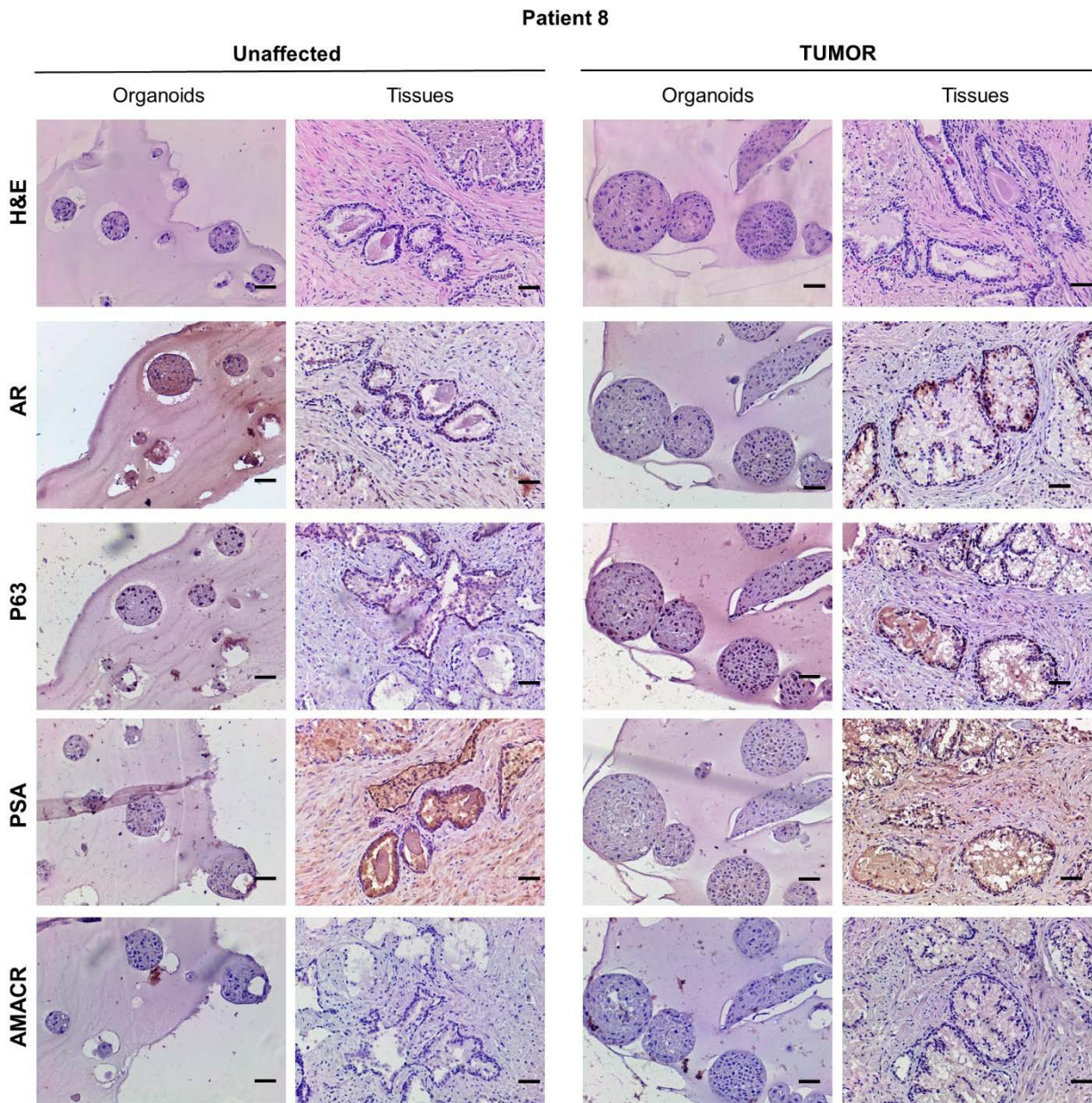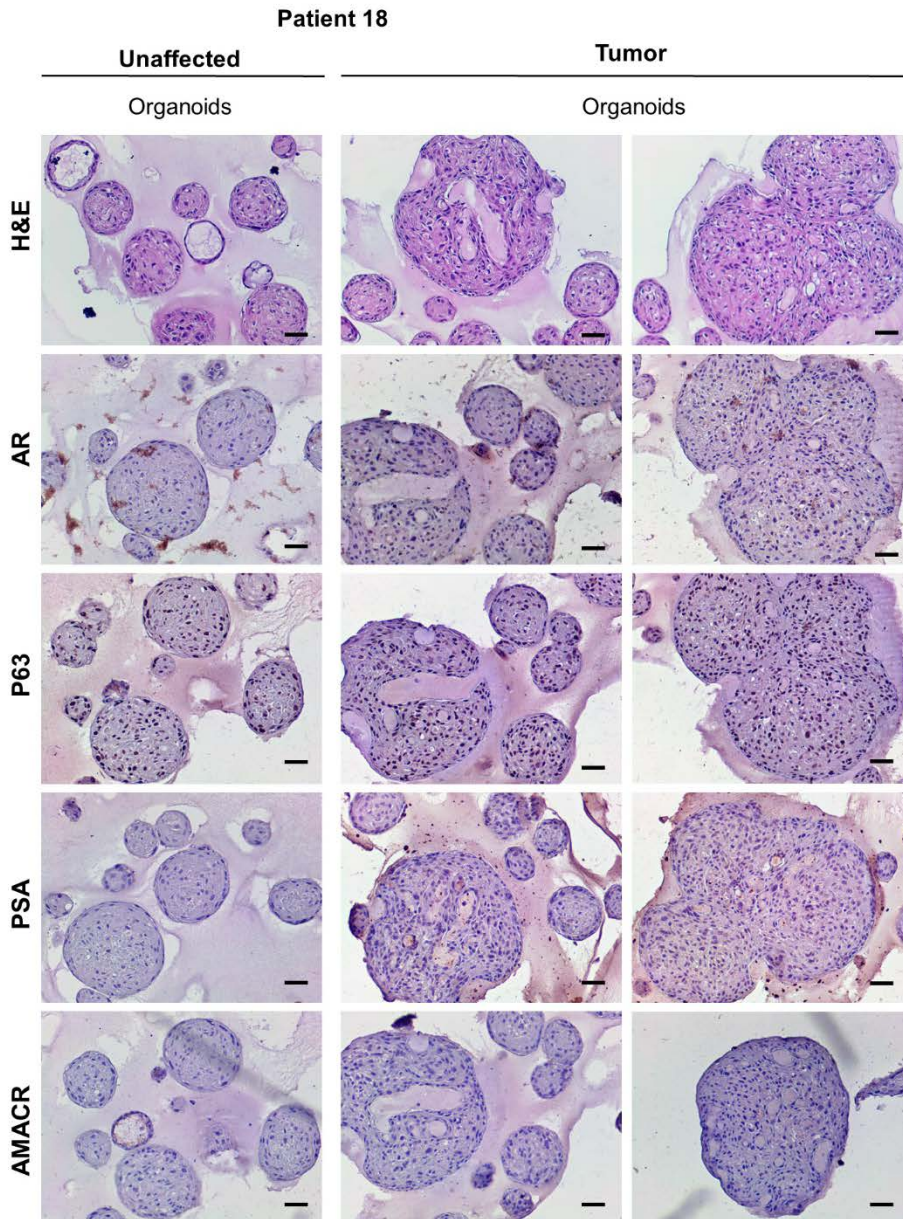**Figure 19. Immunophenotype of patient-derived prostate organoids compared with the corresponding tissue specimen.** Immunofluorescent images of organoids and the corresponding tissue specimens of patient 8 sample with GG A (GS 6) stained with the prostate lineage epithelial markers CK8 and CK5, and the mesenchymal marker VIM. The nuclei were stained with anti-fade reagent Fluorogel II with DAPI. Representative confocal microscopy images were acquired using the Zeiss LSM 710 laser scanning confocal microscope (Zeiss) and images were processed using the Carl Zeiss ZEN 2013 image software.
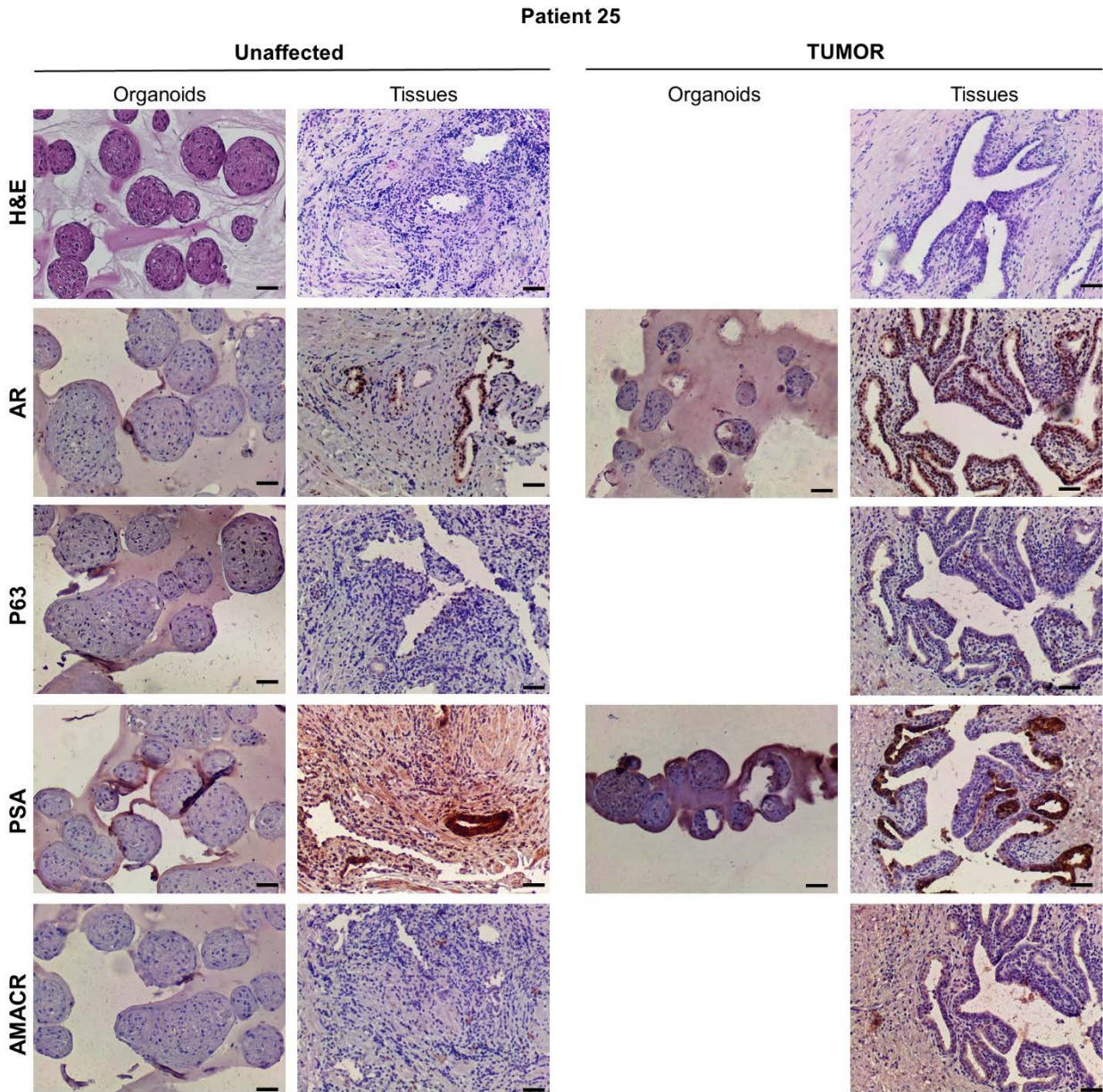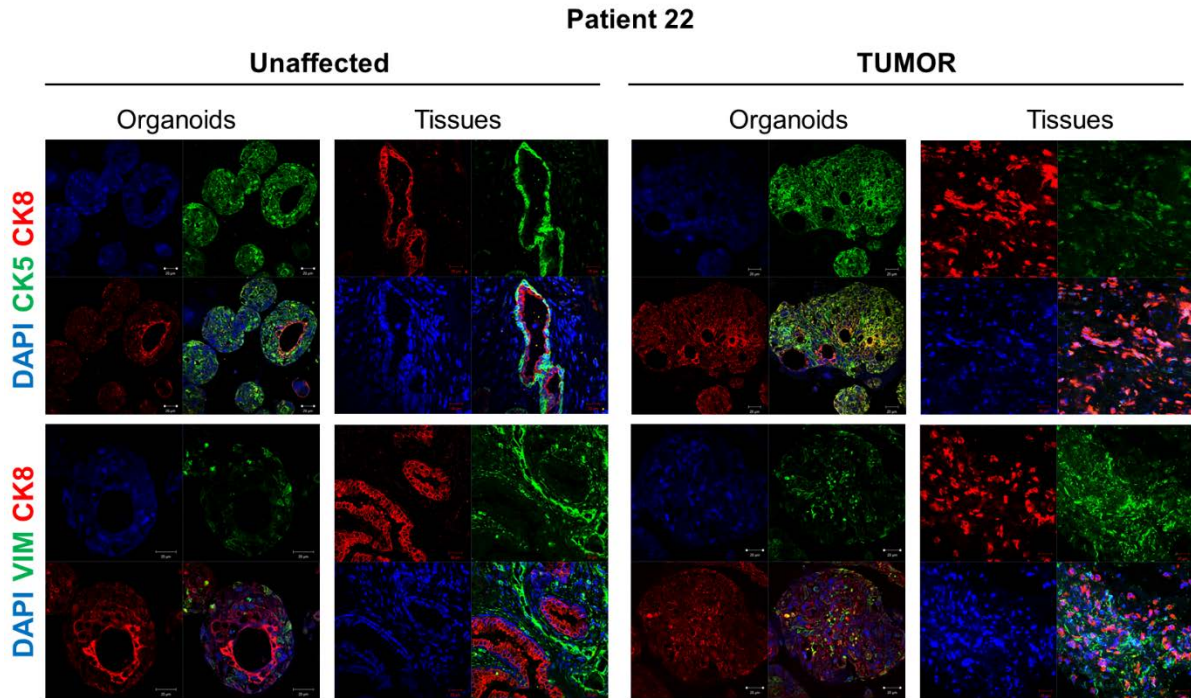
Figure 20. Immunophenotype of patient-derived prostate organoids compared with the corresponding tissue specimen. Immunofluorescent images of organoids and the corresponding tissue specimens of patient 22 sample with GG C (GS 9(5+3)) stained with the prostate lineage epithelial markers CK8 and CK5, and the mesenchymal marker VIM. The nuclei were stained with anti-fade reagent Fluorogel II with DAPI. Representative confocal microscopy images were acquired using the Zeiss LSM 710 laser scanning confocal microscope (Zeiss) and images were processed using the Carl Zeiss ZEN 2013 image software.
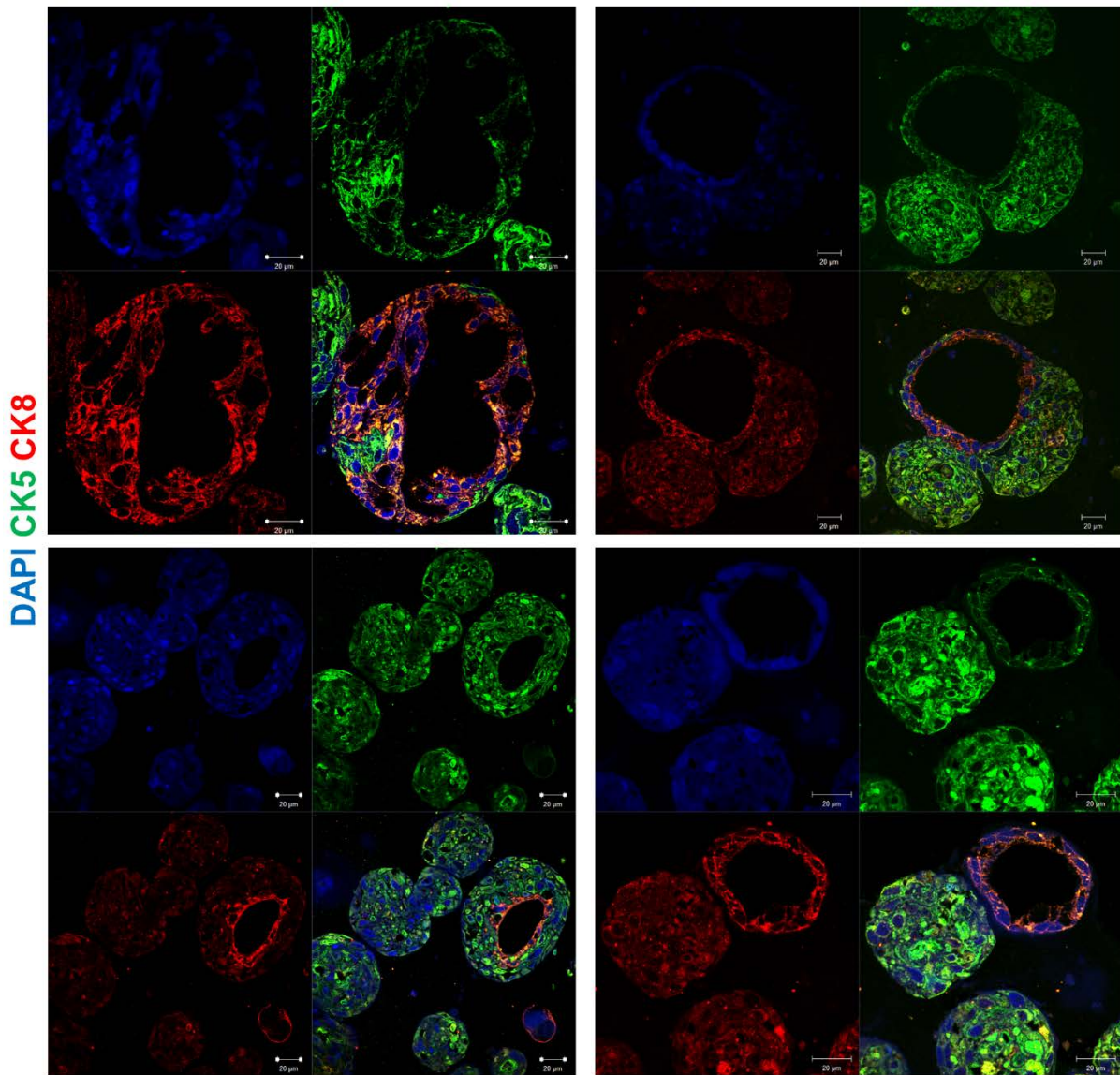
Figure 21. Immunophenotype of patient-derived prostate organoids showing different organoids phenotypes within one sample. Immunofluorescent images of organoids of patient 22 unaffected sample with GG C (GS 9(5+3)) stained with the prostate lineage epithelial markers CK8 and CK5. The nuclei were stained with anti-fade reagent Fluorogel II with DAPI. Representative confocal microscopy images were acquired using the Zeiss LSM 710 laser scanning confocal microscope (Zeiss) and images were processed using the Carl Zeiss ZEN 2013 image software.
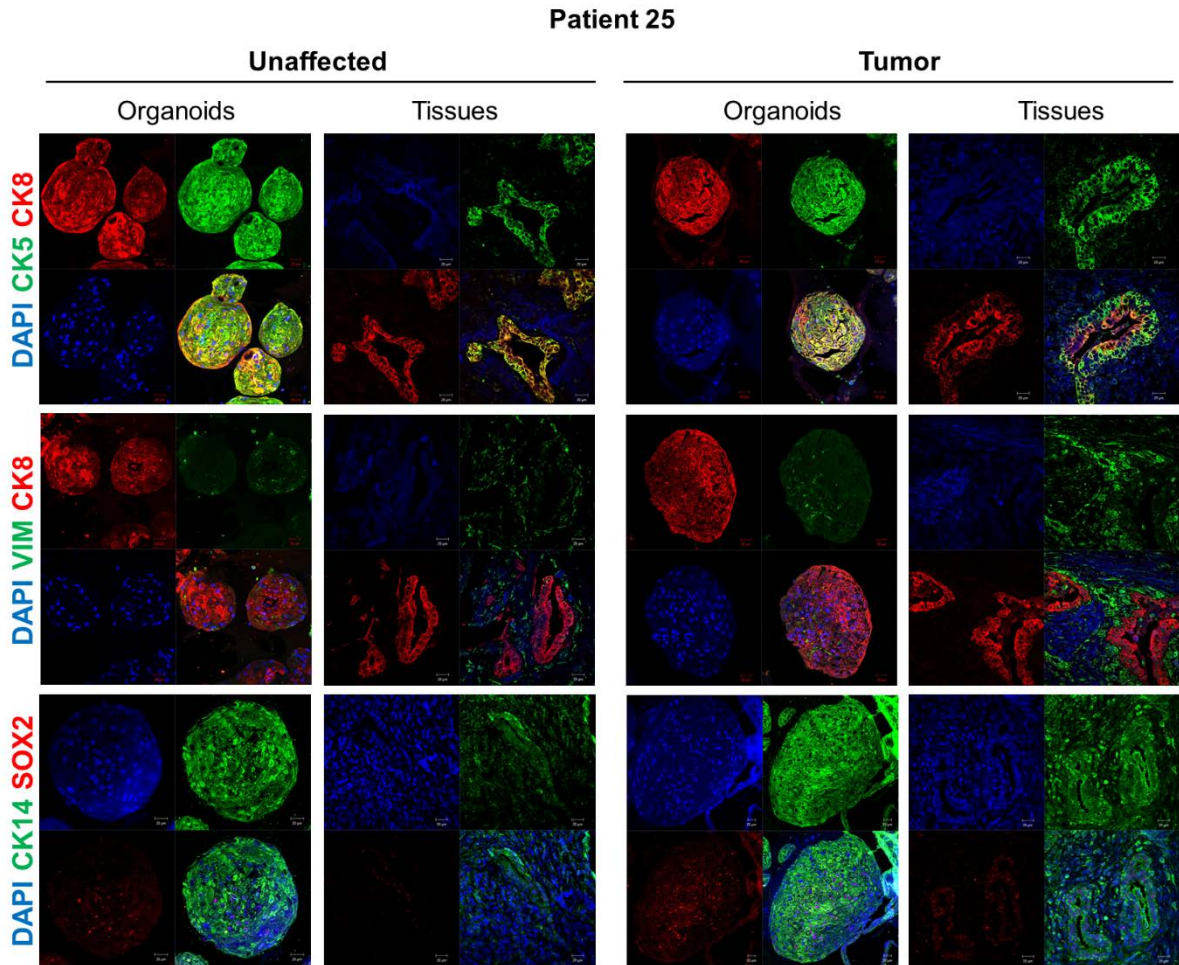
Figure 22. Immunophenotype of patient-derived prostate organoids compared with the corresponding tissue specimen. Immunofluorescent images of organoids and the corresponding tissue specimens of patient 25 sample with GG B (GS 7(4+3)) stained with the prostate lineage epithelial markers CK8 and CK5, the mesenchymal marker VIM, and the stem cell marker SOX2. The nuclei were stained with anti-fade reagent Fluorogel II with DAPI. Representative confocal microscopy images were acquired using the Zeiss LSM 710 laser scanning confocal microscope (Zeiss) and images were processed using the Carl Zeiss ZEN 2013 image software.

3. *The RNA Expression of Selected genes in Organoids vs. Tissues*

RNA expression of selected genes was assessed to evaluate the validity of organoids as a model of the original tissue. In general, a pattern of conserved decreased or increased gene expression was observed when comparing unaffected to tumor tissue and unaffected to tumor organoids. Indeed, for patient 29, with GG A (GS 7(3+4)) an increase of epithelial *CDH1* was detected in both tumor tissue and organoids (Figure 23). An increase in luminal *CK8* expression was detected in tumor organoids when compared with the tumor tissue on one hand and with the unaffected organoids and tissue on the other hand. This increase was accompanied with a decrease in mesenchymal *VIM* in organoids as expected knowing that organoids culture is selective for epithelial cells while the tissue sample includes the stroma and mesenchymal tissue in addition to the glandular epithelial tissue. Nonetheless, the expression of *VIM* is indicative of possible EMT or survival of a mesenchymal component in the culture. Moreover, an increase in the expression of stem cell marker *SOX2* and basal stem cell marker *TP63* was detected in tumor organoids. Similar observations were made for patient 7 with GG A (GS 6(3+3)), however with lower *CDH1* and *SOX2* expression (Figure 24).
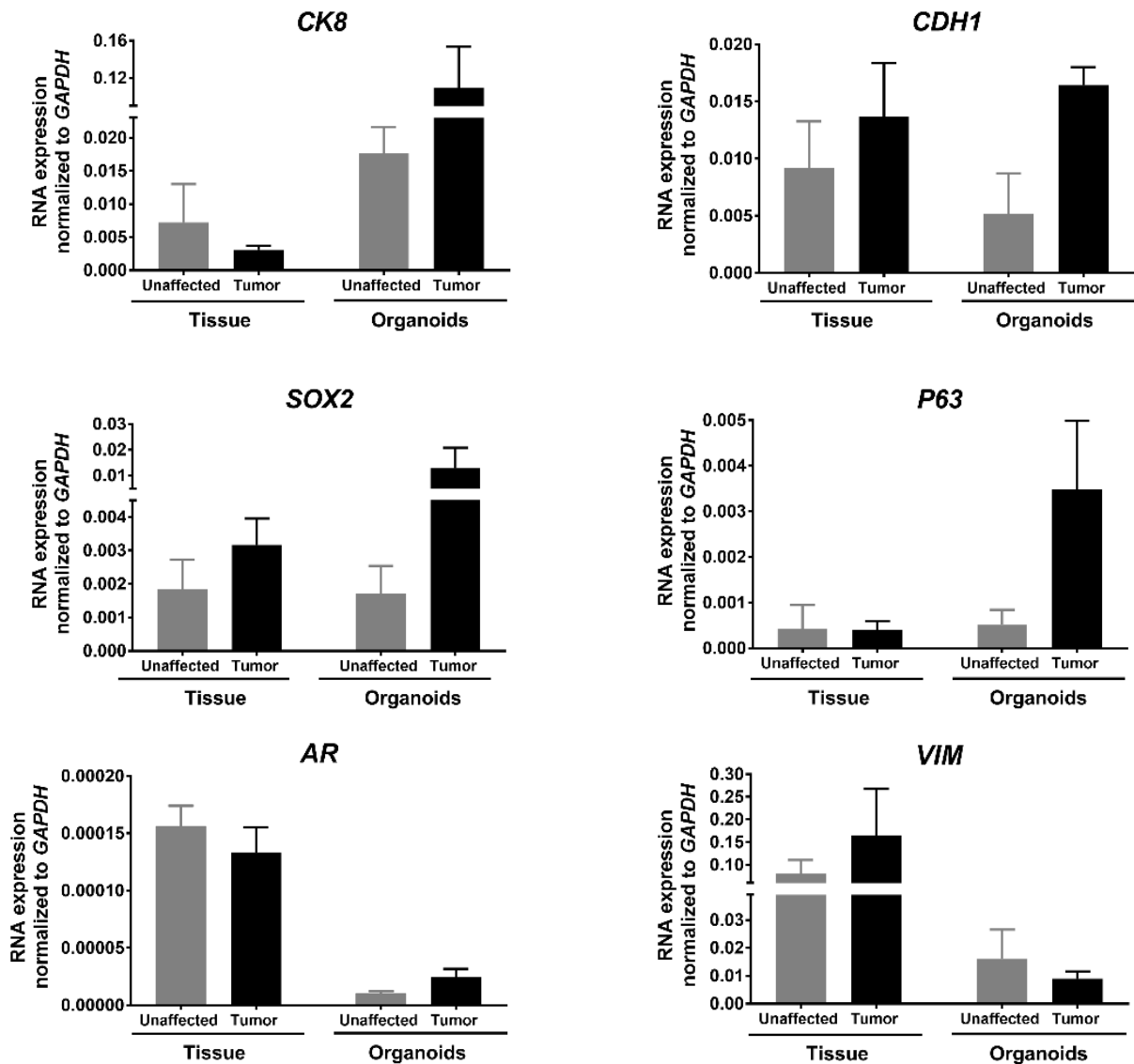
Figure 23. Relative mRNA expression of selected markers to compare organoids with the corresponding tissues of patient 29 with GG A (GS 7(3+4)). The relative mRNA expression of PCa epithelial markers (*CK8*, *CDH1, AR*), mesenchymal markers (*VIM*) and stem cell markers (*SOX2*, *TP63*) was assessed. *GAPDH* expression was used as a reference gene. Average values were reported as mean ± SD (n=3).

84
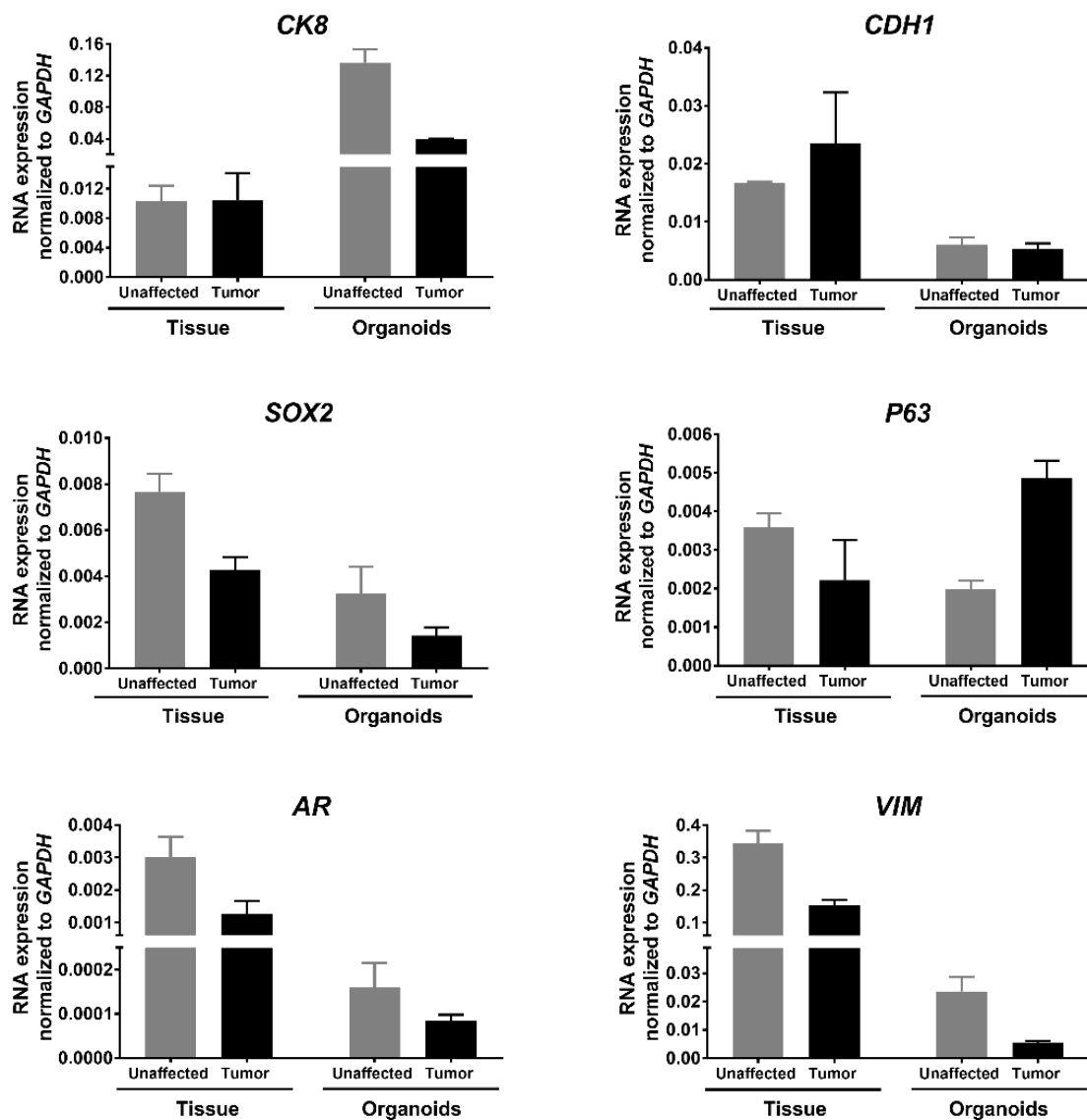
Figure 24. Relative mRNA expression of selected markers to compare organoids with the corresponding tissues of patient 11 with GG A (GS 6(3+3)). The relative mRNA expression of PCa epithelial markers (*CK8*, *CDH1, AR*), mesenchymal markers (*VIM*) and stem cell markers (*SOX2, TP63*) was assessed. *GAPDH* expression was used as a reference gene. Average values were reported as mean ± SD (n=3).

4. *The Use of Established Organoids as Models for Drug assessment*

Cell suspensions derived from freshly digested tissues were plated in Matrigel^{TM} as described in the methods sections. Then, human prostate organoids culture medium was added to each well, in the presence or absence of different drugs in duplicates per treatment to assess the drug effect on the establishment of G1 organoids. Alternatively, G1 organoids were established, then dissociated and propagated to G2, in the presence or absence of different drugs in duplicates per treatment to assess the drug effect on the maintenance of organoids in culture. Drugs tested included the following: Bicalutamide (Bica, 1 and 10uM), Enzalutamide (Enza, 1 and 10uM), and Docetaxel (Doc 0.05, 1 and 50 nM); concentrations were adapted from previously published work by our lab and others [223-225]. We also assessed the effect of radiation therapy on organoids by exposing the organoids on day 1 to 1Gy, 2 Gy or 4 Gy dose. Organoids growth was detected and evaluated by quantifying the number of organoids formed (OFC) and calculating the average size (diameters). The quantification of the average diameter was done by taking images of a minimum of 50 organoids from duplicate wells per condition, and analyzing their sizes using the Carl Zeiss ZEN 2013 image software. The quantification of the OFC was done manually in duplicate wells per condition. Our results show differential drug response between patient samples and between the unaffected and tumor sample of the same patient.

c. <u>Assessing the Effect of Chemotherapy and Irradiation on Organoids Growth</u>

Initially, the potential use of patient-derived PCa organoids was assessed by exposing G2 organoids from 2 different patients, including both the unaffected and tumor sample. After organoids propagation from G1 to G2, dissociated organoids were exposed to a very low dose of chemotherapeutic drug Docetaxel, a taxane that is approved for the treatment of PCa. As for the irradiation, we adapted the dose used in the clinic (2Gy), in addition to half and double the dose. The patients included comprised patient 6 and patient 13 both belong to Gleason group A (GS 7(3+4)). For patient 6, the chemotherapy Doc (0.05 nM) and the different doses of irradiation, showed a highly significant decrease in the size of both unaffected and tumor organoids and a highly significant decrease in the OFC of unaffected organoids only ($P < 0.001$) (Figure 25). Interestingly, for patient 13, the addition of Docetaxel resulted in a significant decrease ($P < 0.05$) in the size of unaffected organoids, while the tumor organoids size and count did not decrease significantly in the presence of Docetaxel. The different doses of irradiation resulted in a significant decrease in both the size and count of both unaffected and tumor organoids ($P < 0.001$) (Figure 26).
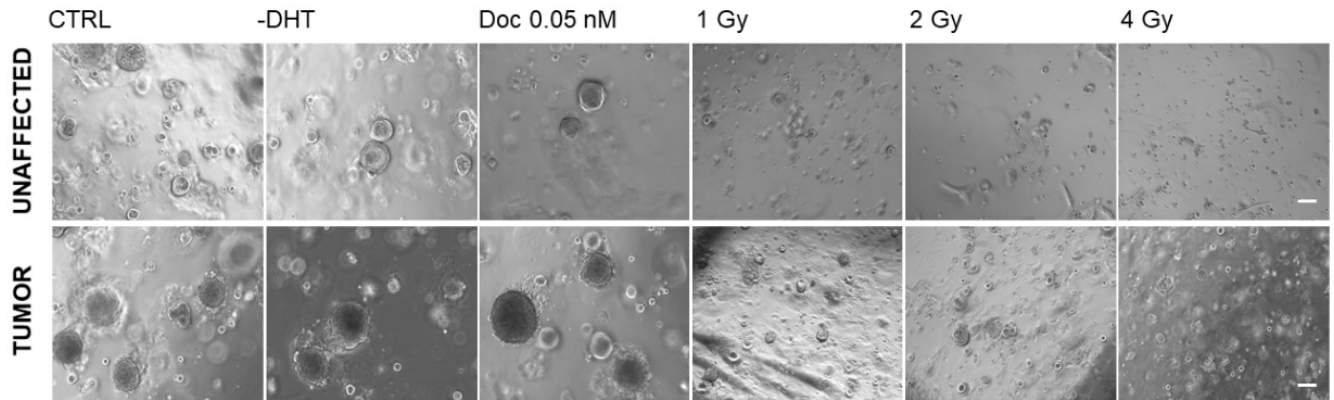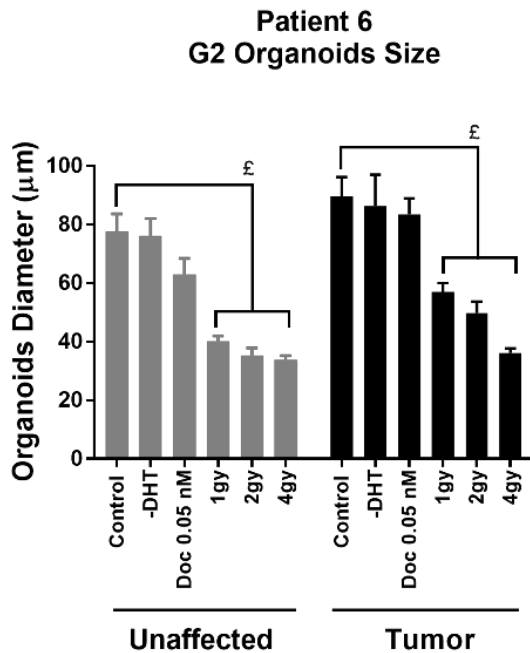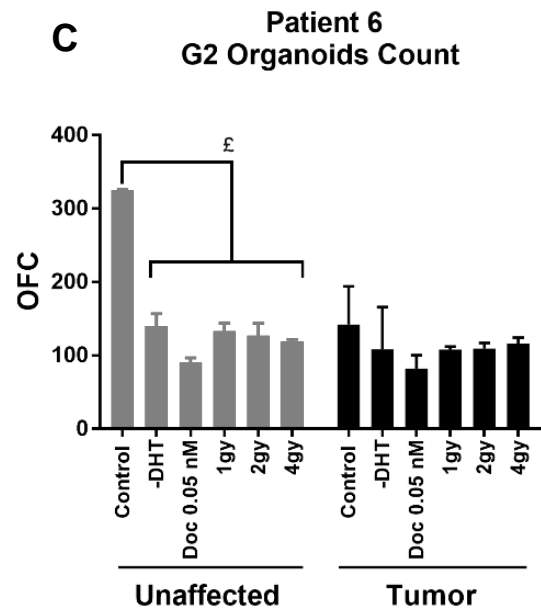
Figure 25. Effect of Docetaxel and different doses of irradiation on G2 organoids growth of patient 6. (A) Representative brightfield images of the unaffected and tumor G2 organoids from patient 6 G2 unaffected and tumor organoids. Scale bar = 100μm. (B) Quantification of the average diameter was done by taking images of a minimum of 50 organoids from duplicate wells per condition. Average values were reported as mean ± SEM. (C) OFC was calculated in duplicate wells per condition. Average values were reported as mean ± SD (*p<0.001*; Two-way ANOVA; £ *P* < 0.001; different conditions compared to the CTRL, Bonferroni's multiple comparisons test).
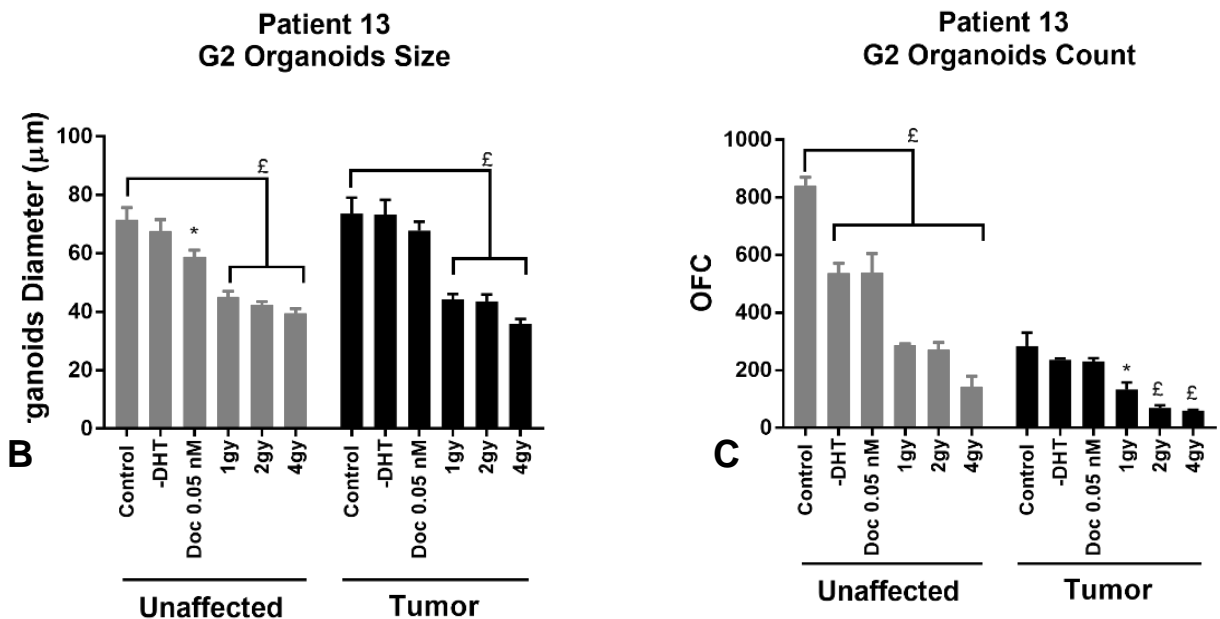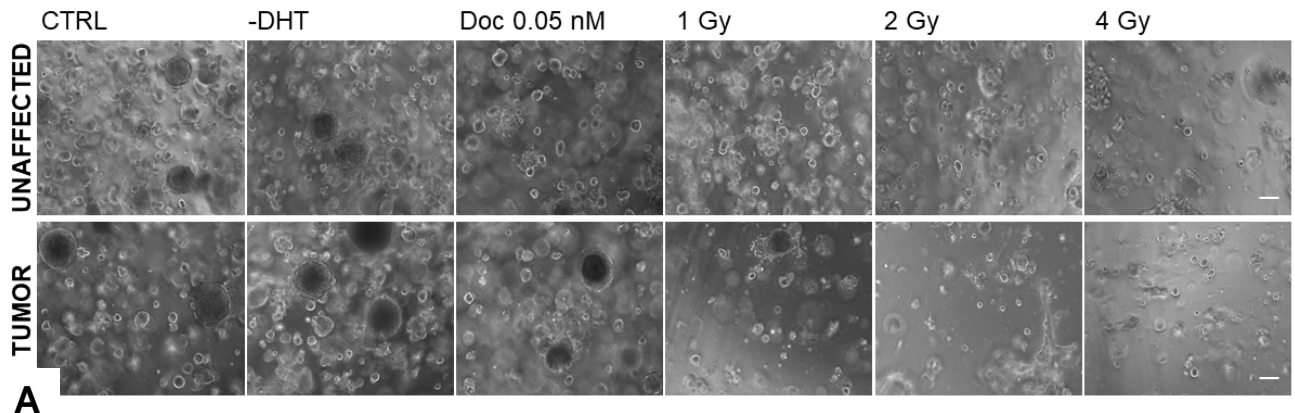
Figure 26. Effect of Docetaxel and different doses of irradiation on G2 organoids growth of patient 13. (A) Representative brightfield images of the unaffected and tumor G2 organoids from patient 13 G2 unaffected and tumor organoids. Scale bar = 100µm. (B) Quantification of the average diameter was done by taking images of a minimum of 50 organoids from duplicate wells per condition. Average values were reported as mean ± SEM. (C) OFC was calculated in duplicate wells per condition. Average values were reported as mean ± SD ($p<0.001$; Two-way ANOVA; * $P<0.05$, £ $P < 0.001$; different conditions compared to the CTRL, Bonferroni's multiple comparisons test).

d. <u>Assessing the Effect of Chemotherapy and Androgen-Deprivation Therapies</u>

To further investigate the potential use of organoids as a model for drug assessment, we included androgen deprivation therapies. We assayed the effect of first generation AR antagonist Bicalutamide and second-generation AR antagonist Enzalutamide alone, or in combination with chemotherapeutic drug Docetaxel. Cell suspensions derived from freshly digested tissues were plated as organoids in the presence or absence of these different drugs in duplicates. G1 organoids from 3 different patients, including both the unaffected and tumor sample, were maintained under these conditions. The patients included comprised patient 21 and patient 32 both belong to GG B (GS 7(4+3)) and patient 22 who belongs to GG C (GS 9(5+4)). The culture medium (with or without the respective drug) was changed every 2-3 days, and organoids growth was assessed after 18-22 days. For patient 21 unaffected sample, the different drugs assayed showed a highly significant decrease of both the size and count of organoids ($P < 0.001$). While, for the tumor sample, Bicalutamide (1 µM) failed at eliciting a significant decrease in the count of organoids, and Enzalutamide (1 µM) did not result in a significant decrease in both the size and the count of organoids. Nonetheless, the addition of Enzalutamide (1 µM) to Docetaxel (1 nM) enhanced the effect of the latter and resulted in additional decrease of both size ($P < 0.001$) and count ($P<0.01$) of organoids (Figure 27 A- C). For patient 22, Bicalutamide (1 and 10 µM) and Docetaxel (1nM) failed at inducing a significant decrease in the size of tumor organoids (Figure 28). On the contrary, for patient 32, the addition of Bicalutamide (1 and 10 µM) resulted in a significant decrease in the tumor organoids size ($P < 0.001$ and $P<0.05$), similarly both Enzalutamide (1 µM) and Docetaxel (1 nM) did not affect the growth (size and OFC) of

organoids from both unaffected and tumor samples. Indeed, only the combination of

Enzalutamide (1 µM) and Docetaxel (1 nM) together resulted in a highly significant

decrease of size and count of organoids of both unaffected and tumor samples of patient 32

($P < 0.001$) (Figure 29).

A

UNAFFECTED

CTRL | No DHT | Doc 50nM | Doc 1nM

Bica 10 µM | Bica 1 µM | Enza 10 µM | Enza 1 µM | Enza 1 µM + Doc 0,5 nM

TUMOR

CTRL | No DHT | Doc 50nM | Doc 1nM

Bica 10 µM | Bica 1 µM | Enza 10 µM | Enza 1 µM | Enza 1 µM + Doc 0,5 nM

B

**Patient 21
G1 Organoids Size**

£

Organoids Diameter (µm)

100
80
60
40
20
0

Control | No DHT | Bica 10 | Bica 1 | Enza 10 | Enza 1 | Doc 1 | Enz 1 + Doc 1

£ £ * £ £

Unaffected   Tumor

92

C

**Patient 21
G1 Organoids Count**

£

OFC

600
400
200
0

Control | No DHT | Bica 10 | Bica 1 | Enza 10 | Enza 1 | Doc 1 | Enz 1 + Doc 1

**

* ** * **

Unaffected   Tumor

Figure 27. Effect of Chemotherapy and Androgen-Deprivation Therapies on G1 patient 21-derived organoids growth. (A) Representative brightfield images of the unaffected and tumor G1 organoids from patient 21 grown in the presence or absence of different drugs, or drug combinations. Scale bar= 100µm**.** (B) Quantification of the average diameter was done by taking images of a minimum of 50 organoids from duplicate wells per condition. Average values were reported as mean ± SEM. (C) OFC was calculated in duplicate wells per condition. Average values were reported as mean ± SD (*p<0.001*; Two-way ANOVA; * *P<0.05*, ** *P<0.01*, £ *P < 0.001*; different conditions compared to the CTRL, Bonferroni's multiple comparisons test).

UNAFFECTED

| CTRL | No DHT | Doc 50nM | Doc 1nM |

| Bica 10 μM | Bica 1 μM | Enza 10 μM | Enza 1 μM | Enza 1 μM + Doc 0,5 nM |

TUMOR

| CTRL | No DHT | Doc 50nM | Doc 1nM |

| Bica 10 μM | Bica 1 μM | Enza 10 μM | Enza 1 μM | Enza 1 μM + Doc 0,5 nM |
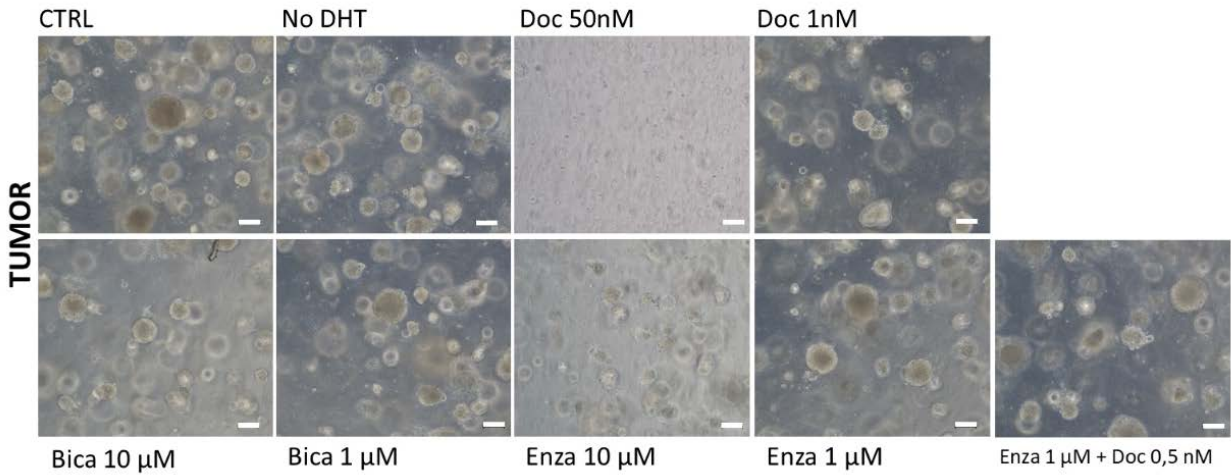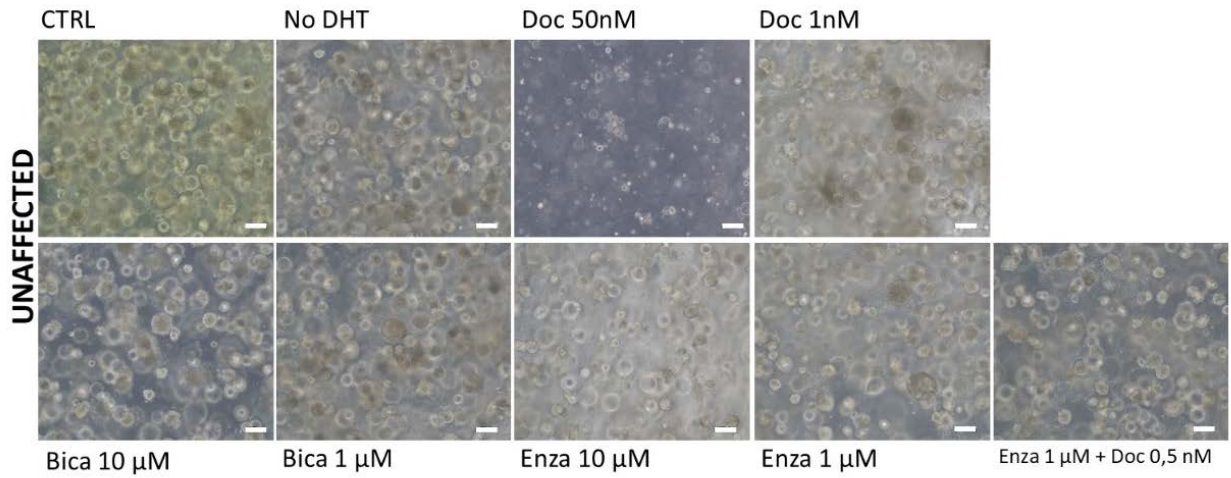
Patient 22
G1 Organoids Size

Patient 22
G1 Organoids Count

A

94
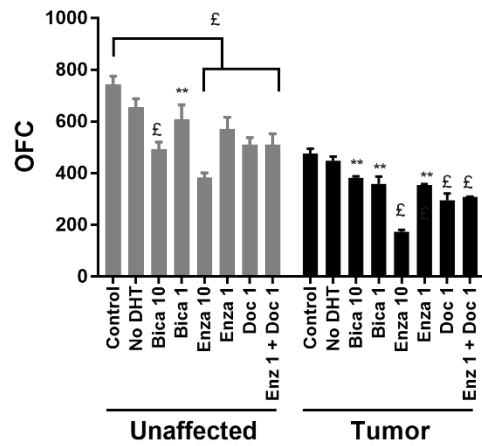
Figure 28. Effect of Chemotherapy and Androgen-Deprivation Therapies on G1 patient 22-deived organoids growth. (A) Representative brightfield images of the unaffected and tumor G1 organoids from patient 21 grown in the presence or absence of different drugs, or drug combinations. Scale bar= 100µm. (B) Quantification of the average diameter was done by taking images of a minimum of 50 organoids from duplicate wells per condition. Average values were reported as mean ± SEM. (C) OFC was calculated in duplicate wells per condition. Average values were reported as mean ± SD (*p<0.001*; Two-way ANOVA; ** *P<0.01*, £ *P<0.001*; different conditions compared to the CTRL, Bonferroni's multiple comparisons test).

A

Patient 32
G1 Organoids Size

B

Patient 32
G1 Organoids Count

Figure 29. Effect of Chemotherapy and Androgen-Deprivation Therapies on G1 patient 32-derived organoids growth. (A) Quantification of the average diameter was done by taking images of a minimum of 50 organoids from duplicate wells per condition. Average values were reported as mean ± SEM. (B) OFC was calculated in duplicate wells per condition. Average values were reported as mean ± SD (*p<0.001*; Two-way ANOVA; * *P<0.05*, £ *P < 0.001*; different conditions compared to the CTRL, Bonferroni's multiple comparisons test).

C. Updating the Patient-Derived Prostate Organoid Culture Systems

1. *Withdrawal of NAC, NOG, and A83 individual components from the pool of prostate organoid culture components significantly reduces organoids' growth*

a. Effect of withdrawal of individual factors from the bulk pool of candidate organoid culture components on organoids growth and maintenance

Knowing the complexity of the growth media that is used in culturing Pca patient-derived organoids, we sought to determine the minimal requirement for establishing patient-derived organoids. In that regard, we developed an assay system in which we examined the effect of withdrawal of individual components from the pool of previously employed culture medium components on the formation of PCa organoids. Organoids growth was detected and evaluated by quantifying the organoids forming count (OFC), calculating the average size (diameters) and assessing maintenance in culture (days). We excluded each of the 10 components (NAC, EGF, NOG, RSPO, A83, FGF10, FGF2, PGE2, SB, DHT) from the culture medium, one at a time, and assessed their withdrawal effect on the organoids' formation efficiency. Based on preliminary data and logistic reasons, B27 and nicotinamide were anticipated to be essential and hence excluded from the withdrawal conditions. Of the 10 remaining components, three were found to instigate a robust inhibitory effect on organoids growth upon their individual withdrawal from the bulk culture medium pool, namely NAC, NOG, and A83 (Figure 30). For patient 29, withdrawal of the three aforementioned components significantly decreased the OFC from 317 ± 9.2 organoids in the CTRL unaffected condition to 169 ± 10.6 (-NAC), 220 ± 13.44 (-NOG), and

96

211±17.68 (-A83) organoids, and from 405±14.14 organoids in the CTRL tumor condition to 227±19.1 (-NAC), 259±10.61 (-NOG), and 328±23.34 (-A83) organoids (Figure 30 B) (p<0.0001), upon withdrawal of NAC, NOG, and A83. Similar effect was observed on the size of cultured organoids where diameters were significantly reduced from 109.98±4.51 µm in the CTRL unaffected condition to 77.59±2.80 µm (-NAC), 74.24±2.48 µm (-NOG), and 90.57±2.68 µm (-A83) (p<0.0001), and from 94.56±3.30 µm in the CTRL tumor condition to 79.68±2.59 µm (-NAC; p<0.01), 78.19±2.24 µm (-NOG; p<0.01), and 86.30±2.39 µm (-A83; p=0.55) (Figure 30 B), upon withdrawal of NAC, NOG, and A83.

A

B

Patient 29
G1 Organoids Size

C

Patient 29
G1 Organoids Count
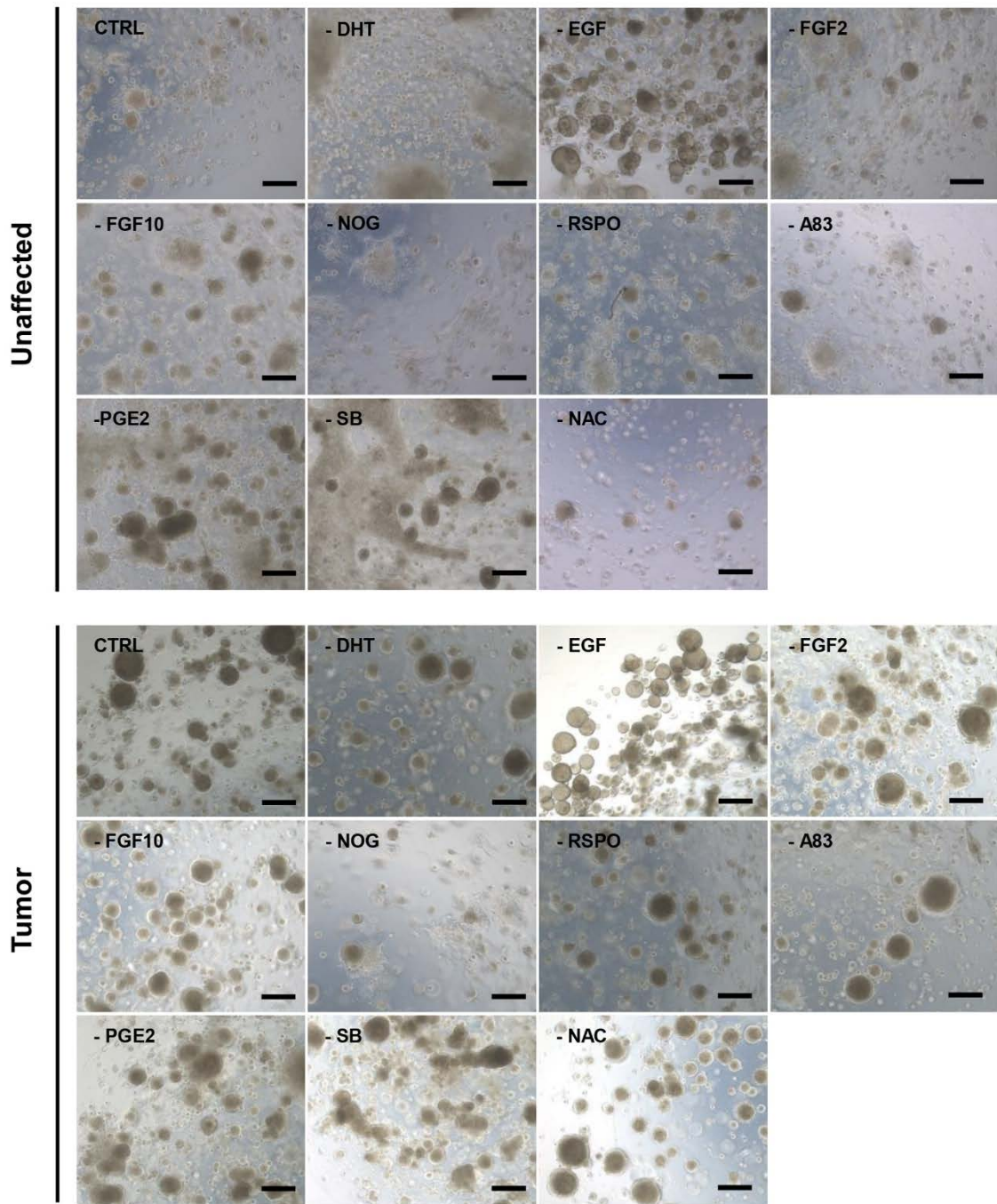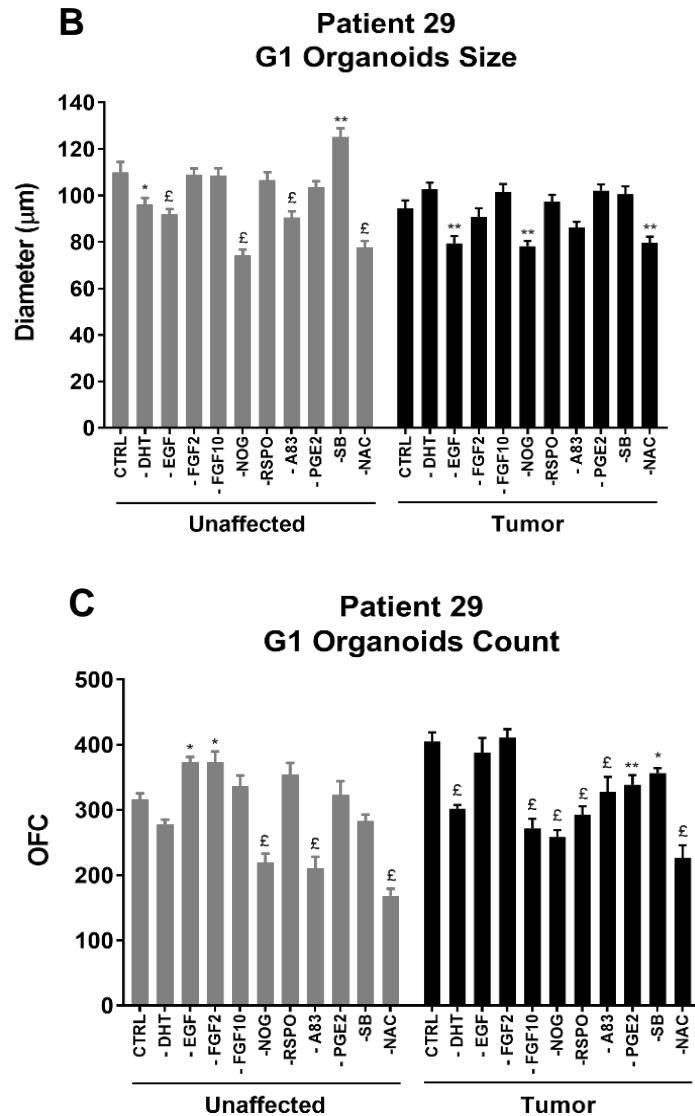
Figure 30. Effect of withdrawal of individual factors from the bulk pool of candidate organoid culture components on organoids growth and maintenance of patient 29. (A) Representative brightfield images of the unaffected and tumor G2 organoids from patient 29. Organoids were grown in AdDMEM/F12 including all 12 components as described in Table 1 (CTRL) or upon withdrawal of each of the components, one at a time. Scale bar = 200 μm. (B) Quantification of the average diameter of G1 unaffected and tumor organoids was done by taking images of a minimum of 50 organoids from duplicate wells per condition using the Carl Zeiss ZEN 2013 image software. Average values were reported as mean ± SEM. (C) OFC was calculated in duplicate wells per condition. Average values were reported as mean ± SD (*p<0.001*; Two-

99

way ANOVA; * *P*<0.05, ** *P*<0.01, £ *P* < 0.001; different conditions compared to the CTRL, Bonferroni's multiple comparisons test).

  b. <u>Confirmation of the effect of withdrawal of individual factors from the bulk pool of candidate organoid culture components on organoids growth and maintenance of patient 27 and patient 31 samples.</u>

This effect was prominent in all three patients (**Figure 33**), for both the unaffected and tumor organoids. Patients 27 and 31 demonstrated comparable effects, and results were consistent with those observed with patient 29, as shown in **Figures 31 and 32**. Therefore, we hypothesized that the 5 factors (NAC, NOG, A83, B27, and nicotinamide) are essential and comprise a minimal requirement for the establishment of patient-derived prostate organoids.
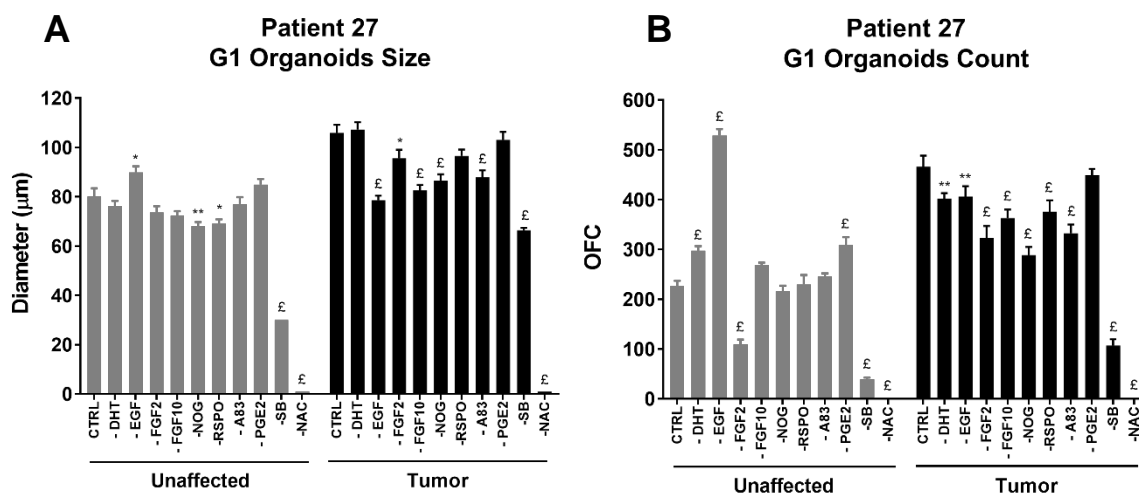
Figure 31. Effect of withdrawal of individual factors from the bulk pool of candidate organoid culture components on organoids growth of patient 27. (**A**) Quantification of the average diameter of G1 unaffected and tumor organoids was done as previously described and average values were reported as mean ± SEM. (**B**) OFC was calculated as previously described and average values were reported as mean ± SD (*p<0.001*; Two-way ANOVA; ** *P*<0.01, £ *P* < 0.001; different conditions compared to the CTRL, Bonferroni's multiple comparisons test).

100

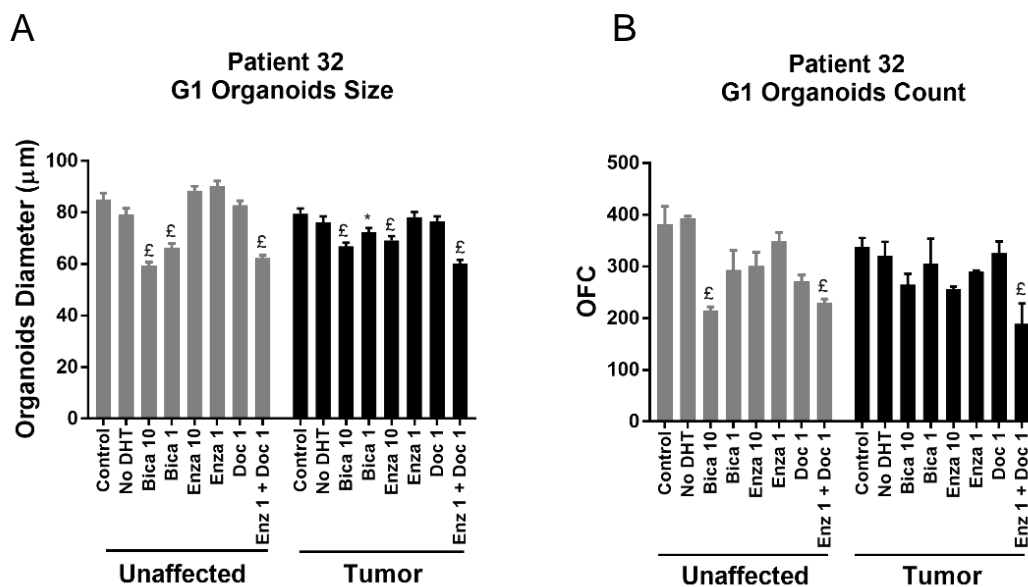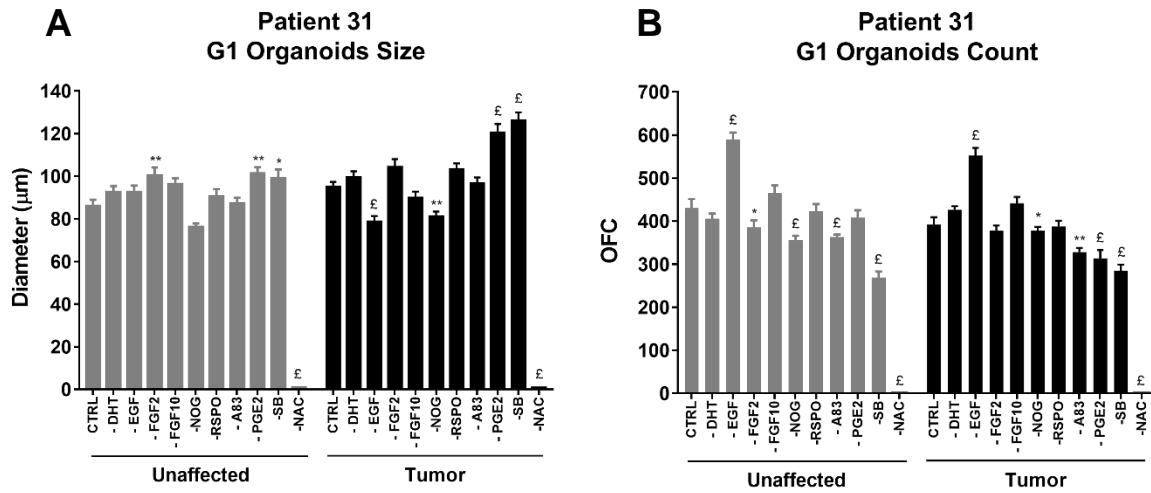**Figure 32. Effect of withdrawal of individual factors from the bulk pool of candidate organoid culture components on organoids growth and maintenance of patient 31. (A)** Quantification of the average diameter of G1 unaffected and tumor organoids was done as previously described and average values were reported as mean ± SEM. **(B)** OFC was calculated as previously described and average values were reported as mean ± SD ($p<0.001$; Two-way ANOVA; ** $P<0.01$, £ $P < 0.001$; different conditions compared to the CTRL, Bonferroni's multiple comparisons test).
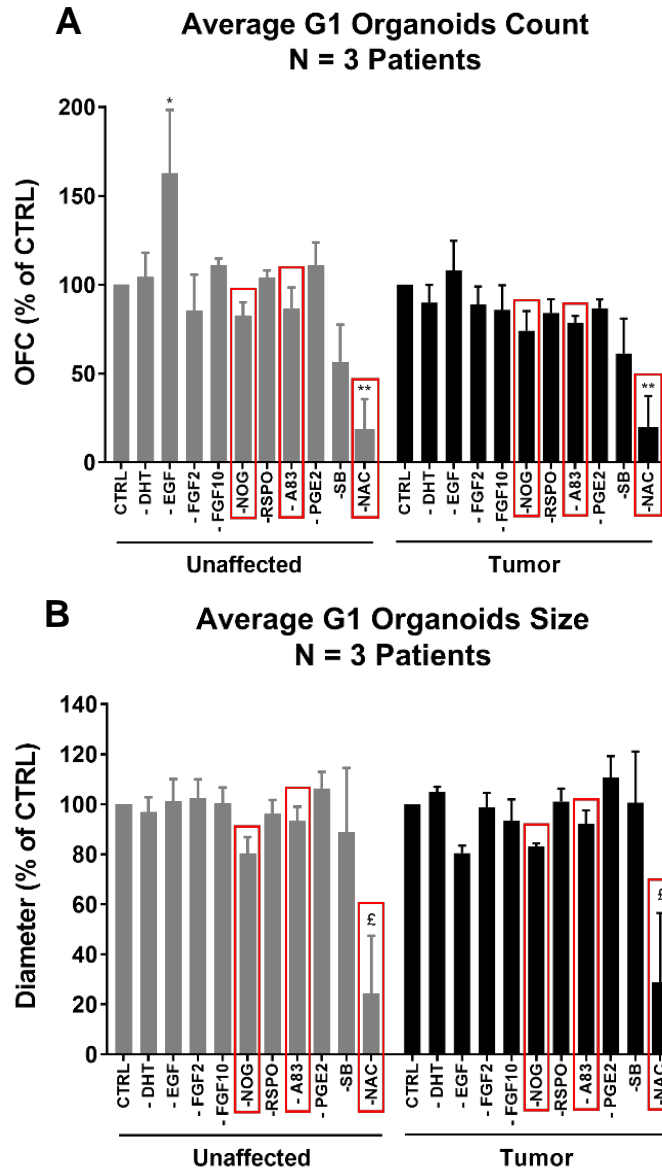
Figure 33. Average effect of withdrawal of individual factors from the bulk pool of candidate organoid culture components on organoids growth and maintenance of all 3 patients. (A) Quantification of the average diameter of all 3 patients G1 unaffected and tumor organoids was done as previously described and average (% of CTRL) values were reported as mean ± SEM. (B) Quantification of OFC of all 3 patients G1 unaffected and tumor organoids was done as previously described and average values (% of CTRL) were reported as mean ± SEM (Two-way ANOVA; * $P<0.05$, ** $P<0.01$, £ $P < 0.001$; different conditions compared to the CTRL, Bonferroni's multiple comparisons test).

2. *The Effect of EGF Withdrawal from the Bulk Pool of Prostate Organoid Culture Components on Organoids Growth and Maintenance*

Interestingly, an increase in the OFC of both unaffected and tumor organoids (G1) was observed upon withdrawal of EGF from the three patients' samples (Figure 33). To validate this effect, we continued cultivating and propagating the organoids of two of our patients, namely patients 1 and 3, under the same factor withdrawal conditions compared to the CTRL. The effect of EGF removal was indeed preserved and maintained wherein only organoids that were grown without EGF survived beyond G3, reaching G7 (an equivalent of 5 months) (Figure 34). Similarly, removal of PGE2 resulted in an increase in the diameter and count of organoids for the three patients 'samples (Figure 33) but did not enhance their maintenance where organoids under this condition (-PGE2) reached at most G3 (Figure 34). In addition, SB removal exerted a positive effect on the diameter of organoids derived from 2 out of 3 patients' samples (Figure 33). Consequently, we hypothesized that these components are negative factors and their effect was further assessed, each alone, in addition to the essential factors (see results below).
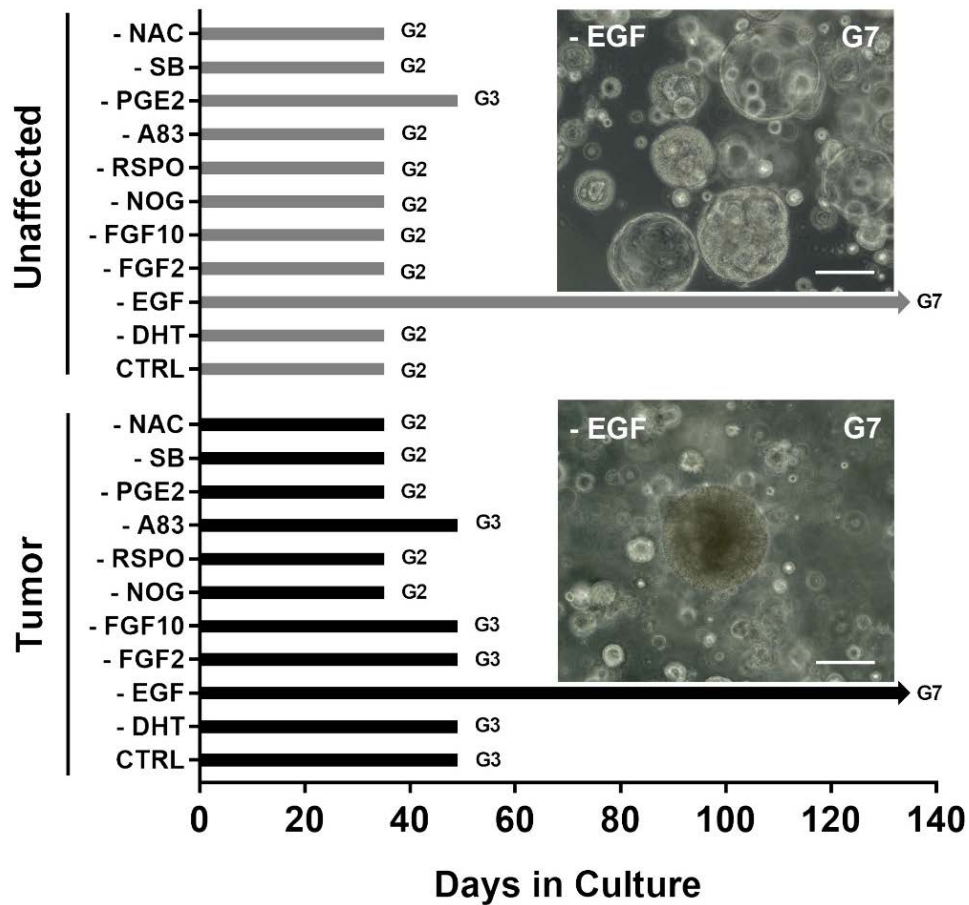
Figure 34. Effect of EGF Withdrawal on long term maintenance of organoids culture. Withdrawal of EGF from the media results in maintenance of both unaffected and tumor organoids beyond G3 and reaching G7 (an equivalent of 5 months). Number of days (and generations) patient 29 unaffected and tumor organoids could be propagated in the absence of the indicated components. Representative brightfield images of the unaffected and tumor G7 organoids from patient 29 grown in AdDMEM/F12 including all components except EGF are shown. Images were visualized by Axiovert inverted microscope from Zeiss at 20x magnification. Scale bar= 100µm.

3. *Combination of the 5 Components (NAC, NOG, A83, B27, and nicotinamide) was Sufficient to Yield Organoids with Higher Efficiency*

To confirm our hypothesis about the ability to grow and maintain patient-derived organoids using only 5 factors (5F) components *(NAC, NOG, A83, B27, and nicotinamide)*, we thawed and cultured frozen P0 patient 1 cells using this minimal medium. Besides, we further validated the role of each of the remaining factors (EGF, RSPO, FGF2, FGF10, PGE2, and SB) in combination with 5F. Interestingly, under 5F condition, organoids diameters and counts increased significantly when compared with the CTRL, where all 12 components were added to the culture medium (Figure 35 A). Addition of RSPO, FGF10, and FGF2 each at a time, further boosted organoids growth; however, presence of 5F alone was enough to enhance the establishment of prostate organoids. Indeed, the OFC increased from 124±12 organoids in the CTRL unaffected condition to 330±2.8 (5F), 280±8.4 (5F+RSPO), 300±10.6 (5F+FGF10), 332±11.3 (5F+FGF2) and from 207±17.6 organoids in the CTRL tumor condition to 394±19.8 (5F), 401.5±10.1 (5F+RSPO), 362±5.7 (5F+FGF10), 409±15.5 (5F+FGF2) (Figure 35 B) (p<0.0001). Similar effect was observed on the size of cultured organoids where diameters significantly increased from 83.43±3.4 µm in the CTRL unaffected condition to 106.67±4.2 µm (5F; p<0.001), 115.74±4.88 µm (5F+RSPO; p<0.0001), 115.31±4.51 µm (5F+FGF10; p<0.0001) and from 79.07±2.95 µm in the CTRL tumor condition to 113.56±4.81 µm (5F; p<0.0001), 117.36±5.04 µm (5F+RSPO; p<0.0001), 103.005±4.79 µm (5F+FGF10; p<0.001), 107.65±4.35 µm (5F+FGF2; p<0.0001) (Figure 35 C).

It is worth mentioning that these organoids were derived from frozen cells of patient 1 where efficiency of organoids formation decreased significantly under the CTRL condition from an OFC of more than 300 organoid with a fresh sample to less than 150 with the frozen cells derived from the same patient specimen, while the 5F medium salvaged the organoids growth from a frozen sample and the OFC was restored to more than 300 organoids.

Interestingly, the addition of EGF, PGE2 and SB, previously predicted as negative components, one at a time to the 5F medium, reduced the OFC and diameter significantly when compared with CTRL condition for tumor samples (p<0.0001). These results further confirm our hypothesis about their negative effect on the culture medium.

A

Unaffected

CTRL | 5F | 5F + RSPO | 5F + FGF10
5F + FGF2 | 5F + SB | 5F + PGE2 | 5F + EGF

Tumor

CTRL | 5F | 5F + RSPO | 5F + FGF10
5F + FGF2 | 5F + SB | 5F + PGE2 | 5F + EGF

B
Patient 29
P0G1 Organoids Size

C
Patient 29
P0G1 Organoids Count
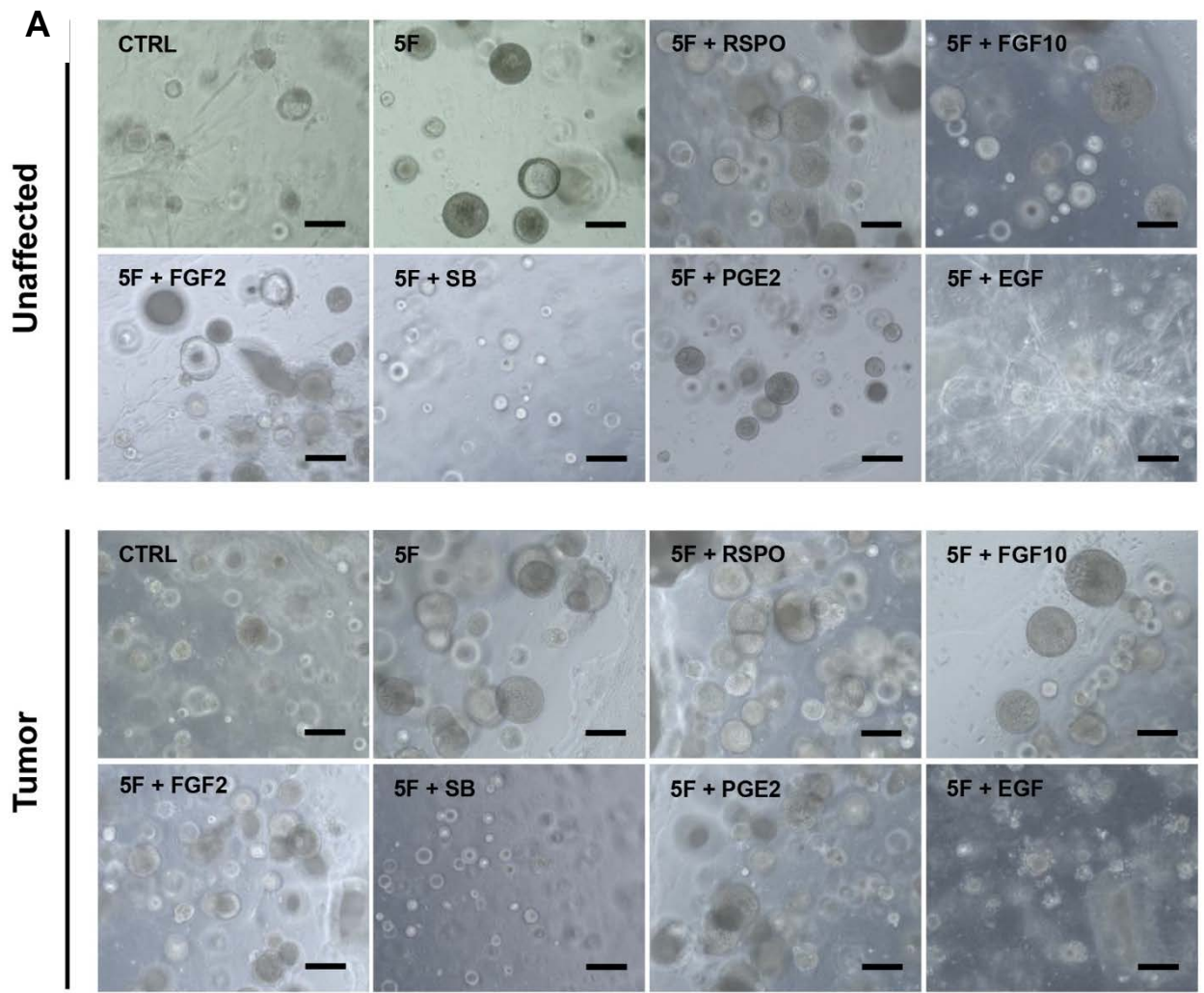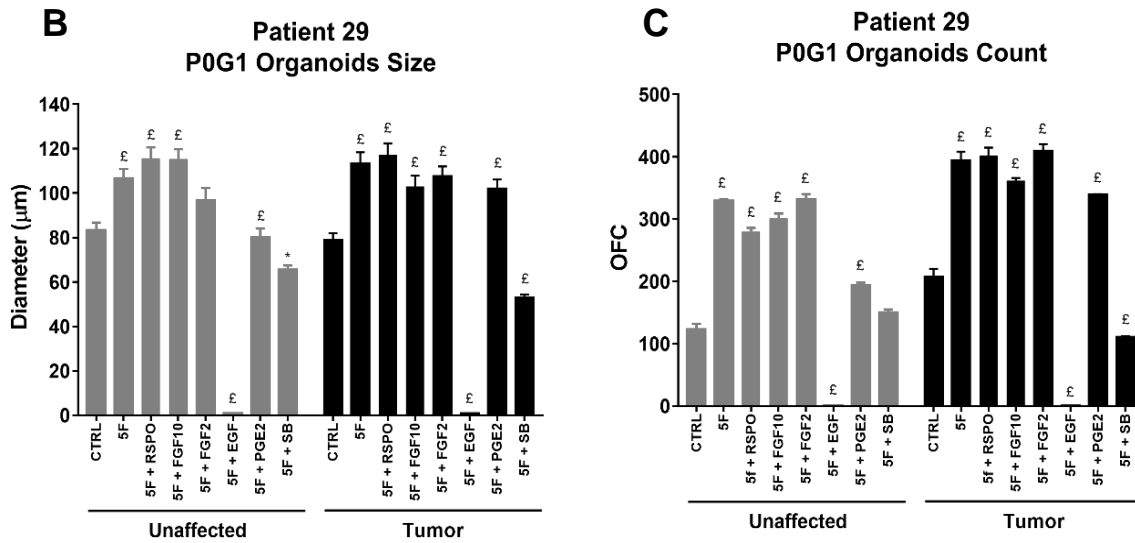
Figure 35. Effect of addition of the individual components (EGF, RSPO, FGF2, FGF10, PGE2, and SB) to the minimal essential 5F components (NAC, NOG, A83, B27, and nicotinamide) on organoids growth. (**A**) Representative brightfield images of the unaffected and tumor organoids from patient 29 grown in AdDMEM/F12 including the 5 minimal essential components (NAC, NOG, A83, B27, and nicotinamide) compared to the CTRL (all 12 components) and upon addition of each of the remaining components one at a time. Scale bar= 100µm. (**B**) Quantification of the average diameter of P0 G1 unaffected and tumor organoids was done as previously described and average values were reported as mean ± SEM. (**C**) OFC was calculated as previously described and average values were reported as mean ± SD (Two-way ANOVA; * $P<0.05$, £ $P < 0.001$; different conditions compared to the CTRL, Bonferroni's multiple comparisons test).

108

4. *FGF10 is an Essential Factor for Long-Term Maintenance in Culture*

The addition of FGF10 to the 5F components seems essential for long-term maintenance beyond G5. Organoids reaching G5 in the presence of FGF10 in addition to 5F reached a size of 350 µm while organoids growing under 5F only reached a maximum size of 150 µm **(Figure 27).** Knowing that FGF10 is an essential growth factor for prostate development [186], we hypothesize that FGF10 is an essential component in this culture system that should be added to the 5F components for the maintenance of long-term culture of organoids in vitro.
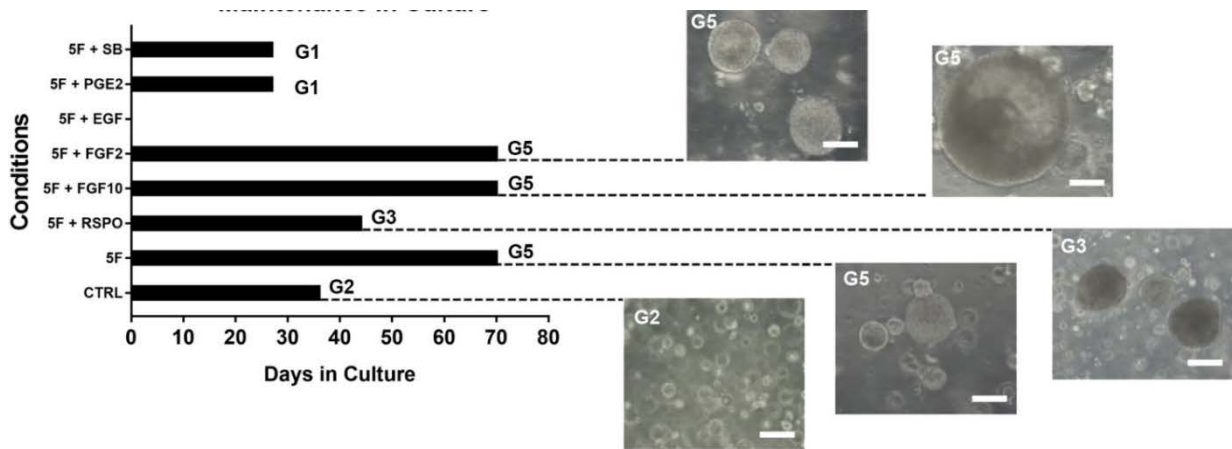
 Figure 36. Effect of addition of the individual components (EGF, RSPO, FGF2, FGF10, PGE2, and SB) to the minimal essential 5F components (NAC, NOG, A83, B27, and nicotinamide) on organoids maintenance. Number of days (and generations) patient 29 tumor organoids could be propagated in the presence of the 5 minimal essential components (NAC, NOG, A83, B27, and nicotinamide) compared to the CTRL (all 12 components) and upon addition of each of the remaining components (EGF, RSPO, FGF2, FGF10, PGE2, and SB), one at a time. Representative brightfield images of the tumor organoids reaching G2, G3, and G5 are shown. Images were visualized by Axiovert inverted microscope from Zeiss at 20x magnification. Scale bar= 100µm.

5. *Immunocharacterization of Prostate Organoids upon Medium Optimization*

The expression of luminal CK8 and basal CK14 markers confirmed the presence of both prostate epithelial lineages in the established organoid cultures, with organoids expressing only luminal, only basal, or luminal and basal double-positive cells within the same organoid as shown in Figure 37 A. Co-expression of both stem cell markers, CD44 and CD49f, has been shown to identify putative prostate stem-like cells [226, 227]. Positive staining of CD44 and CD49f stem cell markers further reinforced the existence of stem-like cells within the bulk of our patient-derived organoids (Figure 37 B). Organoids from the different conditions displayed a heterogeneous population of cells displaying intermediate cytokeratin profiles. Co-expression of CD44 and CD49f was also detected, mainly upon addition of FGF2, FGF10, and PGE2 to the 5F components.
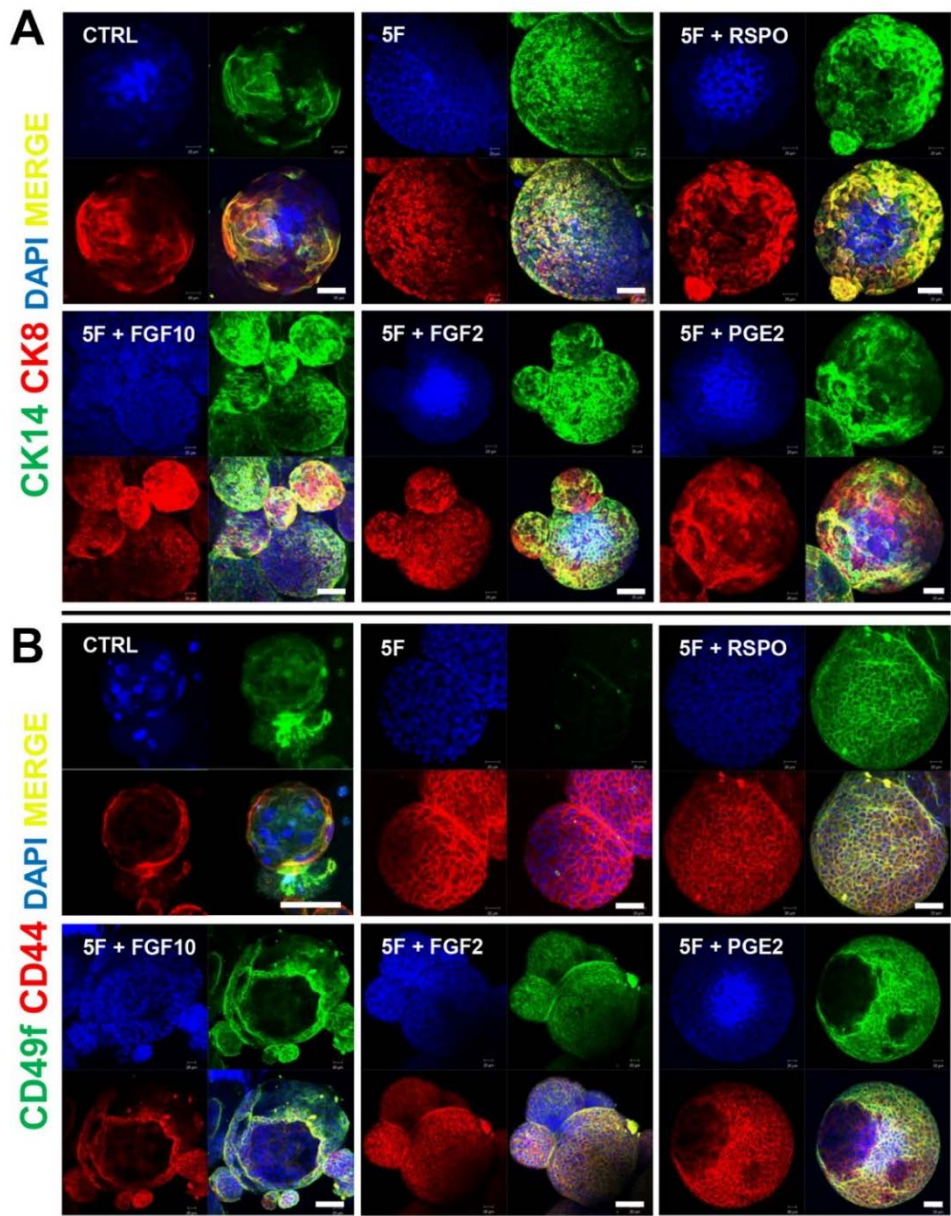
Figure 37. Immunophenotype of prostate tumor organoids upon addition of the individual components (EGF, RSPO, FGF2, FGF10, PGE2, and SB) to the minimal essential 5F components. Immunofluorescent images of tumor P0 G1 organoids from patient 29 stained with the prostate lineage epithelial markers CK8 and CK14 **(A)**, and stem cell markers CD44 and CD49f **(B)**. The nuclei were stained with anti-fade reagent Fluorogel II with DAPI. Scale bars = 40μm. Representative confocal microscopy images were acquired using the Zeiss LSM 710 laser scanning confocal microscope (Zeiss) at 40x oil objective, and images were processed using the Carl Zeiss ZEN 2013 image software.

111

D. Generation of Novel Patient-Derived Prostate Cell Lines

1. *Establishment and Maintenance of 2D Cells in Culture*

The scarcity of human prostate cancer cell lines has always hindered our understanding of the disease etiology and progression, and therefore the need for novel cell lines representing the heterogeneity of the disease is of eminent importance. Along those lines and starting from organoids, human prostate 2D cell lines (unaffected/normal and tumor) were generated using the same culture media used to culture 3D organoids. To optimize the culture conditions, we attempted using different matrices including 1% Matrigel^{TM} and 1% collagen I (Figure 38). Interestingly, collagen I allowed the spreading of cells and maintained their healthy morphology when propagated for continuous passages reaching 30 passages, while cells plated on plates coated with 1% Matrigel^{TM} or on plastic were not maintained in culture. Cells on 1% collagen I were continuously passaged for an
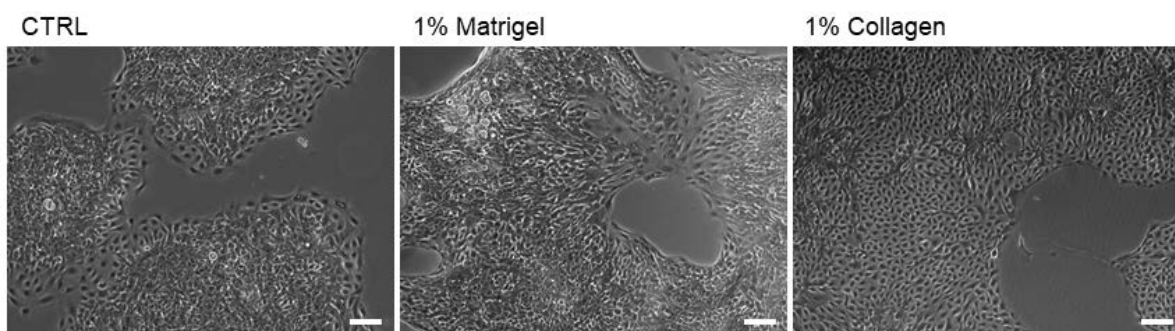
average of 10 passages and up to 30 passages (more than 4 months) (Fig. 39).

Figure 38. Optimization of prostate patient-derived cells culture. Representative bright-field images of the same patient derived prostate cancer cell lines plated on 3 different conditions; on plastic as a control, 1% Matrigel^{TM}, and 1% collagen I at passage 2. Scale bar = 100μm.

112
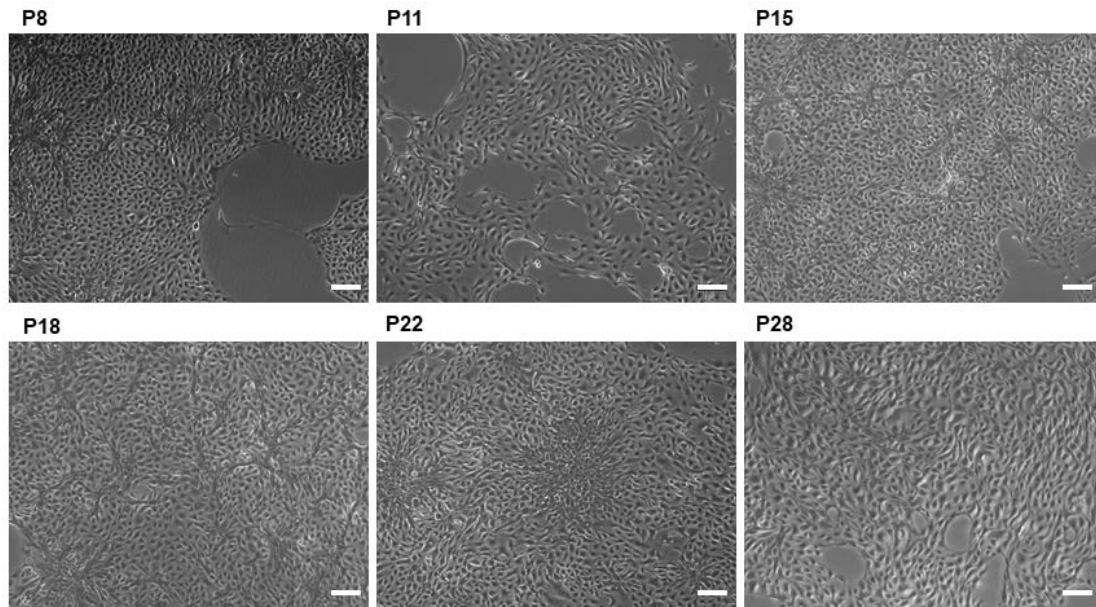
Figure 39. Propagation of Prostate cancer patient-derived 2D cells. Representative bright-field images of human Prostate cells passaged for more than 3 months under all factors condition on 1% collagen I-coated plates. Scale bar = 100μm.

2. *Optimization of Culture Medium Needed to Grow Prostate Patient-Derived 2D Cells in Culture*

Based on an observation made during the organoid's optimization experiment, we noticed that EGF withdrawal from the medium affected the ability to derive 2D cells negatively (Figure 40). Consequently, we sought to further investigate the importance of EGF for the growth of 2D cells by growing cells under 3 conditions; condition 1 includes prostate organoids growth medium (as described in table 1), condition 2 includes prostate organoids growth medium without EGF, and condition 3 includes adDMEM/F12 with EGF only (10 ng/ml) (Figure 41). Cells derived from tissue samples from 3 different patients 25, 26 and 32, including the unaffected and the tumor sample, were seeded at a density of

113

$4x10^3$ cells/well in 100 µL in triplicates under three different conditions. MTT and Trypan Blue assays were performed showing, a significant reduction in cell viability and cell proliferation when EGF was removed from the medium, while EGF alone can maintain the growth of 2D cells. Indeed, there was no significant difference in both cell proliferation and cell viability between condition 1 and condition 3 for all three patients' derived 2D cells (Figures 42-44).
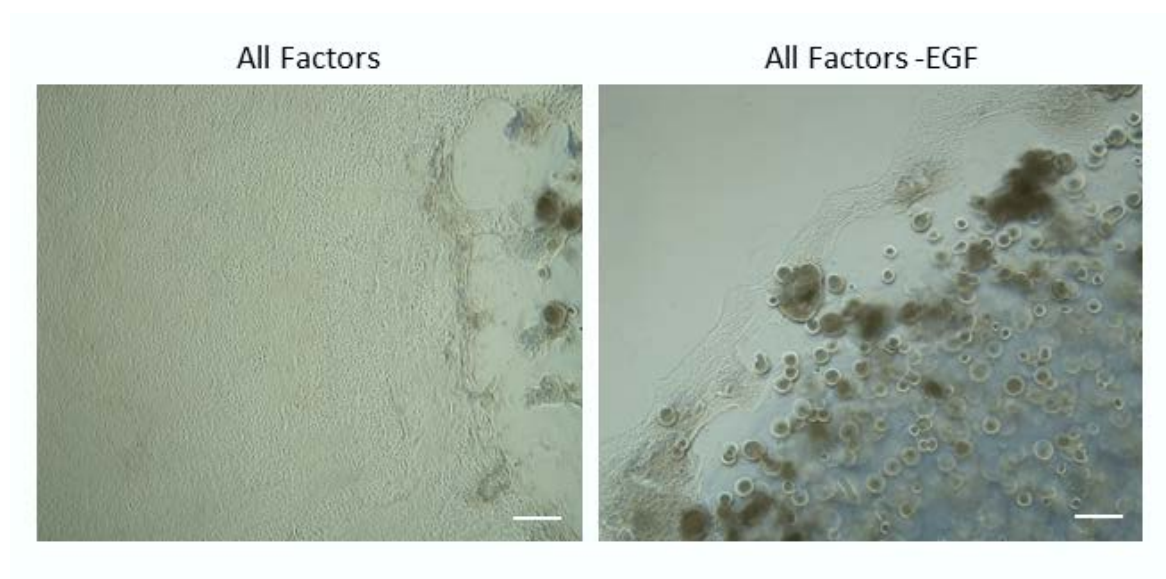
Figure 40. Derivation of patient-derived 2D cells using organoids culture conditions. Representative bright-field images showing 2D cells established around the matrigel droplet of 3D organoids in "All Factors" condition versus "All factors -EGF condition". Scale bar = 200µm.

Figure 41. Optimization of culture conditions to grow prostate patient-derived 2D cells. Representative bright-field images of 2D cells established from unaffected and tumor organoids from patient 32 and grown under different conditions; condition 1 "All factors" with prostate organoids growth medium, condition 2 "All factors -EGF" with prostate organoids growth medium without EGF, and condition 3 "EGF alone" with adDMEM/F12 with EGF only (10 ng/ml). Scale bar = 200μm.
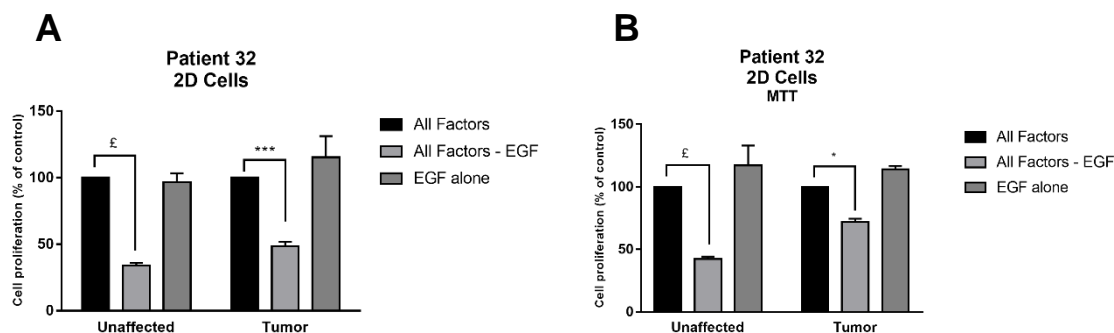
Figure 42. Optimization of culture conditions to grow prostate patient 32-derived 2D cells. (A) Cell viability was determined using the trypan blue exclusion assay. Data represent an average of triplicate measurements and are reported as mean ± SEM. (B) Cell proliferation was determined in triplicates using the MTT cell proliferation assay. (Two-way ANOVA; * $P<0.05$, *** $P<0.01$, £ $P < 0.0001$; different conditions compared to condition 1 "All Factors", Bonferroni's multiple comparisons test).

115
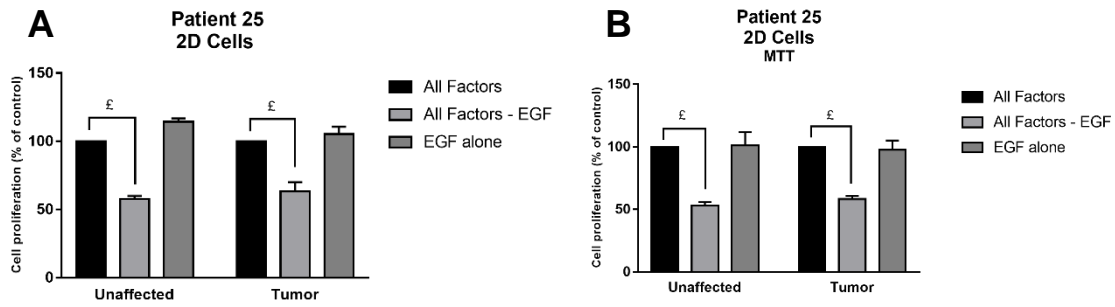
Figure 43. Optimization of culture conditions to grow prostate patient 25-derived 2D cells. (A) Cell viability was determined using the trypan blue exclusion assay. Data represent an average of triplicate measurements and are reported as mean ± SEM. (B) Cell proliferation was determined in triplicates using the MTT cell proliferation assay. (Two-way ANOVA; £ $P < 0.001$; different conditions compared to condition 1 "All Factors", Bonferroni's multiple comparisons test).
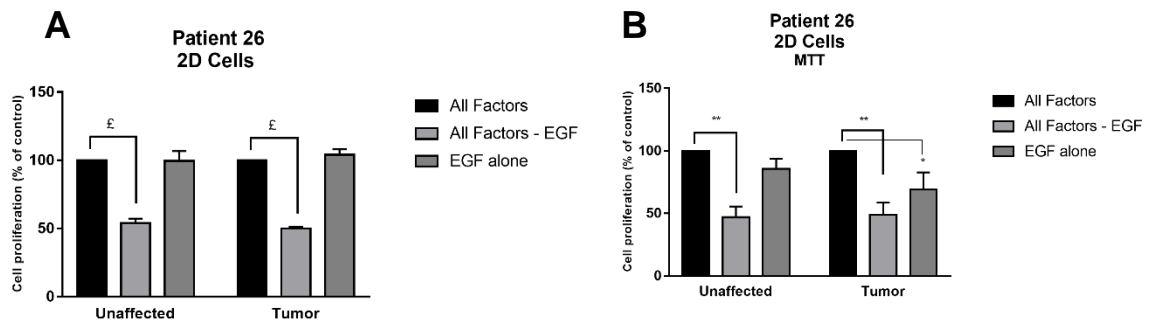
Figure 44. Optimization of culture conditions to grow prostate patient 26-derived 2D cells. (A) Cell viability was determined using the trypan blue exclusion assay. Data represent an average of triplicate measurements and are reported as mean ± SEM. (B) Cell proliferation was determined in triplicates using the MTT cell proliferation assay. (Two-way ANOVA; * $P<0.05$, ** $P<0.01$, £ $P < 0.001$; different conditions compared to condition 1 "All Factors", Bonferroni's multiple comparisons test).

116

3. *Immuno-Characterization of PCa Patient-Derived 2D Cells*

The patient-derived cell lines were characterized by assessing the expression of prostate epithelial lineage markers using immunofluorescence. Patient-derived cells were grown on collagen I-coated coverslips and supplemented with human prostate organoids culture medium plus RI for 3-4 days, then fixed with PFA and immunostained with luminal marker CK8, basal marker CK5 and mesenchymal marker VIM. Our results confirm that cells established from different patients include prostate epithelial luminal and basal lineages, while tumor derived cells show an increased expression of mesenchymal marker VIM indicating a possible increase in EMT which corresponds to an expected increase in EMT in tumor tissue versus unaffected tissue (Figures 45, 46).

To further confirm that condition 3 "EGF alone" can support the growth of both luminal and epithelial cells, 2D cells growing under 3 conditions described above (section D.2) were immunostained with luminal marker CK8 and basal marker CK14. The results obtained show similar morphologies and expression patterns of luminal and basal markers in both condition 1 and condition 3, which confirms that EGF alone can substitute the cocktail of 12 components included in condition 1 (Figure 47).
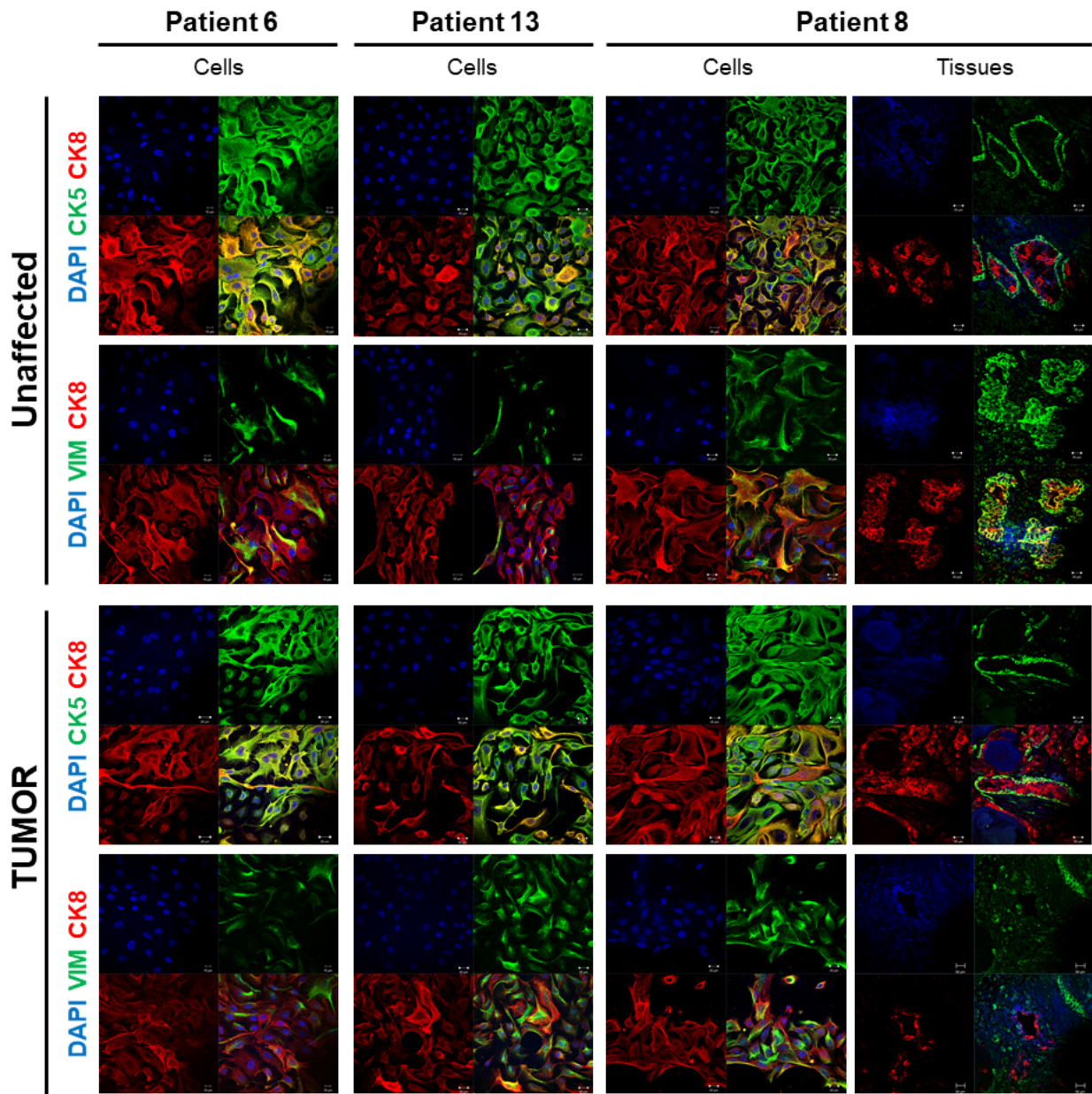
Figure 45. Representative Immunofluorescent images of 2D cells established from Unaffected and tumor organoids from different patients. 2D cells were stained with IF to assess the expression of prostate lineage epithelial markers CK8 and CK5 and mesenchymal VIM. The nuclei were stained with anti-fade reagent Fluorogel II with DAPI. The images were acquired using the Zeiss LSM 710 laser scanning confocal microscope (Zeiss) and images were processed using the Carl Zeiss ZEN 2013 image software.
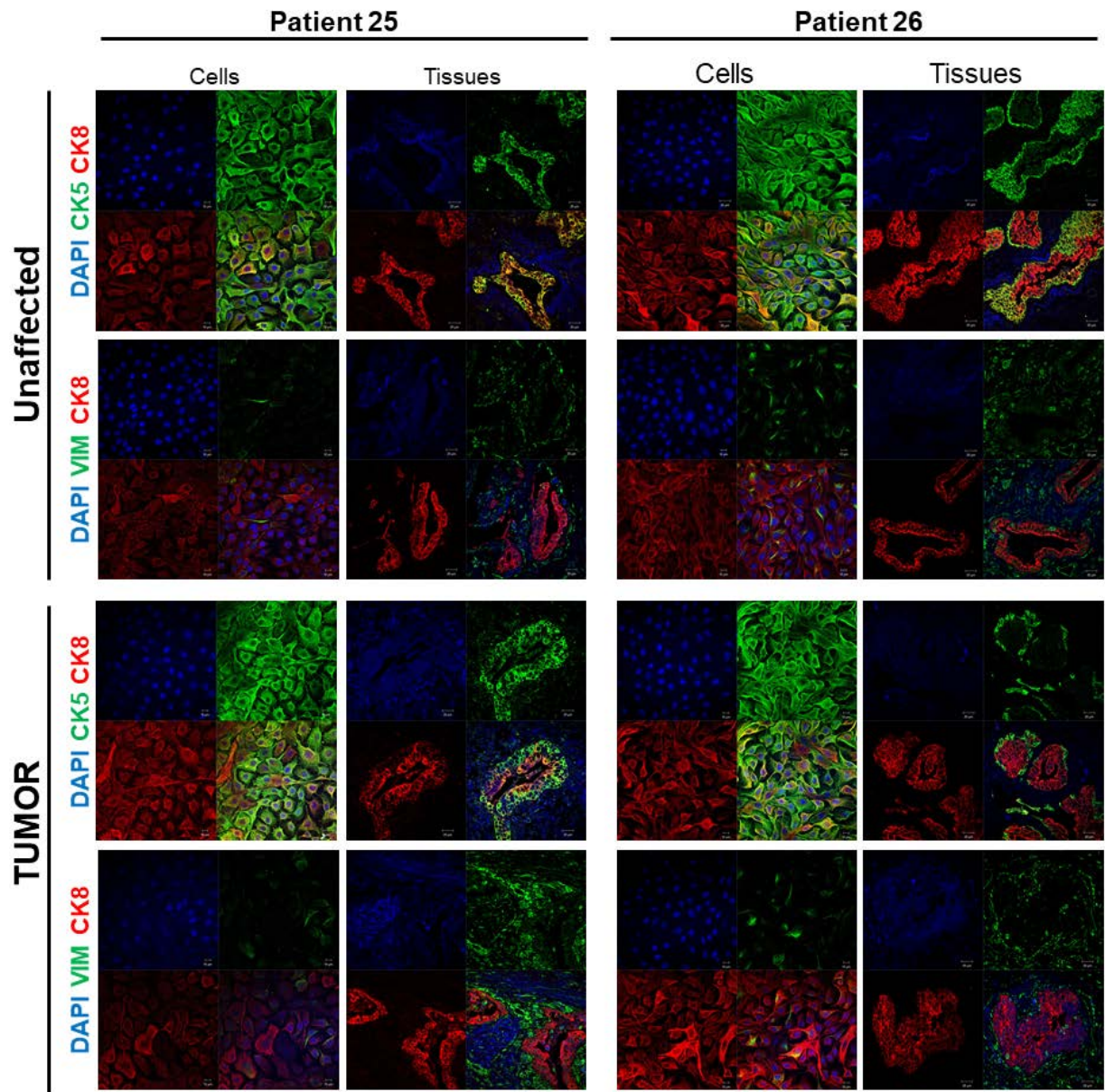
Figure 46. Representative Immunofluorescent images of 2D cells established from Unaffected and tumor organoids from different patients. 2D cells were stained with IF to assess the expression of prostate lineage epithelial markers CK8 and CK5 and mesenchymal VIM. The nuclei were stained with anti-fade reagent Fluorogel II with DAPI. The images were acquired using the Zeiss LSM 710 laser scanning confocal microscope (Zeiss), and images were processed using the Carl Zeiss ZEN 2013 image software.
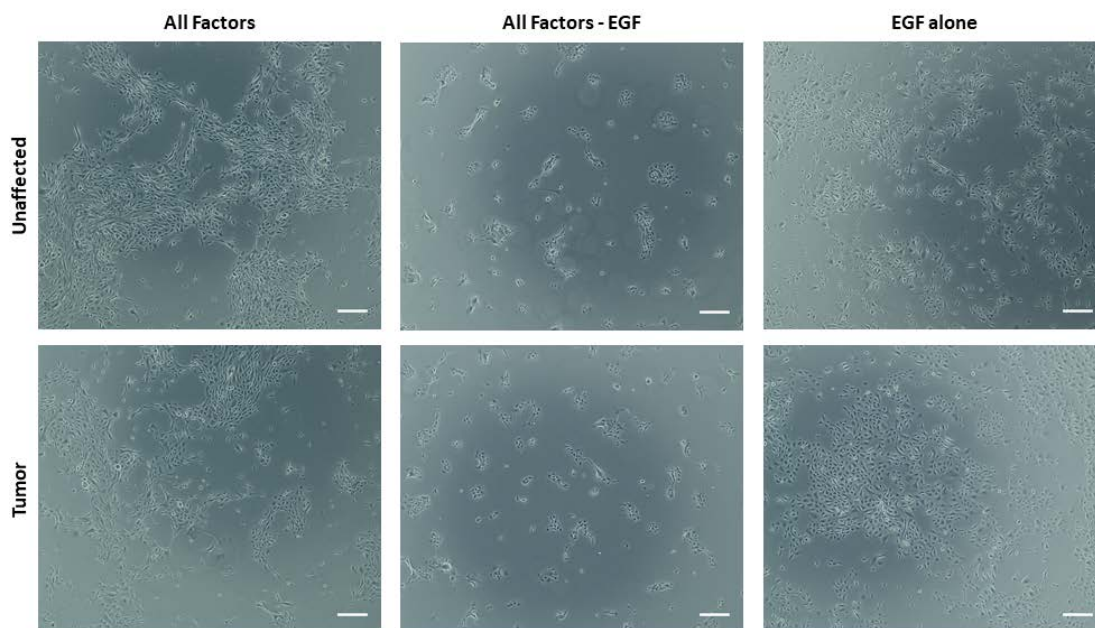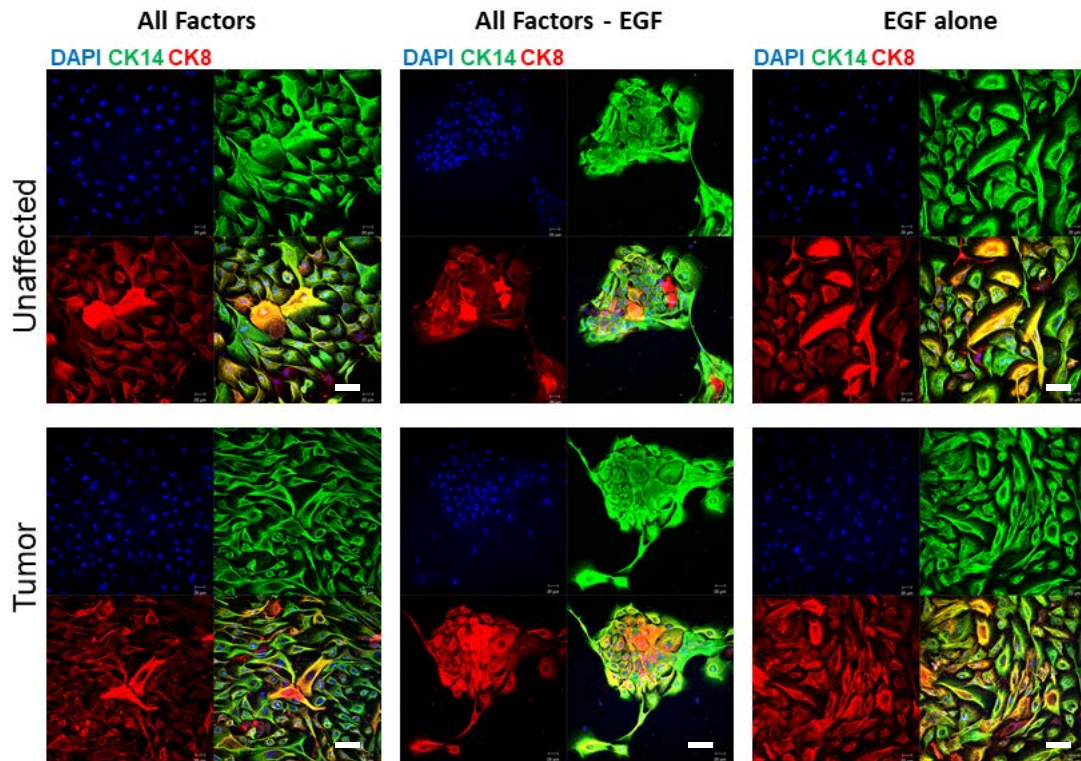
Figure 47. Optimization of culture conditions to grow prostate patient-derived 2D cells. Representative Immunofluorescent images of 2D cells established from tumor organoids from patient 32 and grown under different conditions as described previously and stained with the prostate lineage epithelial markers CK8 and CK14. The nuclei were stained with anti-fade reagent Fluorogel II with DAPI. The images were acquired using the Zeiss LSM 710 laser scanning confocal microscope (Zeiss) at, and images were processed using the Carl Zeiss ZEN 2013 image software.

4. *RNA Expression of Selected Genes in Cells vs. Tissues*

RNA expression of selected genes was assessed to evaluate the expression patterns in cells as compared with the original tissue. In general, the patient-derived cells showed strong expression of epithelial luminal marker *CK8* accompanied with lower expression of *VIM* in cells when compared with corresponding tissue samples. Expression of stem cell

120

marker *SOX2* in tumor cells of patient 5 was 13 folds higher than the corresponding tumor

tissue, while it was not the same case for cells derived from patient 25 sample. *CDH1*

expression was parallel between the (unaffected and tumor) tissues and cells of patient 5,

with tumor tissues and cells showing approximately 5 folds higher expression than

unaffected tissues and cells.
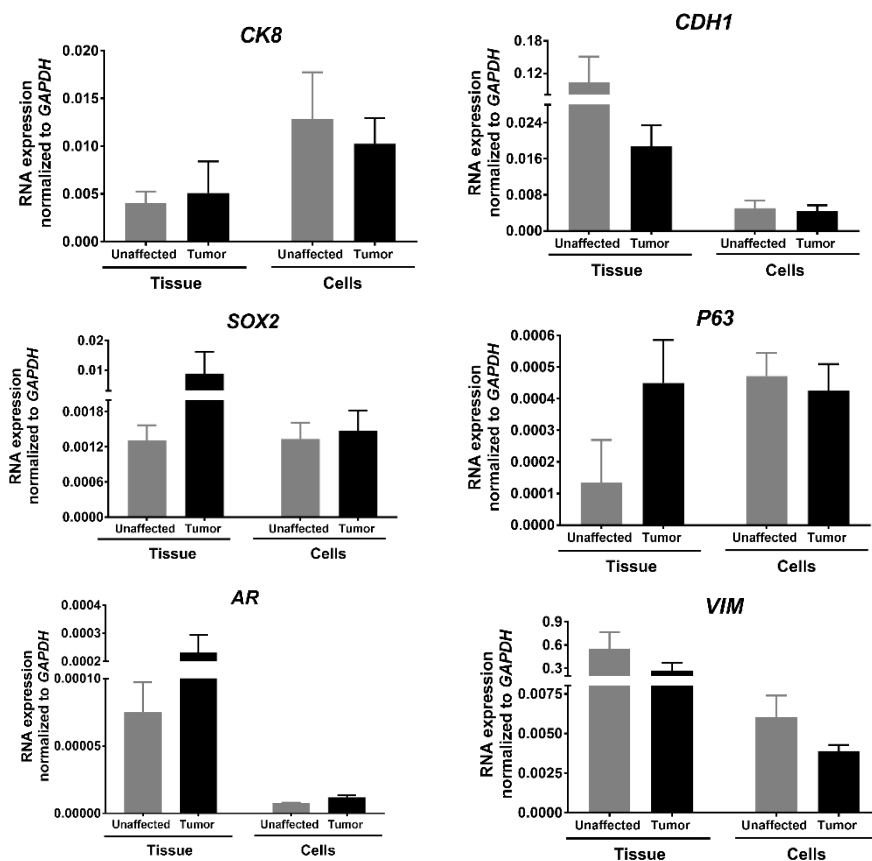
Figure 48. Relative mRNA expression of selected markers to compare cells with the corresponding tissues of patient 25 with GG B (GS 7(4+3)). The relative mRNA expression of PCa epithelial markers (*CK8*, *CDH1, AR*), mesenchymal markers (*VIM*) and stem cell markers (*SOX2, TP63*) was assessed. GAPDH expression was used as a reference gene. Average values were reported as mean ± SD (n=3).
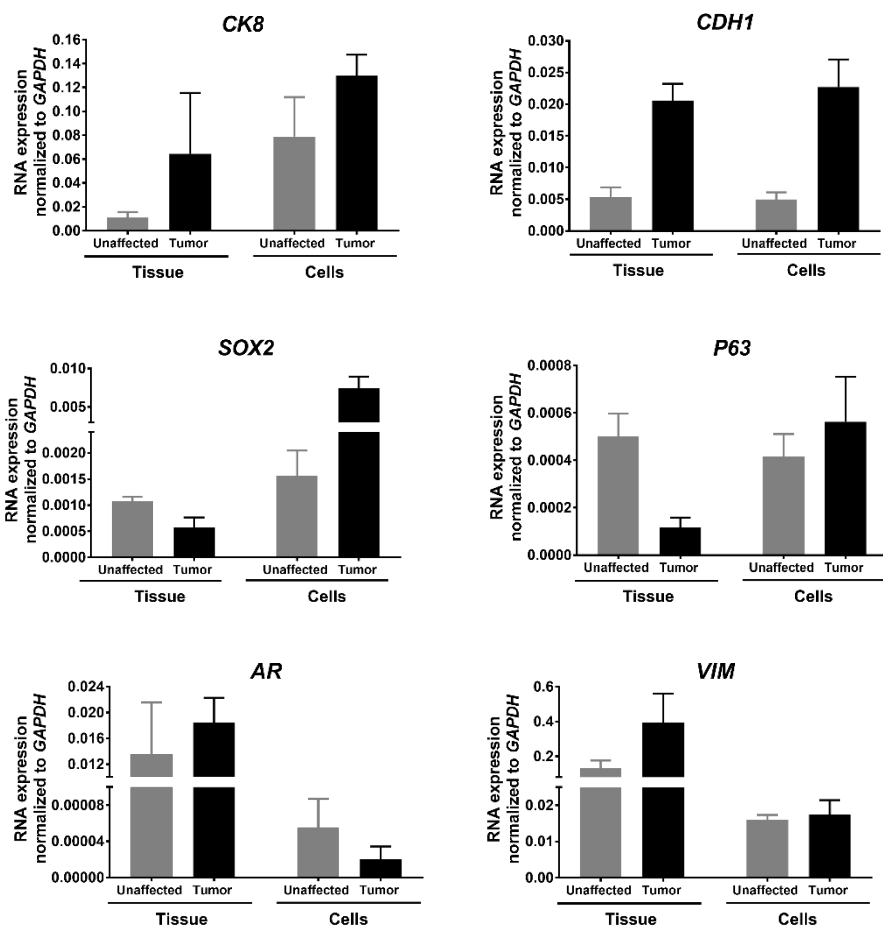
Figure 49. Relative mRNA expression of selected markers to compare cells with the corresponding tissues of patient 5 with GG A (GS 7(3+4)). The relative mRNA expression of PCa epithelial markers (*CK8*, *CDH1, AR*), mesenchymal markers (*VIM*) and stem cell markers (*SOX2, TP63*) was assessed. GAPDH expression was used as a reference gene. Average values were reported as mean ± SD (n=3).

CHAPTER IV

DISCUSSION

A. EMT in Patients with Locally-Advanced PCa to Predict Recurrence

The progression of PCa from a primary stage to an advanced and metastatic castration-resistant PCa (mCRPC) stage involves several mechanisms, including epithelial-to-mesenchymal transition (EMT). The latter is important in endorsing the invasiveness of PCa cells due to increased mobility and migration of mesenchymal cells [80]. Moreover, in carcinoma, invasion and metastasis are associated with transition of cancer cells from an epithelial keratins-expressing phenotype to a mesenchymal vimentin (VIM)-expressing phenotype [228, 229]. Therefore, identifying the onset of metastatic dissemination through assessment of molecular markers of EMT can aid in the development of a novel system for predicting the prognosis of PCa.

The importance of assessing the EMT status through investigating VIM overexpression was highlighted in different solid malignancies. For instance, VIM expression was associated with adverse prognosis in ductal breast carcinoma [230]. Besides, in triple-negative breast cancer, VIM expression was significantly higher compared to other subtypes, and was shown to be associated with a worse prognosis and a more aggressive phenotype, thereby assisting as a biomarker for the prognosis of this aggressive subtype of breast cancer [231]. In addition, VIM was suggested to aid in

123

predicting the risk of developing colon cancer and its use was proposed to serve as an antigen for tumor vaccination [232]. Additionally, a significant increase in VIM expression coupled with a decrease in CK expression were observed in advanced grades of transitional cell carcinoma of the bladder, suggesting the potential use of these biomarkers for early diagnosis of bladder carcinoma [233]. In PCa, the independent relationship between an E-cadherin to N-cadherin switch and patient prognosis unraveled the importance of EMT in PCa progression [234]. Moreover, the value of VIM expression as a predictor of recurrence was established in a previous study where Zhang *et al.* performed an immunohistochemical study and reported that risk of biochemical recurrence is associated with high levels of VIM which was described to be independent of Gleason score [235].

In our study, we were after the transitional stage of EMT where cells are co-expressing both epithelial and mesenchymal markers. Therefore, we investigated the correlation between a novel EMT score on one hand and the various clinicopathological parameters among locally-advanced PCa patients on the other hand [221]. In our patients, representing a cohort of high-risk locally-advanced PCa from the Middle East region, looking at co-expression patterns of CK8 and VIM revealed that the mean EMT score increases significantly as disease becomes more poorly differentiated reflected by higher Gleason group. Our results show that there is a highly significant difference in the mean EMT score between Gleason groups A and C. Furthermore, there is a highly significant linear association based on Mantel Haenszel test whereby higher Gleason groups were associated with higher EMT scores. The added value of this EMT scoring system is that it can predict PSA failure irrespective of Gleason group, pathological stage and surgical

margins [236]. As PSA recurrence is a powerful predictor of distant metastasis, cancer-specific survival, and overall survival, these results suggest that the EMT score can be used to estimate the biochemical recurrence-free survival of a patient irrespective of other clinicopathological parameters. A possible explanation of the link between EMT status and disease progression is the fact that cells with hybrid epithelial/mesenchymal phenotypes possess a large repertoire of survival strategies under many stress conditions [237]. EMT has been linked to circulating tumor cells (CTCs) generation and subsequently metastasis. In colorectal cancer, for instance, the presence of biophenotypic and mesenchymal CTCs, rather than epithelial CTCs, is indicative of a more advanced disease stage and metastasis [238]. This study underscores the importance of EMT markers (increased VIM and decreased CK8 expression) for predicting the prognosis of PCa. Whereas previous studies have indicated reduced expression of epithelial markers and increasing expression of mesenchymal markers, an EMT phenotype and the co-expression of such markers specifically CK8 and Vim and their association with outcome data have not been described. Since these markers could have a significant effect on the management of PCa patients, including projections of targeted therapy, we suggest the extrapolation of this study to larger cohorts of patients from different ethnicities to further validate our findings. Furthermore, assessing the EMT score on pre-operation PCa biopsy might lead to better understanding of post-surgery outcome and to better management.

We recognize that our study has some limitations. First, as a clinical study the sample size is relatively small, therefore the results obtained require further investigation on a larger cohort. Second, samples were collected retrospectively over the period of 18

years with around 75% of the samples having a positive margin and around 70% with a pathological stage greater than pT3. The latter identified the study sample as a high-risk cohort thus restricting the results obtained to such sample characteristics. Third, the retrospective collection of data led to missing information regarding the SVI, PNI and LNM status of the patients; this might explain the lack of significant correlation between the EMT score and the metastatic status.

B. Characteristics of the Prostate Cancer Specimens Established as Organoids

Organoids are rapidly emerging as an effective tool to investigate both basic developmental processes and disease mechanisms [119]. Consequently, in the second aim, we collected fresh tissue specimens from consented treatment-naïve patients undergoing radical prostatectomies at AUB-MC, to establish and characterize the culture system of PCa organoids. The organoids culture system was adapted from a published protocol that has been optimized for human metastatic prostate specimens and to generate new lines that represent the phenotypic spectrum of clinical disease [116, 167]. Using this culture system, it has been shown that human PCa-derived organoids mimic genetically and phenotypically the tumor of origin [116, 166].

A total of 35 fresh radical prostatectomy specimens were received, with one unaffected and one tumor sample resulting in a total of 70 specimens. The success rate was very promising with more than 90% of specimens successfully established as organoids. In published literature, the overall patient success percentage does not exceed 20% for

metastatic biopsies [42, 116]. This can be explained by the advantage of receiving fresh samples directly from a nearby hospital. In addition, cells were plated at a high density 500 cell/µl of Matrigel^{TM}. Indeed, it has been shown that higher cell density can deactivate the mTOR pathway consequently suppressing the senescence [239]. In addition, we added ROCK inhibitor during the tissue digestion step, as well as the first week of organoids plating, which plays a critical role in maintaining the proliferation of cells and inhibiting senescence [146]. Nonetheless, the small size of the tissue fragment was the main limitation in organoids establishment and subsequent applications and characterization.

The organoids forming count (OFC) were relatively lower for organoids derived from tumor specimens compared with their equivalents from unaffected specimens. Accordingly, it has been previously demonstrated that the tumor organoids can even proliferate at slower rates than their normal counterparts, which can be attributed to high levels of mitotic failures and consequent cell death [119]. Moreover, there was substantial variability in organoids formation efficiency between different patients' samples reflected by the large deviation in both OFC and organoids size. This was observed elsewhere where samples derived from advanced PCa exhibited inconsistency in growth speed [146].

Regarding the morphology of organoids, the majority consisted of solid organoids with a minority of luminal-like organoids as detected by bright-field microscopy and H&E staining of sectioned organoids. Indeed, Gao et al (2014) demonstrated that human organoid cultures will mostly comprise solid basal cell-derived organoids [116].

In addition, there was a variability in terms of count, size and morphology between one patient sample and the other, and within cultures established from the same sample. This variability can be attributed to tumor heterogeneity.

To confirm that the organoids are indeed derived from prostate tissue, the expression of luminal-specific markers (CK8, AR, PSA) and basal-specific markers (CK5, p63,) was analyzed. The existence of both lineages was confirmed in the established cultures. The observed expression patterns recapitulate the architecture of prostate tissues where a luminal secretory cell layer expresses prominent levels of CK8, AR and PSA, and an underlying basal cell layer expresses CK5, CK14 and p63 [17, 18]. Interestingly, organoids with a luminal compartment (confirmed by CK8 expression) surrounding a hollow lumen and surrounded by basal cells (confirmed by CK5 expression) were mostly detected in organoids derived from a patient with Gleason group C (GS 9), yet we could not further investigate this observation since we did not receive any additional patient sample with the same Gleason score. In addition, an intermediate cell population is found referred to as intermediate or transit amplifying cells that co-expresses both luminal and basal markers [7, 18]. This population was also detected in organoids including cells that co-express luminal CK8 and basal CK5. Positive nuclear staining of stem cell marker SOX2 was identified in both unaffected and tumor derived organoids which confirms the presence of stem-like/ progenitor cells within the bulk of our patient-derived organoids. Moreover, our IHC results showed a high level of expression of p63 in both unaffected and tumor organoids. This basal marker is involved in various pathways associated with self-renewal

and differentiation of stem cells and cancer stem cells [240-242], which provides an additional validation about the presence of adult stem/progenitor cells among organoids cell populations.

PCa is a heterogeneous disease associated with large-scale genomic rearrangements and extensive copy number alterations involving multiple chromosomes. The heterogeneity of this tumor renders choosing the best treatment for a specific patient very challenging [132]. Therefore, establishing novel and more representative in vitro models for understanding the heterogeneity and the progression of PCa is crucial to define new therapeutic targets for this type of cancer. The recent years witnessed advances in the characterization of the mutational landscape of PCa and the exceptional development of multiple FDA-approved drugs. Nonetheless, there is an extensive variability in therapeutic responses to currently-used drugs [168]. In addition, for therapeutics assessment, the traditional 2D culture systems used for drug screening present significant limitations in the areas of drug dosing, complexity of interactions seen in the *in vivo* environment and translation of results into the clinic. In this context, PCa organoids demonstrated their potential use in personalized drug treatments [119].

Puca *et al* employed prostate tumor organoids from metastatic lesions with a neuroendocrine phenotype for therapeutic assessment [168]. The results obtained showed concordance between drug responses in vitro and patients' responses in the clinic, that corresponded to the molecular background of the tumor; for example, response to AKT inhibition was associated with PTEN loss [168]. Similarly, Beshiri *et al.* demonstrated, by

employing organoids from 20 models of LuCaP mCRPC PDX cohort, conserved genomic heterogeneity between the PDXs and organoids [170]. This cohort provided a platform to investigate responses to therapies; specifically, the cytotoxicity to PARP inhibitor olaparib in $BRCA2^{-/-}$ organoids reflected the patients' response in the clinic. Accordingly, we attempted to employ patient-derived organoids to assess their potential use in predicting a patient's drug response. Our results showed differential drug response between patient samples and between the unaffected and tumor sample of the same patient. Notably, the ability to grow both unaffected and diseased organoids from patients enables clinical screens for drug combinations that selectively target the diseased tissue, and identify more effective therapies with minimal side effects [142]. Initially, we assessed the potential use of patient-derived PCa organoids by exposing G2 organoids to a chemotherapeutic drug and clinicaly achievable doses of irradiation including both the unaffected and tumor sample. Inter-patient variability was demonstrated where the same dose of Docetaxel induced a significant decrease in the size of both unaffected and tumor organoids derived from one patient, but did not elicit an effect on the size of tumor organoids derived from a different patient. This variability was further demonstrated by assessing the drug effect on G1 organoids derived from 3 different patients. Once more, a variability in drug response was observed between the different patients and between the unaffected and tumor samples of the same patient. On one hand, Docetaxel, Bicalutamide, and Enzalutamide failed at eliciting a significant decrease in the count of tumor organoids of one patient while they all induced a significant decrease in both the size and count of unaffected organoids of the same patient. On the second hand, Enzalutamide inhibited the growth (size and count) of

130

unaffected organoids of another patient while Bicalutamide and Docetaxel did not affect the size of tumor organoids of this patient.

Further validation is essential including the comparison of in vitro responses with clinical drug response when applicable and their correlation with genetic mutation profiles through advanced genetic analysis [243]. Therefore, it remains essential to compare the patient's clinical response to the in vitro drug response, therefore, patients are being followed up to collect any clinical data regarding their disease progression and drug response in case they receive one after RP. Moreover, it is necessary to recognize that this methodology employs undefined factors such as Matrigel as ECM substitute, and various growth factors and molecule inhibitors that are included in the culture medium. Consequently, these undefined factors might interfere with the drug responses. Even so, the observed differential effects between one sample and the other is an indication about the validity of this system as a potential model for drug assessment.

Organoid culture systems fail at faithfully recapitulating the in vivo microenvironment since they do not include stromal, immune or endothelial cells [215]. Consequently, substantial efforts are dedicated to developing co-culture systems. Even though it was estimated that organoids can be cultured indefinitely without genetic manipulation [166], we faced the limitation of maintenance in culture and we could not maintain organoids in culture beyond G3-5.

131

C. Updating the Patient-Derived Prostate Organoid Culture Systems

Despite published protocols describing the establishment of PCa organoids, it remains a challenge to successfully culture and maintain them in culture. Consequently, in the third aim, we attempted to enhance the previously established extensive organoids culture system to increase the formation efficiency and minimize the costly requirements. Our results were based on an assay system in which we examined the effect of withdrawal of individual components. We excluded each of the 10 components (NAC, EGF, NOG, RSPO, A83, FGF10, FGF2, PGE2, SB, DHT) from the culture medium, one at a time, and assessed their withdrawal effect on the organoids' formation efficiency; OFC, organoids size, and maintenance in culture. Based on this system, we demonstrated the ability to grow and maintain patient-derived organoids using only 5 factors (5F) components *(NAC, NOG, A83, B27, and nicotinamide)*. Furthermore, our results demonstrate that we succeeded in delineating the essential components needed to grow prostate organoids with a high success rate and long-term maintenance in culture.

In 2014, Gao *et al.* reported the successful generation of fully-characterized organoid lines from 6 metastatic tissue biopsies and one circulating tumor cells specimen [116]. The methodology adapted by this group provided a success percentage of 20% and maintenance in culture for only 1-2 months with no proof of unlimited growth [116]. In the same issue, an accompanying manuscript was published describing the development of a methodology that maintains murine and human benign prostate organoids for a long period of time with verified preserved morphologies and genetics over 7 generations [166]. Although they showed maintenance of benign organoids for over a year in culture, we

could not maintain unaffected or tumor-derived organoids for more than 3 months by adapting the same culture method on our cohort of patients. Nevertheless, we have shown that removing EGF from the culture medium enabled enhanced survival of organoids for more than 8 generations i.e. an equivalent of 6 months. Similarly, our minimal medium, including 5 components only, allowed maintenance of organoids for at least 5 generations and adding FGF10 or FGF2 further enhanced the growth and maintenance of these organoids in culture. In addition, the reported efficiency was doubled for both unaffected and tumor organoids in the 5F medium compared to the previously published protocol where the reported formation efficiency was around 1% [166]. FGF signaling plays a crucial role in maintaining the stemness of prostate cells [185], thus its importance in the enhanced maintenance of organoids in culture. For instance, FGF10 is a highly expressed growth factor in the mesenchyme of a developing prostate gland, while its deletion was shown to impede branching morphogenesis [186]. Indeed, the importance of FGF10 was highlighted in its essential role for the maintenance of organoids in culture.

In 2016, a culture protocol was described as the sole method that maintains the growth of both the luminal and basal prostatic epithelial lineages [146]. Notably, we showed maintenance of both luminal and basal markers over 6 generations using a minimal and less expensive medium. Later, Puca *et al.* reported the derivation of tumor organoids from metastatic lesions of 4 patients focusing on the neuroendocrine phenotype of PCa [168]. However, akin to previous reports, the low total success rate for unlimited propagation and expansion was explained by the scarce starting material [168]. In our case, although specimens received were relatively small (3-5 mm), this limiting factor was

surmounted by adding ROCK inhibitor to the digestion step with collagenase on one hand, and removing p38 MAP kinase inhibitor, prostaglandin E2 (PGE2), and EGF from the medium on the other hand. Interestingly, the efficiency in establishing colorectal cancer derived organoids was reported to be enhanced by removing the p38 kinase inhibitor SB202190 from the medium [200]. Similarly, Beshiri *et al.* showed that inhibiting p38 activity affects the growth of LuCaP-derived organoids and CRPC biopsy–derived organoids [170]. Moreover, it was previously demonstrated that the addition of Rho kinase inhibitor to normal and tumor epithelial cells, including prostate, and to organoids culture can delay senescence and enhance proliferation [146, 166, 168, 244]. Although EGF was designated as an essential component for establishing and maintaining prostate organoids in culture [166], we demonstrated the successful derivation and sustained organoid growth in the absence of EGF from both unaffected and tumor samples. Based on our observations, the removal of EGF enhanced organoids plating efficiency and maintenance by preventing the dissociation of organoids and migration of epithelial cells from 3D Matrigel to 2D compartment.

In line with previously published data, we demonstrated that Noggin and A83-01 are crucial to sustain prostate organoid cultures while R-spondin is not fundamental. Indeed, the BMP antagonist Noggin is essential for stem cell expansion and plays a critical role during prostate development by counteracting BMP-4 inhibitory effect on cell proliferation [142, 191]. TGF-β signaling blocks proliferation of prostate cells and embodies a defense mechanism that suppresses tumorigenesis in various cancer types [192-194]. Therefore, the Alk3/4/5 inhibitor A83-01 plays a substantial role to relieve the

growth barrier and enhance the organoids growth by obstructing the TGF-β signaling

pathway. More recently, the addition of stromal cells in the protocol described by Richards

et al. increased formation efficiency of organoids culture, however, this system does not

demonstrate long term maintenance of organoids in culture where the benign organoids did

not survive passaging and tumor organoids were shown to reach G2 only [169]. Using our

optimized, minimal and cost-effective protocol, we demonstrate successful establishment of

all patient specimens as organoids, with an increased proliferation rate reflected by an

increase in count and diameter of organoids as well as maintenance in culture for more than

6 months. This study demonstrates the successful establishment of organoids from

treatment-naïve primary PCa RP samples with higher efficiency and lower cost than

previously published protocols. Nonetheless, it remains essential to assess this protocol on

metastatic PCa samples. In addition, advanced genetic analysis is needed to further

elucidate the PCa organoids niche requirements and their relationship with genetic mutation

profiles.

D. Generation of Novel Patient-Derived Prostate Cell Lines

Despite its prevalence, PCa is highly underrepresented with a very limited number

of available cell lines in public repositories [120-125]. Indeed, the scarcity of human PCa

cell lines has always hindered our understanding of the disease etiology and progression,

and therefore the need for novel cell lines representing the heterogeneity of the disease is of

eminent importance. Along those lines and starting from organoids our fourth aim was to

generate novel patient-derived cell lines representing unaffected and tumor prostate tissues.

Starting from the organoids protocol and using the same culture medium, human

prostate 2D cell lines (unaffected and tumor) were successfully generated. After the 1st

week of organoids culture, 2D cells started invading the 3D Matrigel^TM droplet and

proliferating on plastic. These cells were successfully derived whenever organoids were

established, nonetheless, their maintenance in culture was very challenging. Consequently,

to maintain them in culture, we attempted to optimize the culture conditions by using

different matrices. Interestingly, Collagen type I allowed the spreading of cells and

maintained their healthy morphology when propagated for continuous passages reaching 30

passages. The favored adhesion of PCa cells to Collagen I represents a possible explanation

for these results. Indeed, the most frequent site of human PCa metastasis is the bone

and collagen type I represents the most abundant protein within the skeleton [245]. In

addition, it has been previously demonstrated that collagen I induces the attachment and

proliferation of PCa cells [246].

To further optimize the culture conditions and minimize the costly requirements and

based on an observation made during the organoid's optimization experiment, we noticed

that EGF withdrawal from the medium affected the ability to derive 2D cells negatively.

Consequently, we sought to further investigate the importance of EGF for the growth of 2D

cells. Remarkably, our results demonstrated a significant reduction in cell viability and cell

proliferation when EGF was removed from the medium, while EGF alone was capable to

support the growth of 2D cells. These data are consistent with the substantial role of EGF in

stimulating cell motility and migration of epithelial cells from various tumors including PCa [183, 184].

E. Conclusions

Our first aim was to develop a novel scoring system to quantify EMT expression (EMT score) in patients with locally-advanced Prostate Cancer (PCa) then explore the correlation between this score and the different clinicopathological outcomes. Our results indicated that the co-expression of CK8/VIM (EMT score), was associated with increasing Gleason group. A highly significant linear association was detected wherein higher Gleason group was associated with higher mean EMT score. Our data also confirmed that the EMT score can predict PSA failure irrespective of Gleason group, pathological stage, or surgical margins. It has to be noted that this work has been published in Frontiers in Oncology [221].

Our second aim was to establish and characterize patient-derived PCa organoids from patients undergoing radical prostatectomies. We demonstrated the successful derivation of organoids with a 90% success rate. We further confirmed the presence of prostate luminal and epithelial lineages among the bulk of organoids cells. In addition, we employed this 3D model for drug assessment and the results showed differential drug response between patient samples and between the unaffected and tumor sample of the same patient.

Our third aim was to enhance the previously established extensive organoids culture system in the attempt to increase the formation efficiency and minimize the costly requirements. We reported the successful establishment of a cost-effective optimized protocol by delineating the essential components needed to grow prostate organoids with a high success rate and long-term maintenance in culture. Our results demonstrated the ability to culture 3D patient-derived unaffected and tumor prostate organoids using 5 instead of the 12 components included in the initial protocol. This work is currently under review in Communications Biology.

Our fourth aim was to generate novel patient-derived cell lines from the 3D organoids representing unaffected and tumor prostate tissues. Starting from the organoids protocol and using the same culture medium, we successfully generated human prostate 2D cell lines. Their maintenance in culture was enhanced by plating on Collagen type I. Furthermore, we optimized the culture medium of 2D cells and reduced it to include EGF alone.

In summary, we were successful in establishing a new assessment score, the EMT score, for the prediction of biochemical recurrence or PSA failure in patients that underwent RP. Future studies are needed on pre-surgery biopsy samples and on larger cohorts of RP tissues to confirm the wide application of this novel EMT score. Furthermore, we were successful in generating patient-derived organoids in 3D and novel cell lines in 2D from a unique cohort of treatment-naïve prostate cancer patients. Future experiments aim at deciphering the genomic and proteomic profiles of the organoids, cells

138

and their respective tissues to better understand the etiology and the makeup of the disease. In addition, prediction of treatment response remains one of the most sought-after future aim for the promises it holds to better manage the disease in a personalized fashion. Lastly, we aim at further enhancing our culture conditions in 3D and 2D to improve the quality, reliability, reproducibility and efficiency of our in vitro cellular models.

BIBLIOGRAPHY

1. The, L., *GLOBOCAN 2018: counting the toll of cancer.* Lancet, 2018. **392**(10152): p. 985.
2. Ferlay, J., et al., *Estimating the global cancer incidence and mortality in 2018: GLOBOCAN sources and methods.* Int J Cancer, 2019. **144**(8): p. 1941-1953.
3. Gronberg, H., *Prostate cancer epidemiology.* Lancet, 2003. **361**(9360): p. 859-64.
4. Hilal, L., et al., *Prostate Cancer in the Arab World: A View From the Inside.* Clin Genitourin Cancer, 2015. **13**(6): p. 505-11.
5. Shamseddine, A., *Cancer Trends in Lebanon & Projections to 2020.* Human & Health, 2015. **32**: p. 8-11.
6. Shamseddine, A., et al., *Cancer trends in Lebanon: a review of incidence rates for the period of 2003–2008 and projections until 2018*, in *Popul Health Metr*. 2014. p. 4.
7. Shen, M.M. and C. Abate-Shen, *Molecular genetics of prostate cancer: new prospects for old challenges.* Genes Dev, 2010. **24**(18): p. 1967-2000.
8. Berry, S.J., et al., *The development of human benign prostatic hyperplasia with age.* J Urol, 1984. **132**(3): p. 474-9.
9. Wilson, A.H., *The prostate gland: a review of its anatomy, pathology, and treatment.* Jama, 2014. **312**(5): p. 562.
10. Verze, P., T. Cai, and S. Lorenzetti, *The role of the prostate in male fertility, health and disease.* Nat Rev Urol, 2016. **13**(7): p. 379-86.
11. McNeal, J.E., *Normal histology of the prostate.* Am J Surg Pathol, 1988. **12**(8): p. 619-33.
12. McNeal, J.E., *The zonal anatomy of the prostate.* Prostate, 1981. **2**(1): p. 35-49.
13. Timms, B.G., *Prostate development: a historical perspective.* Differentiation, 2008. **76**(6): p. 565-77.
14. De Marzo, A.M., et al., *Inflammation in prostate carcinogenesis.* Nat Rev Cancer, 2007. **7**(4): p. 256-69.
15. Toivanen, R. and M.M. Shen, *Prostate organogenesis: tissue induction, hormonal regulation and cell type specification.* Development, 2017. **144**(8): p. 1382-1398.
16. Packer, J.R. and N.J. Maitland, *The molecular and cellular origin of human prostate cancer.* Biochim Biophys Acta, 2016. **1863**(6 Pt A): p. 1238-60.
17. van Leenders, G.J. and J.A. Schalken, *Epithelial cell differentiation in the human prostate epithelium: implications for the pathogenesis and therapy of prostate cancer.* Crit Rev Oncol Hematol, 2003. **46 Suppl**: p. S3-10.
18. Peehl, D.M., *Primary cell cultures as models of prostate cancer development.* Endocr Relat Cancer, 2005. **12**(1): p. 19-47.
19. Tuxhorn, J.A., G.E. Ayala, and D.R. Rowley, *Reactive stroma in prostate cancer progression.* J Urol, 2001. **166**(6): p. 2472-83.
20. Hayward, S.W., et al., *Stromal development in the ventral prostate, anterior prostate and seminal vesicle of the rat.* Acta Anat (Basel), 1996. **155**(2): p. 94-103.
21. Khan, F.U., et al., *Comprehensive overview of prostatitis.* Biomed Pharmacother, 2017. **94**: p. 1064-1076.
22. Wagenlehner, F., et al., *Prostatitis and andrological implications.* Minerva Urol Nefrol, 2013. **65**(2): p. 117-23.
23. Bartoletti, R., et al., *Prevalence, incidence estimation, risk factors and characterization of chronic prostatitis/chronic pelvic pain syndrome in urological hospital outpatients in Italy:*

results of a multicenter case-control observational study. J Urol, 2007. **178**(6): p. 2411-5; discussion 2415.

24. Wagenlehner, F.M., et al., *The role of inflammation and infection in the pathogenesis of prostate carcinoma.* BJU Int, 2007. **100**(4): p. 733-7.

25. Skinder, D., et al., *Benign prostatic hyperplasia: A clinical review.* Jaapa, 2016. **29**(8): p. 19-23.

26. McVary, K.T., *BPH: epidemiology and comorbidities.* Am J Manag Care, 2006. **12**(5 Suppl): p. S122-8.

27. Homma, Y., et al., *Outline of JUA clinical guidelines for benign prostatic hyperplasia.* Int J Urol, 2011. **18**(11): p. 741-56.

28. Guess, H.A., *Benign prostatic hyperplasia and prostate cancer.* Epidemiol Rev, 2001. **23**(1): p. 152-8.

29. Alcaraz, A., et al., *Is there evidence of a relationship between benign prostatic hyperplasia and prostate cancer? Findings of a literature review.* Eur Urol, 2009. **55**(4): p. 864-73.

30. Orsted, D.D. and S.E. Bojesen, *The link between benign prostatic hyperplasia and prostate cancer.* Nat Rev Urol, 2013. **10**(1): p. 49-54.

31. Grignon, D.J., *Unusual subtypes of prostate cancer.* Mod Pathol, 2004. **17**(3): p. 316-27.

32. Yuan, T.C., S. Veeramani, and M.F. Lin, *Neuroendocrine-like prostate cancer cells: neuroendocrine transdifferentiation of prostate adenocarcinoma cells.* Endocr Relat Cancer, 2007. **14**(3): p. 531-47.

33. Aggarwal, R., et al., *Neuroendocrine prostate cancer: subtypes, biology, and clinical outcomes.* J Natl Compr Canc Netw, 2014. **12**(5): p. 719-26.

34. Humphrey, P.A., *Histopathology of Prostate Cancer.* Cold Spring Harb Perspect Med, 2017. **7**(10).

35. Robinson, B.D. and J.I. Epstein, *Intraductal carcinoma of the prostate without invasive carcinoma on needle biopsy: emphasis on radical prostatectomy findings.* J Urol, 2010. **184**(4): p. 1328-33.

36. Epstein, J.I., et al., *The 2014 International Society of Urological Pathology (ISUP) Consensus Conference on Gleason Grading of Prostatic Carcinoma: Definition of Grading Patterns and Proposal for a New Grading System.* Am J Surg Pathol, 2016. **40**(2): p. 244-52.

37. Pierorazio, P.M., et al., *Prognostic Gleason grade grouping: data based on the modified Gleason scoring system.* BJU Int, 2013. **111**(5): p. 753-60.

38. Carter, H.B., et al., *Gleason score 6 adenocarcinoma: should it be labeled as cancer?* J Clin Oncol, 2012. **30**(35): p. 4294-6.

39. Burdick, M.J., et al., *Comparison of biochemical relapse-free survival between primary Gleason score 3 and primary Gleason score 4 for biopsy Gleason score 7 prostate cancer.* Int J Radiat Oncol Biol Phys, 2009. **73**(5): p. 1439-45.

40. Papadakis, M.A., McPhee, S. J., *CURRENT Medical Diagnosis and Treatment.* 55 ed, ed. E.M. Rabow. 2016: McGraw-Hill Education.

41. Kaffenberger, S.D. and C.E. Barbieri, *Molecular subtyping of prostate cancer.* Curr Opin Urol, 2016. **26**(3): p. 213-8.

42. *The Molecular Taxonomy of Primary Prostate Cancer.* Cell, 2015. **163**(4): p. 1011-25.

43. Taylor, B.S., et al., *Integrative genomic profiling of human prostate cancer.* Cancer Cell, 2010. **18**(1): p. 11-22.

44. Tomlins, S.A., et al., *Recurrent fusion of TMPRSS2 and ETS transcription factor genes in prostate cancer.* Science, 2005. **310**(5748): p. 644-8.

45.   Helgeson, B.E., et al., *Characterization of TMPRSS2:ETV5 and SLC45A3:ETV5 gene fusions in prostate cancer.* Cancer Res, 2008. **68**(1): p. 73-80.

46.   Paulo, P., et al., *FLI1 is a novel ETS transcription factor involved in gene fusions in prostate cancer.* Genes Chromosomes Cancer, 2012. **51**(3): p. 240-9.

47.   Perner, S., et al., *TMPRSS2:ERG fusion-associated deletions provide insight into the heterogeneity of prostate cancer.* Cancer Res, 2006. **66**(17): p. 8337-41.

48.   Tomlins, S.A., et al., *TMPRSS2:ETV4 gene fusions define a third molecular subtype of prostate cancer.* Cancer Res, 2006. **66**(7): p. 3396-400.

49.   Pettersson, A., et al., *The TMPRSS2:ERG rearrangement, ERG expression, and prostate cancer outcomes: a cohort study and meta-analysis.* Cancer Epidemiol Biomarkers Prev, 2012. **21**(9): p. 1497-509.

50.   Cerveira, N., et al., *TMPRSS2-ERG gene fusion causing ERG overexpression precedes chromosome copy number changes in prostate carcinomas and paired HGPIN lesions.* Neoplasia, 2006. **8**(10): p. 826-32.

51.   Berg, K.D., et al., *ERG protein expression in diagnostic specimens is associated with increased risk of progression during active surveillance for prostate cancer.* Eur Urol, 2014. **66**(5): p. 851-60.

52.   Barbieri, C.E., et al., *The mutational landscape of prostate cancer.* Eur Urol, 2013. **64**(4): p. 567-76.

53.   Barbieri, C.E., et al., *Exome sequencing identifies recurrent SPOP, FOXA1 and MED12 mutations in prostate cancer.* Nat Genet, 2012. **44**(6): p. 685-9.

54.   Tomlins, S.A., et al., *The role of SPINK1 in ETS rearrangement-negative prostate cancers.* Cancer Cell, 2008. **13**(6): p. 519-28.

55.   Gao, N., et al., *The role of hepatocyte nuclear factor-3 alpha (Forkhead Box A1) and androgen receptor in transcriptional regulation of prostatic genes.* Mol Endocrinol, 2003. **17**(8): p. 1484-507.

56.   Grasso, C.S., et al., *The mutational landscape of lethal castration-resistant prostate cancer.* Nature, 2012. **487**(7406): p. 239-43.

57.   Jenkins, R.B., et al., *Detection of c-myc oncogene amplification and chromosomal anomalies in metastatic prostatic carcinoma by fluorescence in situ hybridization.* Cancer Res, 1997. **57**(3): p. 524-31.

58.   Sato, K., et al., *Clinical significance of alterations of chromosome 8 in high-grade, advanced, nonmetastatic prostate carcinoma.* J Natl Cancer Inst, 1999. **91**(18): p. 1574-80.

59.   Thomas, G.V., et al., *Antibody-based profiling of the phosphoinositide 3-kinase pathway in clinical prostate cancer.* Clin Cancer Res, 2004. **10**(24): p. 8351-6.

60.   Shen, M.M. and C. Abate-Shen, *Pten inactivation and the emergence of androgen-independent prostate cancer.* Cancer Res, 2007. **67**(14): p. 6535-8.

61.   Varambally, S., et al., *The polycomb group protein EZH2 is involved in progression of prostate cancer.* Nature, 2002. **419**(6907): p. 624-9.

62.   Wang, G., J. Wang, and M.D. Sadar, *Crosstalk between the androgen receptor and beta-catenin in castrate-resistant prostate cancer.* Cancer Res, 2008. **68**(23): p. 9918-27.

63.   Wang, G., et al., *Genetics and biology of prostate cancer.* Genes Dev, 2018. **32**(17-18): p. 1105-1140.

64.   Damodaran, S., C.E. Kyriakopoulos, and D.F. Jarrard, *Newly Diagnosed Metastatic Prostate Cancer: Has the Paradigm Changed?* Urol Clin North Am, 2017. **44**(4): p. 611-621.

65. Datta, K., et al., *Mechanism of lymph node metastasis in prostate cancer.* Future Oncol, 2010. **6**(5): p. 823-36.

66. Cai, T., et al., *Clinical importance of lymph node density in predicting outcome of prostate cancer patients.* J Surg Res, 2011. **167**(2): p. 267-72.

67. Bubendorf, L., et al., *Metastatic patterns of prostate cancer: an autopsy study of 1,589 patients.* Hum Pathol, 2000. **31**(5): p. 578-83.

68. Gartrell, B.A., et al., *Metastatic Prostate Cancer and the Bone: Significance and Therapeutic Options.* Eur Urol, 2015. **68**(5): p. 850-8.

69. Logothetis, C.J. and S.H. Lin, *Osteoblasts in prostate cancer metastasis to bone.* Nat Rev Cancer, 2005. **5**(1): p. 21-8.

70. Huggins, C. and C.V. Hodges, *Studies on prostatic cancer: I. The effect of castration, of estrogen and of androgen injection on serum phosphatases in metastatic carcinoma of the prostate. 1941.* J Urol, 2002. **168**(1): p. 9-12.

71. Hussain, M., et al., *Intermittent versus continuous androgen deprivation in prostate cancer.* N Engl J Med, 2013. **368**(14): p. 1314-25.

72. Debes, J.D. and D.J. Tindall, *Mechanisms of androgen-refractory prostate cancer.* N Engl J Med, 2004. **351**(15): p. 1488-90.

73. Feldman, B.J. and D. Feldman, *The development of androgen-independent prostate cancer.* Nat Rev Cancer, 2001. **1**(1): p. 34-45.

74. Grossmann, M.E., H. Huang, and D.J. Tindall, *Androgen receptor signaling in androgen-refractory prostate cancer.* J Natl Cancer Inst, 2001. **93**(22): p. 1687-97.

75. Thiery, J.P., *Epithelial-mesenchymal transitions in development and pathologies.* Curr Opin Cell Biol, 2003. **15**(6): p. 740-6.

76. Kalluri, R. and E.G. Neilson, *Epithelial-mesenchymal transition and its implications for fibrosis.* J Clin Invest, 2003. **112**(12): p. 1776-84.

77. Nawshad, A., et al., *Transforming growth factor-beta signaling during epithelial-mesenchymal transformation: implications for embryogenesis and tumor metastasis.* Cells Tissues Organs, 2005. **179**(1-2): p. 11-23.

78. Kalluri, R. and R.A. Weinberg, *The basics of epithelial-mesenchymal transition.* J Clin Invest, 2009. **119**(6): p. 1420-8.

79. Grant, C.M. and N. Kyprianou, *Epithelial mesenchymal transition (EMT) in prostate growth and tumor progression.* Transl Androl Urol, 2013. **2**(3): p. 202-211.

80. Lo, U.G., et al., *The Role and Mechanism of Epithelial-to-Mesenchymal Transition in Prostate Cancer Progression.* Int J Mol Sci, 2017. **18**(10).

81. Fuchs, I.B., et al., *The prognostic significance of epithelial-mesenchymal transition in breast cancer.* Anticancer Res, 2002. **22**(6a): p. 3415-9.

82. Kokkinos, M.I., et al., *Vimentin and epithelial-mesenchymal transition in human breast cancer--observations in vitro and in vivo.* Cells Tissues Organs, 2007. **185**(1-3): p. 191-203.

83. Takai, M., et al., *The EMT (epithelial-mesenchymal-transition)-related protein expression indicates the metastatic status and prognosis in patients with ovarian cancer.* J Ovarian Res, 2014. **7**: p. 76.

84. Loboda, A., et al., *EMT is the dominant program in human colon cancer.* BMC Med Genomics, 2011. **4**: p. 9.

85. Chen, C.L., et al., *Single-cell analysis of circulating tumor cells identifies cumulative expression patterns of EMT-related genes in metastatic prostate cancer.* Prostate, 2013. **73**(8): p. 813-26.

86.   Nguyen, D.P., J. Li, and A.K. Tewari, *Inflammation and prostate cancer: the role of interleukin 6 (IL-6).* BJU Int, 2014. **113**(6): p. 986-92.

87.   Rojas, A., et al., *IL-6 promotes prostate tumorigenesis and progression through autocrine cross-activation of IGF-IR.* Oncogene, 2011. **30**(20): p. 2345-55.

88.   Wu, C.T., et al., *Significance of IL-6 in the transition of hormone-resistant prostate cancer and the induction of myeloid-derived suppressor cells.* J Mol Med (Berl), 2012. **90**(11): p. 1343-55.

89.   Xu, J. and Y. Qiu, *Role of androgen receptor splice variants in prostate cancer metastasis.* Asian J Urol, 2016. **3**(4): p. 177-184.

90.   Sun, F., et al., *Androgen receptor splice variant AR3 promotes prostate cancer via modulating expression of autocrine/paracrine factors.* J Biol Chem, 2014. **289**(3): p. 1529-39.

91.   Huang, Y., et al., *Overexpression of FGF9 in prostate epithelial cells augments reactive stroma formation and promotes prostate cancer progression.* Int J Biol Sci, 2015. **11**(8): p. 948-60.

92.   Yang, Y., et al., *Dishevelled-2 silencing reduces androgen-dependent prostate tumor cell proliferation and migration and expression of Wnt-3a and matrix metalloproteinases.* Mol Biol Rep, 2013. **40**(7): p. 4241-50.

93.   Baruah, M.M., A.P. Khandwekar, and N. Sharma, *Quercetin modulates Wnt signaling components in prostate cancer cell line by inhibiting cell viability, migration, and metastases.* Tumour Biol, 2016. **37**(10): p. 14025-14034.

94.   Li, Q., et al., *FZD8, a target of p53, promotes bone metastasis in prostate cancer by activating canonical Wnt/beta-catenin signaling.* Cancer Lett, 2017. **402**: p. 166-176.

95.   Stark, T.W., et al., *Predictive value of epithelial-mesenchymal-transition (EMT) signature and PARP-1 in prostate cancer radioresistance.* Prostate, 2017. **77**(16): p. 1583-1591.

96.   Daoud, G., et al., *Primary versus castration-resistant prostate cancer: modeling through novel murine prostate cancer cell lines.* Oncotarget, 2016. **7**(20): p. 28961-75.

97.   Abou-Kheir, W., et al., *Self-renewing Pten-/- TP53-/- protospheres produce metastatic adenocarcinoma cell lines with multipotent progenitor activity.* PLoS One, 2011. **6**(10): p. e26112.

98.   Litwin, M.S. and H.J. Tan, *The Diagnosis and Treatment of Prostate Cancer: A Review.* Jama, 2017. **317**(24): p. 2532-2542.

99.   Filson, C.P., L.S. Marks, and M.S. Litwin, *Expectant management for men with early stage prostate cancer.* CA Cancer J Clin, 2015. **65**(4): p. 265-82.

100.   Bambury, R.M. and H.I. Scher, *Enzalutamide: Development from bench to bedside.* Urol Oncol, 2015. **33**(6): p. 280-8.

101.   Rodriguez-Vida, A., et al., *Enzalutamide for the treatment of metastatic castration-resistant prostate cancer.* Drug Des Devel Ther, 2015. **9**: p. 3325-39.

102.   de Bono, J.S., et al., *Abiraterone and increased survival in metastatic prostate cancer.* N Engl J Med, 2011. **364**(21): p. 1995-2005.

103.   Nguyen, P.L., et al., *Adverse effects of androgen deprivation therapy and strategies to mitigate them.* Eur Urol, 2015. **67**(5): p. 825-36.

104.   Attar, R.M., C.H. Takimoto, and M.M. Gottardis, *Castration-resistant prostate cancer: locking up the molecular escape routes.* Clin Cancer Res, 2009. **15**(10): p. 3251-5.

105.   Collins, A.T., et al., *Prospective identification of tumorigenic prostate cancer stem cells.* Cancer Res, 2005. **65**(23): p. 10946-51.

106. Body, J.J., S. Casimiro, and L. Costa, *Targeting bone metastases in prostate cancer: improving clinical outcome.* Nat Rev Urol, 2015. **12**(6): p. 340-56.

107. Parker, C., et al., *Alpha emitter radium-223 and survival in metastatic prostate cancer.* N Engl J Med, 2013. **369**(3): p. 213-23.

108. Kantoff, P.W., et al., *Sipuleucel-T immunotherapy for castration-resistant prostate cancer.* N Engl J Med, 2010. **363**(5): p. 411-22.

109. Gao, D. and Y. Chen, *Organoid development in cancer genome discovery.* Curr Opin Genet Dev, 2015. **30**: p. 42-8.

110. Barretina, J., et al., *The Cancer Cell Line Encyclopedia enables predictive modelling of anticancer drug sensitivity.* Nature, 2012. **483**(7391): p. 603-7.

111. Lynch, T.J., et al., *Activating mutations in the epidermal growth factor receptor underlying responsiveness of non-small-cell lung cancer to gefitinib.* N Engl J Med, 2004. **350**(21): p. 2129-39.

112. Pao, W., et al., *EGF receptor gene mutations are common in lung cancers from "never smokers" and are associated with sensitivity of tumors to gefitinib and erlotinib.* Proc Natl Acad Sci U S A, 2004. **101**(36): p. 13306-11.

113. Solit, D.B., et al., *BRAF mutation predicts sensitivity to MEK inhibition.* Nature, 2006. **439**(7074): p. 358-62.

114. McDermott, U., et al., *Identification of genotype-correlated sensitivity to selective kinase inhibitors by using high-throughput tumor cell line profiling.* Proc Natl Acad Sci U S A, 2007. **104**(50): p. 19936-41.

115. Garnett, M.J., et al., *Systematic identification of genomic markers of drug sensitivity in cancer cells.* Nature, 2012. **483**(7391): p. 570-5.

116. Gao, D., et al., *Organoid cultures derived from patients with advanced prostate cancer.* Cell, 2014. **159**(1): p. 176-87.

117. Olivotto, M. and P. Dello Sbarba, *Environmental restrictions within tumor ecosystems select for a convergent, hypoxia-resistant phenotype of cancer stem cells.* Cell Cycle, 2008. **7**(2): p. 176-87.

118. O'Driscoll, L., et al., *Phenotypic and global gene expression profile changes between low passage and high passage MIN-6 cells.* J Endocrinol, 2006. **191**(3): p. 665-76.

119. Drost, J. and H. Clevers, *Organoids in cancer research.* Nat Rev Cancer, 2018. **18**(7): p. 407-418.

120. Horoszewicz, J.S., et al., *LNCaP model of human prostatic carcinoma.* Cancer Res, 1983. **43**(4): p. 1809-18.

121. Kaighn, M.E., et al., *Establishment and characterization of a human prostatic carcinoma cell line (PC-3).* Invest Urol, 1979. **17**(1): p. 16-23.

122. Korenchuk, S., et al., *VCaP, a cell-based model system of human prostate cancer.* In Vivo, 2001. **15**(2): p. 163-8.

123. Navone, N.M., et al., *Establishment of two human prostate cancer cell lines derived from a single bone metastasis.* Clin Cancer Res, 1997. **3**(12 Pt 1): p. 2493-500.

124. Sramkoski, R.M., et al., *A new human prostate carcinoma cell line, 22Rv1.* In Vitro Cell Dev Biol Anim, 1999. **35**(7): p. 403-9.

125. Mertz, K.D., et al., *Molecular characterization of TMPRSS2-ERG gene fusion in the NCI-H660 prostate cancer cell line: a new perspective for an old model.* Neoplasia, 2007. **9**(3): p. 200-6.

126. Sobel, R.E. and M.D. Sadar, *Cell lines used in prostate cancer research: a compendium of old and new lines--part 2.* J Urol, 2005. **173**(2): p. 360-72.

145

127. Sachs, N. and H. Clevers, *Organoid cultures for the analysis of cancer phenotypes.* Curr Opin Genet Dev, 2014. **24**: p. 68-73.

128. MacLeod, R.A., et al., *Widespread intraspecies cross-contamination of human tumor cell lines arising at source.* Int J Cancer, 1999. **83**(4): p. 555-63.

129. van Bokhoven, A., et al., *TSU-Pr1 and JCA-1 cells are derivatives of T24 bladder carcinoma cells and are not of prostatic origin.* Cancer Res, 2001. **61**(17): p. 6340-4.

130. van Bokhoven, A., et al., *Molecular characterization of human prostate carcinoma cell lines.* Prostate, 2003. **57**(3): p. 205-25.

131. Stone, K.R., et al., *Isolation of a human prostate carcinoma cell line (DU 145).* Int J Cancer, 1978. **21**(3): p. 274-81.

132. Baca, S.C., et al., *Punctuated evolution of prostate cancer genomes.* Cell, 2013. **153**(3): p. 666-77.

133. Barcellos-Hoff, M.H., et al., *Functional differentiation and alveolar morphogenesis of primary mammary cultures on reconstituted basement membrane.* Development, 1989. **105**(2): p. 223-35.

134. Simian, M. and M.J. Bissell, *Organoids: A historical perspective of thinking in three dimensions.* J Cell Biol, 2017. **216**(1): p. 31-40.

135. Korinek, V., et al., *Depletion of epithelial stem-cell compartments in the small intestine of mice lacking Tcf-4.* Nat Genet, 1998. **19**(4): p. 379-83.

136. Barker, N., et al., *Lgr5(+ve) stem cells drive self-renewal in the stomach and build long-lived gastric units in vitro.* Cell Stem Cell, 2010. **6**(1): p. 25-36.

137. Kim, K.A., et al., *Mitogenic influence of human R-spondin1 on the intestinal epithelium.* Science, 2005. **309**(5738): p. 1256-9.

138. Sato, T., et al., *Single Lgr5 stem cells build crypt-villus structures in vitro without a mesenchymal niche.* Nature, 2009. **459**(7244): p. 262-5.

139. Shamir, E.R. and A.J. Ewald, *Three-dimensional organotypic culture: experimental models of mammalian biology and disease.* Nat Rev Mol Cell Biol, 2014. **15**(10): p. 647-64.

140. Lancaster, M.A. and J.A. Knoblich, *Organogenesis in a dish: modeling development and disease using organoid technologies.* Science, 2014. **345**(6194): p. 1247125.

141. Clevers, H., *Modeling Development and Disease with Organoids.* Cell, 2016. **165**(7): p. 1586-1597.

142. Fatehullah, A., S.H. Tan, and N. Barker, *Organoids as an in vitro model of human development and disease.* Nat Cell Biol, 2016. **18**(3): p. 246-54.

143. Sato, T., et al., *Long-term expansion of epithelial organoids from human colon, adenoma, adenocarcinoma, and Barrett's epithelium.* Gastroenterology, 2011. **141**(5): p. 1762-72.

144. Stange, D.E., et al., *Differentiated Troy+ chief cells act as reserve stem cells to generate all lineages of the stomach epithelium.* Cell, 2013. **155**(2): p. 357-68.

145. Huch, M., et al., *In vitro expansion of single Lgr5+ liver stem cells induced by Wnt-driven regeneration.* Nature, 2013. **494**(7436): p. 247-50.

146. Drost, J., et al., *Organoid culture systems for prostate epithelial tissue and prostate cancer tissue.* Nat Protoc, 2016. **11**(2): p. 347-58.

147. Jung, P., et al., *Isolation and in vitro expansion of human colonic stem cells.* Nat Med, 2011. **17**(10): p. 1225-7.

148. Taguchi, A., et al., *Redefining the in vivo origin of metanephric nephron progenitors enables generation of complex kidney structures from pluripotent stem cells.* Cell Stem Cell, 2014. **14**(1): p. 53-67.

149.   Takasato, M., et al., *Directing human embryonic stem cell differentiation towards a renal lineage generates a self-organizing kidney.* Nat Cell Biol, 2014. **16**(1): p. 118-26.

150.   Antonica, F., et al., *Generation of functional thyroid from embryonic stem cells.* Nature, 2012. **491**(7422): p. 66-71.

151.   Koehler, K.R., et al., *Generation of inner ear sensory epithelia from pluripotent stem cells in 3D culture.* Nature, 2013. **500**(7461): p. 217-21.

152.   Eiraku, M., et al., *Self-organizing optic-cup morphogenesis in three-dimensional culture.* Nature, 2011. **472**(7341): p. 51-6.

153.   Lancaster, M.A., et al., *Cerebral organoids model human brain development and microcephaly.* Nature, 2013. **501**(7467): p. 373-9.

154.   Agarwal, S., et al., *Identification of Different Classes of Luminal Progenitor Cells within Prostate Tumors.* Cell Rep, 2015. **13**(10): p. 2147-58.

155.   Drost, J., et al., *Sequential cancer mutations in cultured human intestinal stem cells.* Nature, 2015. **521**(7550): p. 43-7.

156.   Matano, M., et al., *Modeling colorectal cancer using CRISPR-Cas9-mediated engineering of human intestinal organoids.* Nat Med, 2015. **21**(3): p. 256-62.

157.   van de Wetering, M., et al., *Prospective derivation of a living organoid biobank of colorectal cancer patients.* Cell, 2015. **161**(4): p. 933-45.

158.   Dekkers, J.F., et al., *Characterizing responses to CFTR-modulating drugs using rectal organoids derived from subjects with cystic fibrosis.* Sci Transl Med, 2016. **8**(344): p. 344ra84.

159.   Sachs, N., et al., *A Living Biobank of Breast Cancer Organoids Captures Disease Heterogeneity.* Cell, 2018. **172**(1-2): p. 373-386.e10.

160.   Boj, S.F., et al., *Organoid models of human and mouse ductal pancreatic cancer.* Cell, 2015. **160**(1-2): p. 324-38.

161.   Li, Y., et al., *Induction of Expansion and Folding in Human Cerebral Organoids.* Cell Stem Cell, 2017. **20**(3): p. 385-396.e3.

162.   Bershteyn, M. and A.R. Kriegstein, *Cerebral organoids in a dish: progress and prospects.* Cell, 2013. **155**(1): p. 19-20.

163.   Bershteyn, M., et al., *Human iPSC-Derived Cerebral Organoids Model Cellular Features of Lissencephaly and Reveal Prolonged Mitosis of Outer Radial Glia.* Cell Stem Cell, 2017. **20**(4): p. 435-449.e4.

164.   Mondal, S., et al., *Antigenicity of cells derived from mouse prostate cells after malignant transformation in vitro by carcinogenic hydrocarbons.* Cancer Res, 1970. **30**(6): p. 1593-7.

165.   Centenera, M.M., et al., *Ex vivo culture of human prostate tissue and drug development.* Nat Rev Urol, 2013. **10**(8): p. 483-7.

166.   Karthaus, W.R., et al., *Identification of multipotent luminal progenitor cells in human prostate organoid cultures.* Cell, 2014. **159**(1): p. 163-75.

167.   Vela, I. and Y. Chen, *Prostate cancer organoids: a potential new tool for testing drug sensitivity.* Expert Rev Anticancer Ther, 2015. **15**(3): p. 261-3.

168.   Puca, L., et al., *Patient derived organoids to model rare prostate cancer phenotypes.* Nat Commun, 2018. **9**(1): p. 2404.

169.   Richards, Z., et al., *Prostate Stroma Increases the Viability and Maintains the Branching Phenotype of Human Prostate Organoids.* iScience, 2019. **12**: p. 304-317.

170.   Beshiri, M.L., et al., *A PDX/Organoid Biobank of Advanced Prostate Cancers Captures Genomic and Phenotypic Heterogeneity for Disease Modeling and Therapeutic Screening.* Clin Cancer Res, 2018. **24**(17): p. 4332-4345.

171.   Njoroge, R.N., et al., *Organoids model distinct Vitamin E effects at different stages of prostate cancer evolution.* Sci Rep, 2017. **7**(1): p. 16285.

172.   Santamaria, P.G., et al., *EMT: present and future in clinical oncology.* Molecular oncology, 2017. **11**(7): p. 718-738.

173.   Park, J.W., et al., *Prostate epithelial cell of origin determines cancer differentiation state in an organoid transformation assay.* Proc Natl Acad Sci U S A, 2016. **113**(16): p. 4482-7.

174.   Drost, J. and H. Clevers, *Translational applications of adult stem cell-derived organoids.* Development, 2017. **144**(6): p. 968-975.

175.   Orkin, R.W., et al., *A murine tumor producing a matrix of basement membrane.* J Exp Med, 1977. **145**(1): p. 204-20.

176.   Hughes, C.S., L.M. Postovit, and G.A. Lajoie, *Matrigel: a complex protein mixture required for optimal growth of cell culture.* Proteomics, 2010. **10**(9): p. 1886-90.

177.   Xu, H., et al., *Organoid technology and applications in cancer research.* J Hematol Oncol, 2018. **11**(1): p. 116.

178.   Romijn, H.J., *Development and advantages of serum-free, chemically defined nutrient media for culturing of nerve tissue.* Biol Cell, 1988. **63**(3): p. 263-8.

179.   Brewer, G.J., *Serum-free B27/neurobasal medium supports differentiated growth of neurons from the striatum, substantia nigra, septum, cerebral cortex, cerebellum, and dentate gyrus.* J Neurosci Res, 1995. **42**(5): p. 674-83.

180.   Date, S. and T. Sato, *Mini-gut organoids: reconstitution of the stem cell niche.* Annu Rev Cell Dev Biol, 2015. **31**: p. 269-89.

181.   Davies, C.C., et al., *Impaired JNK signaling cooperates with KrasG12D expression to accelerate pancreatic ductal adenocarcinoma.* Cancer Res, 2014. **74**(12): p. 3344-56.

182.   Feng, Y., et al., *Mutant KRAS promotes hyperplasia and alters differentiation in the colon epithelium but does not expand the presumptive stem cell pool.* Gastroenterology, 2011. **141**(3): p. 1003-1013.e1-10.

183.   Montanari, M., et al., *Epithelial-mesenchymal transition in prostate cancer: an overview.* Oncotarget, 2017. **8**(21): p. 35376-35389.

184.   Lu, X. and Y. Kang, *Epidermal growth factor signalling and bone metastasis.* Br J Cancer, 2010. **102**(3): p. 457-61.

185.   Huang, Y., et al., *Type 2 Fibroblast Growth Factor Receptor Signaling Preserves Stemness and Prevents Differentiation of Prostate Stem Cells from the Basal Compartment.* J Biol Chem, 2015. **290**(29): p. 17753-61.

186.   Donjacour, A.A., A.A. Thomson, and G.R. Cunha, *FGF-10 plays an essential role in the growth of the fetal prostate.* Dev Biol, 2003. **261**(1): p. 39-54.

187.   Cronauer, M.V., et al., *Fibroblast growth factors and their receptors in urological cancers: basic research and clinical implications.* Eur Urol, 2003. **43**(3): p. 309-19.

188.   Pecqueux, C., et al., *FGF-2 is a driving force for chromosomal instability and a stromal factor associated with adverse clinico-pathological features in prostate cancer.* Urol Oncol, 2018. **36**(8): p. 365.e15-365.e26.

189.   de Lau, W.B., B. Snel, and H.C. Clevers, *The R-spondin protein family.* Genome Biol, 2012. **13**(3): p. 242.

190.   de Lau, W., et al., *The R-spondin/Lgr5/Rnf43 module: regulator of Wnt signal strength.* Genes Dev, 2014. **28**(4): p. 305-16.

191.   Cook, C., et al., *Noggin is required for normal lobe patterning and ductal budding in the mouse prostate.* Dev Biol, 2007. **312**(1): p. 217-30.

192. Bjerke, G.A., et al., *Activation of Akt signaling in prostate induces a TGFbeta-mediated restraint on cancer progression and metastasis.* Oncogene, 2014. **33**(28): p. 3660-7.

193. Qin, J., et al., *COUP-TFII inhibits TGF-beta-induced growth barrier to promote prostate tumorigenesis.* Nature, 2013. **493**(7431): p. 236-40.

194. Ding, Z., et al., *SMAD4-dependent barrier constrains prostate cancer growth and metastatic progression.* Nature, 2011. **470**(7333): p. 269-73.

195. Park, J.I., et al., *Transforming growth factor-beta1 activates interleukin-6 expression in prostate cancer cells through the synergistic collaboration of the Smad2, p38-NF-kappaB, JNK, and Ras signaling pathways.* Oncogene, 2003. **22**(28): p. 4314-32.

196. Maroni, P.D., et al., *Mitogen Activated Protein kinase signal transduction pathways in the prostate.* Cell Commun Signal, 2004. **2**(1): p. 5.

197. Bhowmick, N.A., et al., *Transforming growth factor-beta1 mediates epithelial to mesenchymal transdifferentiation through a RhoA-dependent mechanism.* Mol Biol Cell, 2001. **12**(1): p. 27-36.

198. Bhowmick, N.A., et al., *Integrin beta 1 signaling is necessary for transforming growth factor-beta activation of p38MAPK and epithelial plasticity.* J Biol Chem, 2001. **276**(50): p. 46707-13.

199. Cheng, T.L., M. Symons, and T.S. Jou, *Regulation of anoikis by Cdc42 and Rac1.* Exp Cell Res, 2004. **295**(2): p. 497-511.

200. Fujii, M., et al., *A Colorectal Tumor Organoid Library Demonstrates Progressive Loss of Niche Factor Requirements during Tumorigenesis.* Cell Stem Cell, 2016. **18**(6): p. 827-38.

201. Legler, D.F., et al., *Prostaglandin E2 at new glance: novel insights in functional diversity offer therapeutic chances.* Int J Biochem Cell Biol, 2010. **42**(2): p. 198-201.

202. Tjandrawinata, R.R., R. Dahiya, and M. Hughes-Fulford, *Induction of cyclo-oxygenase-2 mRNA by prostaglandin E2 in human prostatic carcinoma cells.* Br J Cancer, 1997. **75**(8): p. 1111-8.

203. Jain, S., et al., *Prostaglandin E2 regulates tumor angiogenesis in prostate cancer.* Cancer Res, 2008. **68**(19): p. 7750-9.

204. Fulton, A.M., X. Ma, and N. Kundu, *Targeting prostaglandin E EP receptors to inhibit metastasis.* Cancer Res, 2006. **66**(20): p. 9794-7.

205. Meng, Y., et al., *Nicotinamide Promotes Cell Survival and Differentiation as Kinase Inhibitor in Human Pluripotent Stem Cells.* Stem Cell Reports, 2018. **11**(6): p. 1347-1356.

206. Bagcchi, S., *Nicotinamide yields impressive results in skin cancer.* Lancet Oncol, 2015. **16**(16): p. e591.

207. Chase, P., et al., *Nicotinamide and prevention of diabetes.* Lancet, 1992. **339**(8800): p. 1051-2.

208. Aisen, P.S., et al., *High-dose B vitamin supplementation and cognitive decline in Alzheimer disease: a randomized controlled trial.* Jama, 2008. **300**(15): p. 1774-83.

209. Huch, M., et al., *Unlimited in vitro expansion of adult bi-potent pancreas progenitors through the Lgr5/R-spondin axis.* Embo j, 2013. **32**(20): p. 2708-21.

210. Minarini, A., et al., *N-acetylcysteine in the treatment of psychiatric disorders: current status and future prospects.* Expert Opin Drug Metab Toxicol, 2017. **13**(3): p. 279-292.

211. Zafarullah, M., et al., *Molecular mechanisms of N-acetylcysteine actions.* Cell Mol Life Sci, 2003. **60**(1): p. 6-20.

212. Curtin, J.F., M. Donovan, and T.G. Cotter, *Regulation and measurement of oxidative stress in apoptosis.* J Immunol Methods, 2002. **265**(1-2): p. 49-72.

213. Deepmala, et al., *Clinical trials of N-acetylcysteine in psychiatry and neurology: A systematic review.* Neurosci Biobehav Rev, 2015. **55**: p. 294-321.

214. Zhang, L., et al., *ROCK inhibitor Y-27632 suppresses dissociation-induced apoptosis of murine prostate stem/progenitor cells and increases their cloning efficiency.* PLoS One, 2011. **6**(3): p. e18271.

215. Wang, S., D. Gao, and Y. Chen, *The potential of organoids in urological cancer research.* Nat Rev Urol, 2017. **14**(7): p. 401-414.

216. Epstein, J.I., et al., *A Contemporary Prostate Cancer Grading System: A Validated Alternative to the Gleason Score.* European urology, 2016. **69**(3): p. 428-435.

217. Strober, W., *Trypan blue exclusion test of cell viability.* Curr Protoc Immunol, 2001. **Appendix 3**: p. Appendix 3B.

218. van Meerloo, J., G.J. Kaspers, and J. Cloos, *Cell sensitivity assays: the MTT assay.* Methods Mol Biol, 2011. **731**: p. 237-45.

219. Mosmann, T., *Rapid colorimetric assay for cellular growth and survival: application to proliferation and cytotoxicity assays.* J Immunol Methods, 1983. **65**(1-2): p. 55-63.

220. Riss, T.L., et al., *Cell Viability Assays*, in *Assay Guidance Manual*, G.S. Sittampalam, et al., Editors. 2004, Eli Lilly & Company and the National Center for Advancing Translational Sciences: Bethesda (MD).

221. Cheaito, K.A., et al., *EMT Markers in Locally-Advanced Prostate Cancer: Predicting Recurrence?* Front Oncol, 2019. **9**: p. 131.

222. Zhou, M., et al., *Alpha-Methylacyl-CoA racemase: a novel tumor marker over-expressed in several human cancers and their precursor lesions.* Am J Surg Pathol, 2002. **26**(7): p. 926-31.

223. Abou-Kheir, W.G., et al., *Characterizing the contribution of stem/progenitor cells to tumorigenesis in the Pten-/-TP53-/- prostate cancer model.* Stem Cells, 2010. **28**(12): p. 2129-40.

224. Lawrence, M.G., et al., *Patient-derived Models of Abiraterone- and Enzalutamide-resistant Prostate Cancer Reveal Sensitivity to Ribosome-directed Therapy.* Eur Urol, 2018. **74**(5): p. 562-572.

225. Linxweiler, J., et al., *Patient-derived, three-dimensional spheroid cultures provide a versatile translational model for the study of organ-confined prostate cancer.* J Cancer Res Clin Oncol, 2019. **145**(3): p. 551-559.

226. Yamamoto, H., et al., *CD49f Is an Efficient Marker of Monolayer- and Spheroid Colony-Forming Cells of the Benign and Malignant Human Prostate.* PLOS ONE, 2012. **7**(10): p. e46979.

227. Guo, C., et al., *Epcam, CD44, and CD49f Distinguish Sphere-Forming Human Prostate Basal Cells from a Subpopulation with Predominant Tubule Initiation Capability.* PLOS ONE, 2012. **7**(4): p. e34219.

228. Boyer, B., et al., *Rearrangements of desmosomal and cytoskeletal proteins during the transition from epithelial to fibroblastoid organization in cultured rat bladder carcinoma cells.* J Cell Biol, 1989. **109**(4 Pt 1): p. 1495-509.

229. Valles, A.M., et al., *Acidic fibroblast growth factor is a modulator of epithelial plasticity in a rat bladder carcinoma cell line.* Proc Natl Acad Sci U S A, 1990. **87**(3): p. 1124-8.

230. Hemalatha, A., T.N. Suresh, and M.L. Kumar, *Expression of vimentin in breast carcinoma, its correlation with Ki67 and other histopathological parameters.* Indian J Cancer, 2013. **50**(3): p. 189-94.

231. Yamashita, N., et al., *Vimentin as a poor prognostic factor for triple-negative breast cancer.* J Cancer Res Clin Oncol, 2013. **139**(5): p. 739-46.

232. Bukhari, S., et al., *Affinity proteomics led identification of vimentin as a potential biomarker in colon cancers: insights from serological screening and computational modelling.* Mol Biosyst, 2015. **11**(1): p. 159-69.

233. Rahmani, A.H., et al., *Association of Cytokeratin and Vimentin Protein in the Genesis of Transitional Cell Carcinoma of Urinary Bladder Patients.* Dis Markers, 2015. **2015**: p. 204759.

234. Gravdal, K., et al., *A switch from E-cadherin to N-cadherin expression indicates epithelial to mesenchymal transition and is of strong and independent importance for the progress of prostate cancer.* Clin Cancer Res, 2007. **13**(23): p. 7003-11.

235. Zhang, Q., et al., *Nuclear factor-kappaB-mediated transforming growth factor-beta-induced expression of vimentin is an independent predictor of biochemical recurrence after radical prostatectomy.* Clin Cancer Res, 2009. **15**(10): p. 3557-67.

236. Lee, D.K., et al., *Progression of prostate cancer despite an extremely low serum level of prostate-specific antigen.* Korean J Urol, 2010. **51**(5): p. 358-61.

237. Jolly, M.K., et al., *Implications of the Hybrid Epithelial/Mesenchymal Phenotype in Metastasis.* Front Oncol, 2015. **5**: p. 155.

238. Zhao, R., et al., *Expression and clinical relevance of epithelial and mesenchymal markers in circulating tumor cells from colorectal cancer.* Oncotarget, 2017. **8**(6): p. 9293-9302.

239. Leontieva, O.V., Z.N. Demidenko, and M.V. Blagosklonny, *Contact inhibition and high cell density deactivate the mammalian target of rapamycin pathway, thus suppressing the senescence program.* Proc Natl Acad Sci U S A, 2014. **111**(24): p. 8832-7.

240. Nekulova, M., et al., *The role of p63 in cancer, stem cells and cancer stem cells.* Cell Mol Biol Lett, 2011. **16**(2): p. 296-327.

241. Pellegrini, G., et al., *p63 identifies keratinocyte stem cells.* Proc Natl Acad Sci U S A, 2001. **98**(6): p. 3156-61.

242. Memmi, E.M., et al., *p63 Sustains self-renewal of mammary cancer stem cells through regulation of Sonic Hedgehog signaling.* Proc Natl Acad Sci U S A, 2015. **112**(11): p. 3499-504.

243. Gjorevski, N., et al., *Designer matrices for intestinal stem cell and organoid culture.* Nature, 2016. **539**(7630): p. 560-564.

244. Liu, X., et al., *ROCK inhibitor and feeder cells induce the conditional reprogramming of epithelial cells.* Am J Pathol, 2012. **180**(2): p. 599-607.

245. Buckwalter, J.A., et al., *Bone biology. I: Structure, blood supply, cells, matrix, and mineralization.* Instr Course Lect, 1996. **45**: p. 371-86.

246. Kiefer, J.A. and M.C. Farach-Carson, *Type I collagen-mediated proliferation of PC3 prostate carcinoma cell line: implications for enhanced growth in the bone microenvironment.* Matrix Biol, 2001. **20**(7): p. 429-37.